DEVELOPMENT OF A TETHERED BILAYER LIPID MEMBRANE (TBLM) LIPASE AND PHOSPHOLIPASE SENSOR

A thesis submitted in fulfilment of the requirements for the degree of Doctor of Philosophy

University of Technology Sydney

School of Life Sciences

Faculty of Science

Upeksha Shashikala Randunu Mirissa Lankage

2023

CERTIFICATE OF ORIGINAL AUTHORSHIP

I, Upeksha Shashikala Randunu Mirissa Lankage declare that this thesis is submitted in fulfilment of the requirements for the award of Doctor of Philosophy, in the School of Life Sciences of the Faculty of Science at the University of Technology Sydney.

This thesis is wholly my own work unless otherwise referenced or acknowledged. In addition, I certify that all information sources and literature used are indicated in the thesis. This document has not been submitted for qualifications at any other academic institution.

This research is supported by the ARC Research Hub for Integrated Device for End-user Analysis at Low-levels (IDEAL) and we acknowledge the support of the Australian Nuclear Science and Technology Organsiation (ANSTO) for providing valuable beamtime and neutron reflectometry expertise.

This research is supported by the Australian Government Research Training Program.

Signature: Production Note: Signature removed prior to publication. Date: 21/01/2023

Acknowledgements

Firstly, I want to thank my principal supervisor, Associate Professor Charles Cranfield from the University of Technology Sydney (UTS), for his high enthusiasm, dedication, motivation and continuous help and support throughout my PhD. I was able to conduct experiments at the Australian Nuclear Science and Technology Organisation (ANSTO) and present my research findings at conferences. These experiences and research opportunities have been rewarding and would not have been possible without Associate professor Charles Cranfield.

I would like to acknowledge the support of my co-supervisor, Adjunct Professor Bruce Cornell, for his dedication and continued support, and guidance throughout my PhD.

I want to acknowledge my other co-supervisor, Dr Stephen Holt, for his support during the experiments at ANSTO and for helping me learn new data analysation methods.

Also, I would like to thank you Dr Evelyne Deplazes, Dr Alvaro Garcia, Dr Amani Alghalayini, Dr Krishanthi Jayasundara for helping with my membrane work in the early stages and for the insights they provided during the many discussions of my results.

I would like to express my gratitude towards Professor Stell Valenzuela for the support and the insights she provided during the many discussions of my results during the IDEAL Hub meetings. Also, I would like to thank UTS IDEAL Hub for providing funding and my scholarship during my PhD.

I want to express gratitude towards the people who helped develop my understanding of different techniques and complete the experiments I have performed for this study. Thank you to Dr Matt Padula for his help with the mass spectroscopy experiments and Dr Anton LeBrun from ANSTO with the Neutron reflectometry experiments. A special thank you to IBD sensor collaborators Dr Catherine Burke and Professor Georgina Hold from UNSW for supplying samples for the IBD study.

Lastly, I thank my Mom, Dad, three sisters, uncle, aunt and friends who believed in me and supported me in various ways while undertaking this work. Their mental and emotional support has been significant in helping me to complete this research study.

Awards and Grants

2022, co-investigator in UTS Research Translation Competition. **2nd prize. $25,000** grant for further research into colorectal cancer diagnostic.

2022, Runner-up selected student presentation award at the Australian Society for Biophysics Meeting, Hobart.

2021: Chief-investigator Australian Centre for Neutron Scattering Neutron Proposal (Platypus) Acute pancreatitis point-of-care sensor based on a triolein tethered bilayer lipid membrane (tBLM) technology. 3 days ($31,235) (ANSTO, Proposal 9765).

2021, The best 3-minute thesis PhD presenter at IDEAL Research Hub annual meeting with the University of South Australia.

2019, International Research Scholarship and IDEAL Research Hub - Biochemistry Scholarship with a $5000 per annum top-up scholarship.

Publications

Publications

Garcia, A., Deplazes, E., Aili, S., Padula, M.P., Touchard, A., Murphy, C., **Mirissa Lankage, U**., Nicholson, G.M., Cornell, B. and Cranfield, C.G., 2020. Label-Free, Real-Time Phospholipase-A Isoform Assay. ACS Biomaterials Science & Engineering, 6(8), pp.4714-4721.

Conference presentations

Talk and Runner-up selected student presentation award: **Upeksha Mirissa Lankage**, Stephen Holt, Bruce Cornell, and Charles Cranfield, 2022, 'A novel triglyceride tethered bilayer lipid membrane (tBLM) architecture': 2022 AuPS/ASB Scientific Meeting, 20th -23rd November, Hobart.

Poster of co-supervised student: Samara Bridge, **Shashikala Randunu**, Bruce Cornell, Charles G. Cranfield, 2022, 'Identifying lipid mixture for optimal tethered bilayer lipid membrane sensing of lipase activity: 2022 AuPS/ASB Scientific Meeting, 20th -23rd November, Hobart.

Poster and 5-minute talk: **Upeksha Mirissa Lankage**, Stephen Hold, Charles Cranfield and Bruce Cornell, 2022, 'Lipase and phospholipase point-of-care sensor based on a triolein tethered bilayer lipid membrane (tBLM) technology': The Australian Nuclear Science and Technology Organisation (ANSTO) and the Helmholtz Zentrum Berlin (HZB) neutron school, 9th -14th October, Lucas Height, Sydney, NSW, Australia.

Poster: **Upeksha Mirissa Lankage**, Evelyne Deplazes, Alvaro Garcia and Charles Cranfield, 2019, 'Development of a tethered bilayer lipid membrane (tBLM) pancreatic lipase sensor': 2019 AuPS/ASB Scientific Meeting, 1st-4th December, Canberra ACT.

List of Abbreviations

ANSTO	Australian nuclear science and technology organisation
AP	acute pancreatitis
Au	gold
ANL	*Aspergillus niger* lipase
AUC	area under the curve
$BaTiO_3$	Barium titanate
BLM	black lipid membranes
$CaCl_2$	calcium chloride
$cPLA_2$	cytosolic phospholipase A_2
C_m	capacitance
CPP	critical packing parameter
CPE	constant phase element
CRL	*Candida rugosa* lipase
CT	computed tomography
D_2O	heavy water
DOPC	1,2-dioleoyl-sn-glycero-3-phosphocholine
d-triolein	deuterated triolein
diether-PC	1-O-hexadecanyl-2-O-(9Z-octadecenyl)-sn-glycero-3-phosphocholine

EDTA	Ethylenediaminetetraacetic acid
ELISA	enzyme-linked immunosorbent assay
EPJ	European Physical Journal
EIS	Electrochemical impedance spectroscopy
FDA	Food and Drug Administration
G_m	conductance
He	helium
HPL	human pancreatic lipase
HRP	horse radish peroxidase
IBDs	inflammatory bowel diseases
IBS	irritable bowel syndrome
ISFET	ion-sensitive field-effect transistor
Lyso PC	1-oleoyl-2-hydroxy-sn-glycero-3-phosphocholine
MES	ethanesulfonic acid
MRI	magnetic resonance imaging
NaCl	sodium chloride
NR	neutron reflectometry
PAF	platelet-activating factor
PC	phosphatidylcholine
PLA	phospholipase A

PLA_1	phospholipase A_1
PLA_2	phospholipase A_2
PLC	phospholipase C
PLD	phospholipase D
PLRP	pancreatic lipase-related protein
PPL	porcine pancreatic lipase
Q	scattering vector
Q_s	close capacitive term
RA	rheumatoid arthritis
R_m	resistance
ROC	receiver operating characteristic
ROL	*Rhizopus oryzae* lipase
$sPLA_2$	secreted phospholipase A_2
SLD	scattering length density
spacers	benzyl-disulfide-tetra-ethyleneglycol-OH
SIRS	systemic inflammatory response syndrome
SLMs	supported lipid membranes
tBLMs	tethered bilayer lipid membranes
tethers	(tetra-ethyleneglycol)n=2 C20-phytanyl
tMLM	tethered monolayer lipid membrane

tris	trisaminomethane
TMB	3,3',5,5'-Tetramethylbenzidine
TPE	dyetetraphenylethylene
UC	ulcerative colitis
WGL	wheat germ lipase
$\propto_s$	dimensional constant in constant phase element

List of Figures and Tables

Table of contents

Abstract

Tethered bilayer lipid membrane (tBLMs) is the name for lipid bilayers that can be anchored to a conductive metal substrate. Used in conjunction with electrical impedance spectroscopy (EIS), they are a valuable tool for research into the properties of lipid bilayer interactions with proteins, peptides and toxins. This project sought to create a phospholipase biosensor that can detect Inflammatory bowel diseases (IBDs) using phospholipid tBLMs.

IBDs are a group of chronic bowel conditions that includes ulcerative colitis and Crohn's disease. Currently, the diagnosis of IBD conditions typically involves colonoscopies and biopsies. However, attempts have been made to diagnose IBD conditions by the levels of phospholipase A_2 (PLA_2) enzyme in serum and stool samples. A blind trial using 40 stool samples was tested on the DOPC tBLMs and the presence of PLA_2 activity was measured using EIS. The data suggest that tBLM arrays are capable of detecting PLA_2 activity in fecal samples and that this has the potential to be developed into a point-of-care diagnostic for IBDs.

Another part of this project was to investigate biomedical diagnostics for acute pancreatitis, which is a life-threatening inflammatory condition that causes severe abdominal pain in patients. Current tests for acute pancreatitis involve the use of enzyme-linked immunosorbent assays (ELISAs) of pancreatic lipase (PL) levels in blood samples which aren’t conducive to a rapid point-of-care diagnosis.

So this project also reports on developing an impedance sensor that uses a novel tethered membrane architecture that incorporates the triglyceride triolein as a substrate to identify the presence of PL. The hydrolysis of triolein leads to membrane disruption that can then be detected using EIS. The creation of a triglyceride tethered membrane and the ability to rapidly measure pancreatic lipase activity shows great potential for the use of this technology as a point-of-care acute pancreatitis diagnostic. This would have a particular benefit to many remote communities where there is no access to rapid pathology testing currently. These triglyceride-tethered membranes were further tested with multiple

lipases that are produced commercially to demonstrate their potential to be used as a sensor in industrial research and other biomedical diagnostics.

Finally, this project tested triolein tethered membranes using neutron reflectometry (NR) in order to determine their membrane thickness and water volume fraction. The NR data shows that triolein membranes typically form as a monolayer around the tethering molecules and are really a tethered monolayer lipid membrane (tMLM) architecture.

1 Introduction to phospholipase and lipase sensors tethered bilayer lipid membranes and electrical impedance spectroscopy

1.1 Introduction

This chapter delivers background information about phospholipases, lipases, and current lipase and phospholipase sensors. It also describes the development of lipase and phospholipase sensors using tethered bilayer lipid membrane (tBLM) technology. The sensors are targeted to have multiple applications, such as diagnosing acute pancreatitis (AP) and inflammatory bowel diseases (IBDs) and monitoring industrial lipase production.

1.2 Lipases and phospholipases

1.2.1 Lipases

The human body contains lipase enzymes that hydrolyse triglycerides into free fatty acids and glycerol in the digestive system. Lipase production mainly occurs in the pancreas as well as in the mouth and stomach [1]. The role of the lipases is mainly digestion, along with the transport and processing of dietary lipids in most living organisms. Lipases catalyse the hydrolysis of ester bonds in triacylglycerides leading to the formation of free fatty acids, di-acylglycerols, mono-acylglycerols and glycerols.

Lipases are part of the α/β hydrolyse superfamily [2]. The lipase structure includes active sites that contain the Ser-His-Asp catalytic triad and the residues in the *oxyanion hole* (Figure 1.1). The oxyanion hole is formed by Gly133, Thr134 and Ser135 and the NH_2 groups are usually inaccessible due to the helical structure or surface loop loops. However, when they are exposed to the substrate molecules or micelles, there is a change in the overall structure of the protein, offering access to the active site to the substrate [3].

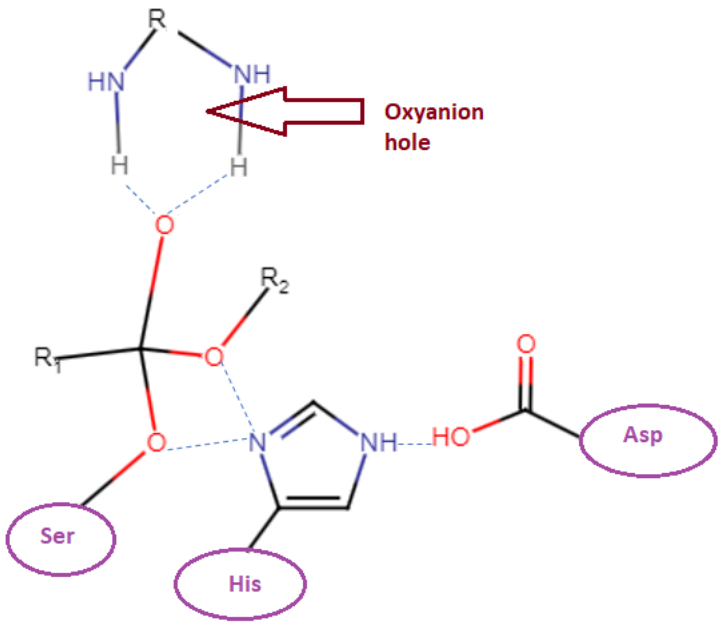

Figure 1.1: The N-H bonds of the oxyanion hole or the active site in lipase enzymnes.

A typical triglyceride structure with three fatty acid chains is shown in Figure 1.2 The positional specificity can be subdivided into non-positional and 1,3-positional specificity. Most fungi-produced lipases are 1,3-positional specific lipases [4, 5], while microbial lipases are a combination of both. In general, microbial lipases have diversified properties which can be significantly impacted by temperature, pH, presence of surfactants, organic solvents, and metal ions that can promote or inhibit the enzymatic reaction [6]. Also, these microbial lipases have substrate specificity that includes non-specific, 1,3 position specific and fatty acid-specific lipases.

The 1,3 position-specific lipases can hydrolyse triglycerides at positions 1 and 3 and are not capable of hydrolysing the middle ester bonds, which improves their biotechnological importance. The fatty acid-specific lipases target the long-chain fatty acids with cis double bonds between carbon 9 and 10 [7]. These substrate specificities are commonly used in industrial applications where lipases have been used for bioenergy processes, food and pharmaceuticals production, detergents, cosmetics and textiles [8-10]. Due to

industrial demand, lipase production has increased in the past decades [11-15], and the microbial lipase market is estimated to reach USD $590 million by 2023 [16].

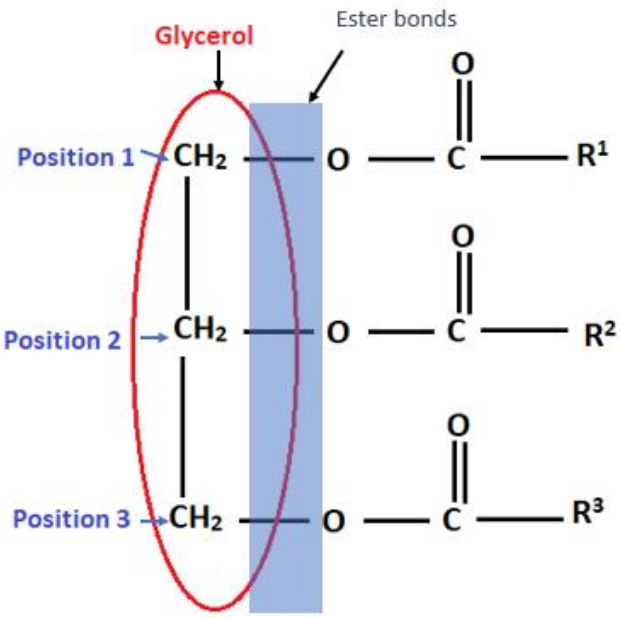

Figure 1.2: The typical structure of triglyceride with three fatty-acid-linked ester moieties.

1.2.1.1 Pancreatic lipase

Human pancreatic lipase (HPL), shown in Figure 1.3, is the main enzyme in the mammalian digestive system responsible for the breakdown of dietary triglycerides into monoglycerides and free fatty acids [17]. HPL is a single polypeptide chain with a size of ~50kDa. HPL is secreted from the pancreas in their final enzymatic form, where they are typically produced as proenzymes. Pancreatic lipase was identified in the early 90s when it was found that they were distinct from lipoprotein and hepatic lipases [18, 19].

HPLs typically contain a single-chain glycoprotein of 449 amino acids [20]. These enzymes have three different subclasses based on their substrate specificity and activity: classical pancreatic lipase, pancreatic lipase-related protein 1 (PLRP1) and pancreatic lipase-related protein 2 (PLRP2) [19]. The PLRP 1 and 2 are 65 to 68% similar to the

classical pancreatic lipase, respectively. Human PPL has three active sites; two of them are a charge relay system (position 193 and 280) and one nucleophile (position 169), see highlighted areas of Figure 1.3. There are four different binding sites in the HPL at positions 204, 207, 209 and 212.

Colipase is the co-enzyme of pancreatic lipase that is required during the activation of enzymatic reactions in the presence of bile salts. Trypsin works in the intestine to cleave the precursor molecule pro-colipase into colipase. This small protein contains five conserved disulphate bonds and it can bind to the non-catalytic domain and C-terminal of pancreatic lipases [21]. The non-catalytic domains of C and N-terminal domains are then more able to interact with the membrane [22].

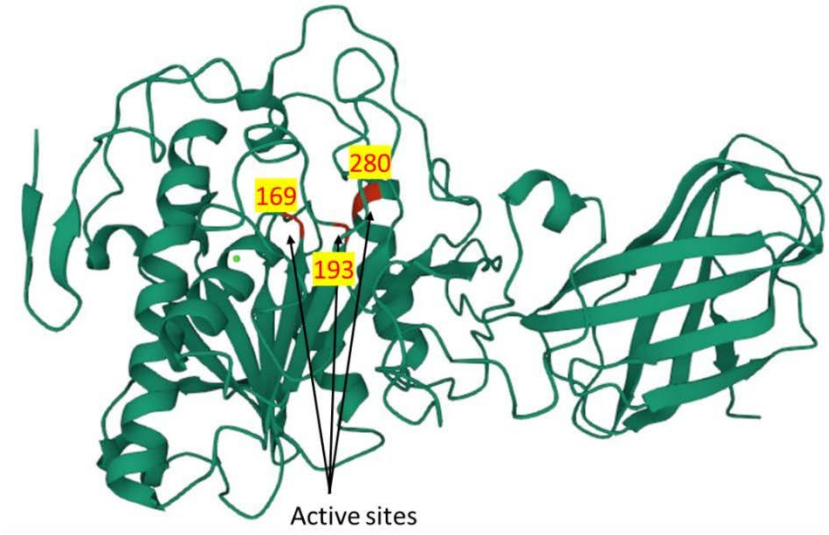

Figure 1.3: 3D structure of human pancreatic lipase with three active sites in positions 169,193 and 280 in the amino acid sequence. There are four different binding sites in the HPL at positions 204, 207, 209 and 212. This structure was created using the RCSB protein data bank.

Blood PL level is important for human health, and generally, a PL activity of 10 to 140 U/L is known as a healthy, or normal lipase range, for adults younger than 60. For adults aged 60 and older, it is 24 to 151 U/L [23, 24]. If the blood contains 3 to 10 times that normal level, it is indicative of the *inflammatory disease*, *acute pancreatitis*. High levels of pancreatic lipase can increase the risk of kidney failure, cirrhosis or bowel problems.

1.2.1.2 Porcine and human pancreatic lipases

One Aim of this project is an attempt to create a point-of-care sensor to detect pancreatic lipase in blood or serum as a diagnostic for acute pancreatitis. To develop the experimental method, porcine pancreatic lipase was used instead of human pancreatic lipase. These two enzymes' similarities were checked using the UniProt database, a universal database for protein resources. The human and porcine pancreatic lipase has 86.19% similarity in their amino acid sequence, Figure 1.4. There are three active sites and four Ca^{2+} binding sites in both species' enzymes.

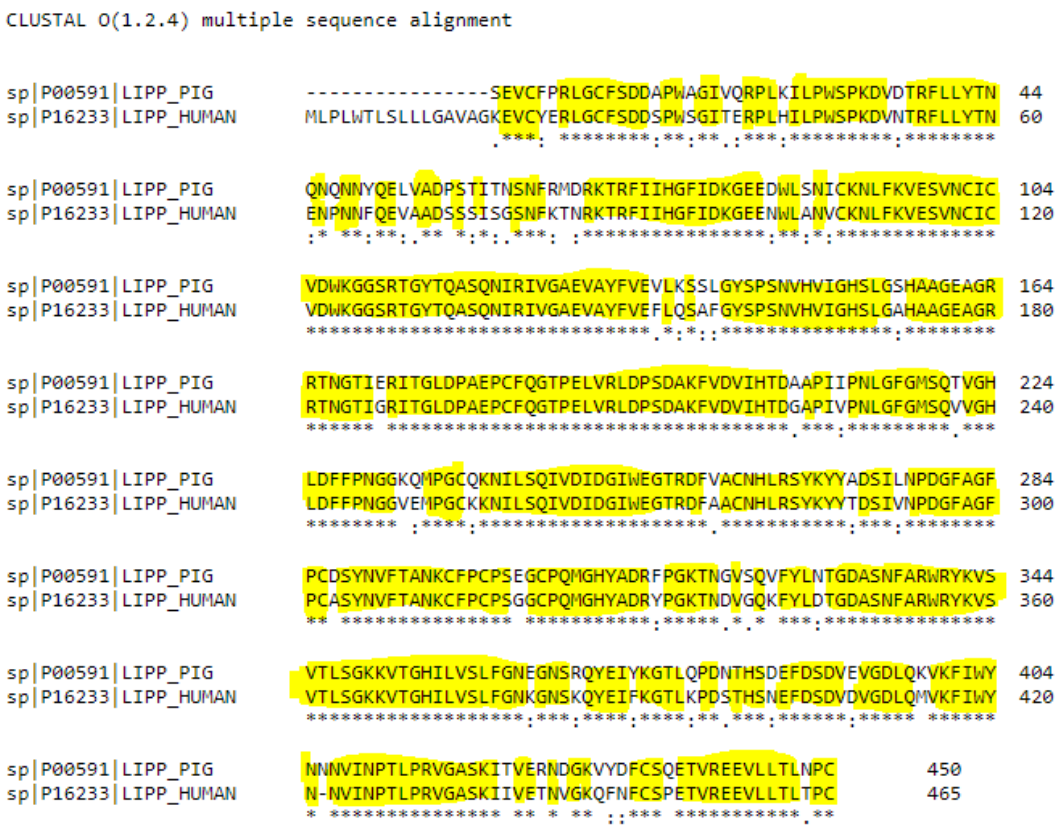

Figure 1.4: The human and porcine pancreatic lipase's protein sequence and functional information from the UniProt database. The human pancreatic lipase has 465 amino acid residues, and the porcine pancreatic lipase has 450 residues.

1.2.1.3 Industrial lipases

Lipases have been used in many industries, such as bioenergy, cosmetics, leather, paper, food, pharmaceuticals, detergents, cosmetics and textiles industry [8-10]. 75% of all the industrial enzymes are of microbial origin of the nearly 200 enzymes that are used industrially [25]. Therefore, for this project, the most common type of industrial lipases used were selected for this project, namely: *Aspergillus niger* lipase (ANL), *Candida rugosa* lipase (CRL), *Rhizopus oryzae* lipase (ROL) and lipase from the wheat germ (WGL).

1.2.1.3.1 *Aspergillus niger* lipase (ANL)

Aspergillus is a genus of filamentous fungus that can be found in agro-industrial solid waste such as rice, wheat and soybean bran [26]. There are 180 officially recognised *Aspergillus* species. 20 Aspergillus species are recognised pathogens, however, there are beneficial species, such as those that produce industrial lipase enzymes [27].

The lipase from these species is known to have many industrial benefits. According to the Food and Drug Administration (FDA) in the United States, *Aspergillus oryzae* and *Aspergillus niger* are the safest lipases used in industrial applications. These species produce limited toxic components compared to most fungi [28]. The *Aspergillus* lipases can hydrolyse natural and synthetic lipids [29]. As well as being used as a biocatalyst in food processing, AN lipases have been utilised in the synthesis of biodiesel using solid-state fermentation techniques [30].

There are a few ANLs with more-pronounced enzymatic properties with altered amino acid sequences. They are lipases from *A. niger* NRRL3 [31], *A. niger* MTCC 872 [32], *A. niger* GZUF36 [33], *A. niger* F044 [34], *A. niger* CBE 332.1 [35], and *A. niger* INCIM 1207 [36]. ANL enzymes function optimally at pH 4 to 7. This chemical property has been useful in *Aspergillus niger* lipase industrial production [37]. This lipase is Ca^{2+} ion-dependent [38].

1.2.1.3.2 *Candida rugosa* lipase (CRL)

Candida rugosa (CR) is a fungal pathogen found in Europe, North America, and Latin America [39]. *Candida* species can cause serious fungal infections [40]. The lipase from CR (CRL) is used as a digestive enzyme in dietary supplements for fat hydrolysation [41]. This lipolytic food-grade enzyme is commonly used in the dairy industry as a biocatalyst of lipids and oils to enhance flavours [42].

This lipase can hydrolyse triglycerides and sterol esters, and it is a non-position-specific lipase so can hydrolyse all three positions in the triglyceride molecule [43]. This lipase can also catalyse transesterification reactions replacing one fatty acid tail with another [44]. There are five different types of CRL (1 to 5) based on their structural traits and catalytic versatility [45-47]. The affinity for some of these enzymes is different such as the CRL2 shows more activity on cholesterol esters than triglycerides [48]. These enzymes work best at pH 7.5 [49] and at 30 °C [50]. This lipase's enzymatic reaction is Ca^{2+} ion-dependent and also there are increases in their activity in the presence of Cr^{+3} and Co^{+2} [51].

CR lipase is also one of the digestive enzyme supplements that are available as over-the-counter products, especially for people with cystic fibrosis [52]. When a patient suffers from cystic fibrosis, a thick mucus layer prevents enzymes from entering the gut; therefore, these patients suffer from lipase deficiency. As a result, cystic fibrosis patients can take CR lipases as a pancreatic lipase enzyme replacement [41, 53].

1.2.1.3.3 *Rhizopus oryzae* (RO) lipase (ROL)

The *Rhizopus oryzae* (RO) *is* a micro-fungus that can be found in rotting vegetation and dung. *Rhizopus oryzae* lipase is used in the food industry, biodiesel production and the synthesis of organic acids. The production of RO lipase started with fungi growing on palm fruit [54]. As this is a fungus-produced lipase, it has a 1,3-positional specificity. This lipase has a molecular weight of 32 kDa with 28 N-terminal amino acids in the RO's structure. [55]. This lipase deactivates at a lower pH than 4 and is most stable at pH 5-7 [56, 57].

1.2.1.3.4 Wheat germ lipase (WGL)

Wheat germ is part of the wheat kernel that assists plants in reproducing and spawning new wheat. The lipase from the wheat germ (WGL) is one of the largest industrially produced enzymes. As well as being a biocatalyst for glycerides and simple carboxylic acid esters [58], applications of WGL include esterification reactions in organic media, oils and triglyceride (fat) modifications and chiral racemic intermediates [59]. As a result of the hydrolysation of plant lipid substrates, this lipase can enhance flavours. Therefore these enzymes are widely used in the baking industry [60]. This lipase is also used as a fine chemistry application in pharmaceutical and chemical industries [61], such as to determine the kinetic resolution of secondary alcohols [62].

The enzyme shows the highest activity at 6.6 to 6.8 pH [63] and is even active at 40°C [64]. Jing, F at el. 2003, have characterised the hydrolysation of triolein by WGL and showed the highest activity at pH 7.4 [60]. Most of the research with WGL is involved with short-chain fatty acids with less than six carbon in the chain substrates [65].

1.2.1.4 Phospholipases

The enzymes that can hydrolyse *phospholipids* into fatty acids are phospholipases [66]. Phospholipases are categorised into four classes based on the cleavage sites of enzyme activity, namely, phospholipase A, B, C, and D. Figure 1.5 shows the cleavage sites in the phospholipid molecule in response to the various classes of phospholipases. Phospholipase A (PLA) catalyses cleavage at the ester moieties in the phospholipid acyl chains. There are two isomers of PLA, A_1 and A_2, that cleave *sn-1* and *sn-2* acyl chains, respectively. The role of PLA_1 is to assist in the production of various lysophospholipid mediators that regulate cellular metabolic pathways [67]. Phospholipase B (PLB) catalyses the cleavage of both acyl chains in phospholipids. Phospholipase C (PLC) catalyses cleavage between the phosphate head group and the glycerol moiety of phospholipids. In contrast, phospholipase D (PLD) catalyses cleavage at the phosphate group, distal to the glycerol moiety.

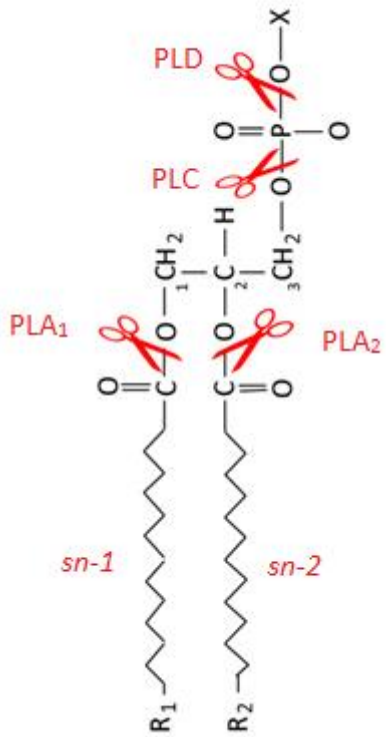

Figure 1.5: The phospholipase cleavage sites in a typical phospholipid structure. Phospholipase A_1 and A_2 actions on the phospholipid result in the release of free fatty acids and lysophospholipids, whereas diacylglycerol and phosphatidic acids are produced with PLC and PLD, respectively. PLB has the PLA_1 and PLA_2 both combined enzymatic property where can cleave sn-1 and sn-2 in the acyl chains [68]

.

1.2.1.4.1 Phospholipase A_2

In 1890, phospholipase A_2 was first studied using snake venoms from Cobras. This was found to have similar properties to porcine pancreas-secreted enzymes [69]. PLA_2 has since been subdivided into 18 groups based on their molecular structures, disulphide bond positions, extensions and unique loops [70]. PLA_2 can also be grouped into secreted phospholipase A_2 ($sPLA_2$), cytosolic phospholipase A_2 ($cPLA_2$), and Ca^{2+}-independent phospholipase A_2 ($iPLA_2$). These groups are further classified into subgroups (Table 1.1) based on their primary sequences [71].

Mammalian pancreatic PLA_2 and digestive enzymes have a similar structure to the snake venoms and have been grouped into Group I (GI), which are further sub-grouped into A and B [72]. GI phospholipases are secretory ($sPLA_2$) and are relatively small, being just 13 to 15kDa in size. GIB enzymes have a more positively charged interfacial surface [73] and can bind to an anionic lipid interface [74].

Group IIA is also highly cationic with positively charged arginine and lysine residues. It is one of the main enzymes in inflammation processes, where it regulates the production of inflammatory mediators such as lysophospholipids and eicosanoids such as arachidonic acid. This enzyme can be found in many organs during inflammation, such as in the lungs, kidneys and gastrointestinal tract [75-77]. Intestinal secretion of Group II (GII) phospholipases has gram-positive and negative bacteria-killing properties [78, 79]. The anti-bacterial properties depend on their surface cationic charges [80]. Anti-bactericidal properties have also been identified in human and murine GI, GII, GV, GX and GXII PLA_2 enzymes. The presence of GIIA in synovial fluid can be used to diagnose rheumatoid arthritis (RA). This subgroup can increase inflammation and autoimmunity [81].

Group	Sources	Size (kDa)
IA	Cobra, Krait venom	13 -15
IB	Mammal pancreas	13 -15
IIA	Human Synovial fluid, platelets rattlesnake, viper venom	13 - 15
IIB	Gaboon viper	13 - 15
IIC	Rat (murine) testis	15
III	Human, murine, lizard, bee	15 -18
V	Human and murine in heart, lung, macrophages	14
IX	Snail venom	14
X	Human spleen, thymus, leukocyte	14
XII	Human, murine	19
XIII	Parvovirus	<10
XIV	Symbiotic fungi, bacteria	13 - 19

Table 1.1: Phospholipase A_2 groups and their sources [82, 83].

1.3 Lipase and phospholipase A_2 sensors

Biosensors are becoming essential in food processing, environmental remediation, and the pharmaceutical and biotechnology industries [84]. Typical components of biosensors are the physio-chemical transducer or the sensor, and the biorecognition element required to impart specificity. Lipases are frequently used in biosensor construction because of their wide substrate specificity, and commercial availability. [85, 86].

In nature, PLA_2 is primarily active on lipid substrates like micelles and lipid membranes. Therefore, many PLA_2 sensor studies are based on liposome-related release assays [87-91]. There are various lipase and phospholipase sensors, such as pH sensors, impedance sensors, and nanoparticle aggregation sensors [92-96].

The lipase and phospholipase activity test is performed for many purposes and is fairly standard in microbiology as well as biochemical laboratories. They are mainly based on the physicochemical properties of the medium such as conductivity, pH and optical properties. These enzymes are capable of generating organic acid and alcohol after the hydrolysation of triglycerides and phospholipids. This leads to a change in the pH of the surrounding solution. Therefore, many lipase/phospholipase sensors function by detecting pH changes after the hydrolysation of specific substrates.

Pijanowska et al. (2001) have described an ion-sensitive field-effect transistor (ISFET) sensor for pancreatic lipases. They have created 100% triglycerides coated on glass rods using three triglycerides, triacetin, tributyrin and triolein [97]. Lipase activity was measured by monitoring changes in pH using the ISFET. According to their results, tributyrin has the highest sensitivity to responding to the lipase, and this sensor's detection range for tributyrin is <4 mM at 0.478 pH/mM.

Kartal et al. (2007) used glass electrodes to identify the *Candida rugosa* lipase activity on organophosphorus pesticides. This pesticide contains the triglyceride *tributyrin* [45]. Tributyrin is hydrolysed into butyric acid and glycerol, and the pH change is due to the increase of butyric acid formation. This sensor is capable of measuring tributyrin in the range of 65 to 455 μM. However, this tributyrin pH sensor has low stability and slow response time, taking up to 7 hrs to see significant changes in phospholipase activity.

The biggest advantage of these pH sensors is that direct measurements can be done with existing sensor technologies. However, the biggest disadvantage is that sample environment changes might also alter the pH of the test fluid. The pH sensors that rely on a fluorescence change also require the presence of a reporter molecule which might introduce its own artefact [98].

Shi et al. (2017) experimented with fluorometric probing using gold nanoparticles to create a sensor to detect acute pancreatitis [99]. This study used the aggregation of the nanoparticles as the probe. The nanoparticles are coated with glutamate functionalised with the dyetetraphenylethylene (TPE). When the lipase cleaves the ester groups in the probe, a transformation happens which releases 4,4′-dihydroxy tetraphenylethylene which aggregates and emits the blue colour. This study tested a few porcine pancreases and serum forms with and without acute pancreatitis patients. The porcine pancreatic lipase (PPL) in the buffer detection range is 0.13 to 90 U/L, the standard lipase level in the human blood is 10- 140 U/L for people aged 60 and below, 18- 180 U/L for ages greater than 60 years [100]. This study also tested human serum samples of patients with and without acute pancreatitis. The blood samples had to be centrifugated at 3000 rpm for 5 minutes and then diluted ten-fold with PBS buffer.

The nanoparticle aggregation PLA_2 sensors such as Aili, D., et al. (2011) are targeting pharmaceutical screening and point-of-care diagnostics [101]. They developed this assay with gold nanoparticles that can attach to liposomal surfaces. This assay is able to detect the enzymatic concentration as low as 700 pM in real-time and in rapid testing mode as low as 10 nM within 5 mins.

Impedance enzymatic sensors are based on a method to determine the enzymatic activity using sensing electrodes [102, 103]. Most impedance sensors require a phospholipid or the lipase substrate that is attached to electrodes using a liposome deposition method or Langmuir-Blodgett technique. Typically, membrane capacitance changes after the enzymatic reaction can be measured [104]. The disadvantages of these techniques might be that the deposition of the membrane might not be even or replicable between sensors, which could cause a difference in the electrical measurements. The advantage, however, is that impedance sensors can give quick responses.

A recent study showed an attempt to create a low-cost rapid sensor to detect lipase activity in an industrial application using impedance sensing [105]. This sensor consists of lipase sensitive substrate deposited on the electrode surface. The substrate in this instance was a mixture of 70% olive oil and 30% triolein mixed with $BaTiO_3$ nanoparticles coated onto an electrode. The $BaTiO_3$ was added to increase its sensitivity. The experimental results show the presence of the nanoparticles gives the layer a high electrical resistance and dielectric constant. This sensor is capable of detecting 0.73×10^{-2} to 3.9 U/mL enzymatic activity with a response time of 70 to 140 s.

1.4 Acute pancreatitis

Pancreatitis is an inflammation of the pancreas, which, depending on its severity, can lead to long-term damage to the pancreas [106]. Excessive use of alcohol and gallstones are significant causes of pancreatitis and other pancreatic disorders [107]. Other causes of pancreatitis include metabolic disorders, cystic fibrosis and autoimmune disease [108]. Acute pancreatitis causes severe abdominal pain in patients with symptoms such as vomiting and nausea, and chronic pancreatitis presents with symptoms that include diarrhoea, nausea, vomiting and shortness of breath [109, 110]. Upper abdominal pain can persist for several days [111]. In some circumstances, the pancreatic ducts' enzyme pathways to the small intestine are blocked, and there is a build-up of pressure inside the ducts, which leads to pancreatic swelling and inflammation [112].

This disease is common among men 30 to 40 years old, mostly due to alcohol abuse. Excessive alcohol consumption is believed to affect pancreas immune responses, including innate and adaptive immunity [113]. According to the Australian pancreatic research group, 50 % of alcoholic pancreatitis patients die within 20 years of diagnosis [114]. Acute pancreatitis is a life-threatening condition, with 20 to 40% of patients experiencing body organ failure. According to the "World Congress of Emergency Surgery", in 2018, acute pancreatitis patients' hospital mortality rate was about 15% and has increased within the last few years [115]. 20% to 40% of patients may experience heart, lung or kidney failure. The cause of this is due to the build-up of inflammatory mediators such as TNF-α, IL-1-β, IL-6, IL-8, platelet-activating factor (PAF), IL-10, C5a,

ICAM-1, and Substance P. This, in turn, can lead to systemic inflammatory response syndrome (SIRS) [116]. According to an Alice Springs hospital report in 2001, most of the acute and chronic pancreatitis patients reported in Australia were from remote hospitals, and 77% of pancreatitis patients were indigenous Australians. 64% presenting with acute pancreatitis were due to excessive alcohol consumption [117]. From March 2004 to July 2007, in regional Australian hospitals, 61.4% of reported acute pancreatitis patients were male, and of those, 41.2% were reported to be Indigenous Australians from remote regions [118].

1.4.1 Current pancreatitis diagnoses

Pancreatic disorders are challenging to diagnose due to pancreas inaccessibility. There are two steps to diagnosing pancreatitis. The first step involves a physical examination by a general medical practitioner, which is then followed by a laboratory-based pathology test [119]. Diagnosis is then made based on measures of body temperature, mean blood pressure, respiratory rate, arterial pH, serum sodium and potassium levels, serum glucose and creatinine levels, blood urea nitrogen and blood amylase tests [120].

Diagnosis of acute pancreatitis does not have a specific biochemical test that can be considered a "gold standard" [121]. Pancreatic auto-digestion from the release of pancreatic enzymes during acute inflammation releases lipases, phospholipase A_2, trypsinogen and amylases into the body's circulating serum. As such, serum amylases, lipase, trypsinogen and stool chymotrypsin have all been mooted as tests for acute pancreatitis [122, 123]. Table 1.2 shows the pancreatic enzyme reference range in sera for these analytes in diagnosing acute pancreatitis. Amylase and lipases are active enzymes, whereas trypsinogen is the pro-enzyme of trypsin, which also gets released into the bloodstream as a result of pancreatic inflammation.

Acute pancreatitis patients have amylase levels that are typically 5 to 10 times higher than average. Amylase has the highest clinical advantage in identifying acute pancreatitis due to its sensitivity, availability (easy to collect) and technical simplicity. However, current commercially available tests for amylase in sera have low specificity compared to lipase

tests [124]. This is the most considerable disadvantage for amylase assays. Urine amylase tests have a higher specificity than serum amylase tests. However, these tests are usually immunological lateral flow assays, and as such, they are not usually quantitative [125]. Urine trypsinogen levels have been studied as an early predictor of acute pancreatitis [126]. Here, urine trypsinogen concentration was measured using a radioimmunoassay. This assay had a trypsinogen cut-off concentration of 2 nmol/L optimal cut-off points with 80% of sensitivity and 90% of specificity. Unfortunately, radio-immunoassays are not conducive to point-of-care diagnostics.

There are other clinical tests for pancreatitis involving the use of computed tomography (CT), magnetic resonance imaging (MRI), ultrasound and enzyme-linked immunosorbent assays (ELISAs) of pancreatic lipase levels in blood samples. Nevertheless, these tests are not conducive to rapid point-of-care diagnoses [122]. Remote areas have small medical centres rather than fully equipped hospitals; therefore, patients do not receive a proper diagnosis in the early stage of pancreatitis. As a result, this delay in diagnosis provides pancreatic inflammatory factors time to damage the pancreas and other organs. There is a need for a rapid, highly specific point-of-care quantitative diagnostic sensor for acute pancreatitis. In this regard, lipases and phospholipases could be ideal analytical targets.

	Normal	**Enzyme activity where Pancreatitis suspected**
Amylase levels	20 – 300 U/L (some lab results up to 140U/L)	> 300 U/L [127]
Lipase levels	0 – 180 U/L [100]	> 200 U/L [128]
Trypsinogen	10 – 57 ng/ mL	Not reported [123, 129]

Table 1.2: Pancreatitis enzymes amylase, lipase and trypsinogen reference levels and pancreatitis suspect levels in serum.

1.5 Inflammatory bowel diseases (IBDs)

Inflammatory bowel diseases (IBDs) are a group of chronic bowel conditions that includes *ulcerative colitis* and *Crohn's disease* [130]. Crohn's disease can occur anywhere in the gastrointestinal tract and is an inflammatory disorder that presents with symptoms such as abdominal pain, weight loss, diarrhoea, nausea, tiredness, constipation, and delayed or impaired growth in children [131, 132]. Ulcerative colitis, on the other hand, is confined to the surface of the bowel regions [133]. The underlying causes of these IBDs are thought to be a combination of immunological, genetic and environmental factors, although the exact causes of IBDs are still unknown [134-137]. IBDs could also be due to bacterial or virus proteins, which can destroy the immune defence mechanisms [138].

1.5.1 Inflammatory bowel diseases diagnoses

IBDs are typically incurable, and treatment involves managing the inflammatory response with chemotherapies. Treatments include antibiotics to control and kill pathogens; corticosteroids to relieve inflammation; mesalamine, an anti-inflammatory agent; and immunosuppressant drugs [139]. IBD and irritable bowel syndrome (IBS) have similar symptoms. To diagnose IBD, patients have to do blood tests, stool tests, and endoscopies which include upper gastrointestinal endoscopy, colonoscopy and sigmoidoscopy, as also bowel imaging, scans and biopsies [140, 141].

However, attempts have been made to diagnose IBD conditions by the levels of phospholipase A_2 (PLA_2) enzyme in serum and stool samples [142]. In the gut, it is thought that bacterial ecto-phospholipase A_2 attacks the mucus lipids, facilitating the bacterial invasion of the gut epithelium, leading to inflammation and the phospholipase A_2 level increase in blood and stool in IBD patients [143]. There are a few acute-phase protein and fecal markers, novel genetic markers and several antibodies for detecting IBDs.

Previous research has been conducted to find the sub-group of the phospholipase A_2 isoforms that might cause inflammatory bowel diseases, and these studies have shown the Phospholipase A_2 group II (PLA_2-GII) is increased in UC and Crohn’s disease patients

[144-147]. This subgroup of PLA_2 is bactericidal [78, 148] and can inhibit bacterial activity during inflammation [149]. Conversely, research has shown that certain bacteria are able to secrete PLA_2 [150].

Fecal markers for IBD patients are a very common approach to the detection of the disease, as stool samples are easily accessible. Markers of IBDs include *fecal calprotectin*, *elastase*, *lysozyme*, *lactoferrin* and *myeloperoxidase* [151-154]. Calprotectin, especially, is a very sensitive marker to identify any inflammation in the gastrointestinal tract. Also, it helps to differentiate IBD from *irritable bowel syndrome* (IBS). During inflammation, neutrophils, monocytes and macrophages are increased in the blood, and they release calprotectin. This 36 kDa protein plays a major role in inducing cell adhesion, receptor expression and innate immune responses, as well as phagocytosis of neutrophils [155]. There are commercially available fecal calprotectin enzyme-linked immunosorbent assays (ELISAs) [156], and these will be used to compare to the sensor developed in this project.

Ideal makers for any disease should have a few qualities, such as being specific to the disease, being able to measure disease activity and being able to monitor the effect of treatments. The ideal maker for IBDs would be a rapid test that helps patients as well as gastroenterologists or surgeons who treat IBD patients. Therefore, there is a need for detection or gold started for IBD diagnosis, and this project will attempt to create a sensor that can detect the PLA_2 activity in the IBD patient's stool samples.

1.6 Tethered bilayer lipid membranes (tBLMs)

Bilayer lipid membrane models can be free-standing bilayer membranes, solid-supported membranes or tethered bilayer lipid membranes. When used with electrical impedance spectroscopy, these membrane models are useful in investigating how small molecules and proteins interact with lipid membranes, Figure 1.6.

Another bilayer lipid membrane model is known as *black lipid membrane*s (BLM). This is a free-standing bilayer membrane, Figure 1.6A, that is formed across a small cavity (100 μm diameter) in a nonconducting Teflon layer [157]. BLMs are typically created using lipids that are dissolved in an organic solvent which are 'painted' on the electrode to create the membranes. This model can be useful to measure the potential across the membrane, which is then a measure for ions transport through ion channels embedded in the BLM [158].

Figure 1.6B shows supported lipid membranes (SLMs) [159]. These membranes are typically separated from their substrate by a thin aqueous layer of ~1 nm thickness. The solid support should be a hydrophilic substrate such as silicon oxide, glass or gold. The bilayer can be formed using a Langmuir-Blodgett film, with the bilayer leaflets being transferred onto the solid substrate using Schaefer dipping [160]. Alternatively, vesicle fusion is used [161]. A problem with this model is that molecules and ions are not always able to interact with the membrane due to its close proximity to the substrate. A solution to this problem is to use tethered bilayer lipid membranes (tBLMs) architectures, Figure 1.6C.

Hydrogel-Tethered tBLMs: A hydrogel layer is used as an intermediate tether between the solid substrate and the lipid bilayer to provide mechanical support. This improves the membrane's stability and compatibility with delicate membrane proteins; however, hydrogel properties may affect membrane behavior [162].

tBLMs usually have higher stability than other models because they are chemically anchored to the solid substrate [163]. Gold is commonly used as a substrate to which coordinated tethering molecules, usually via thiol groups, terminate in a hydrophobic moiety to which the fatty acid chains of lipids can self-assemble around to form an

anchored lipid bilayer. This architecture provides an ionic reservoir region between the substrate and the membrane. [164]. This hydrophilic space helps to minimise the interaction of the lipid bilayer with the substrate.

Because of their stability and rapid self-assembly, this work will utilise *sparsely tethered* tBLMs to characterise and detect the changes in membrane morphology as a result of lipase and phospholipase enzyme activity.

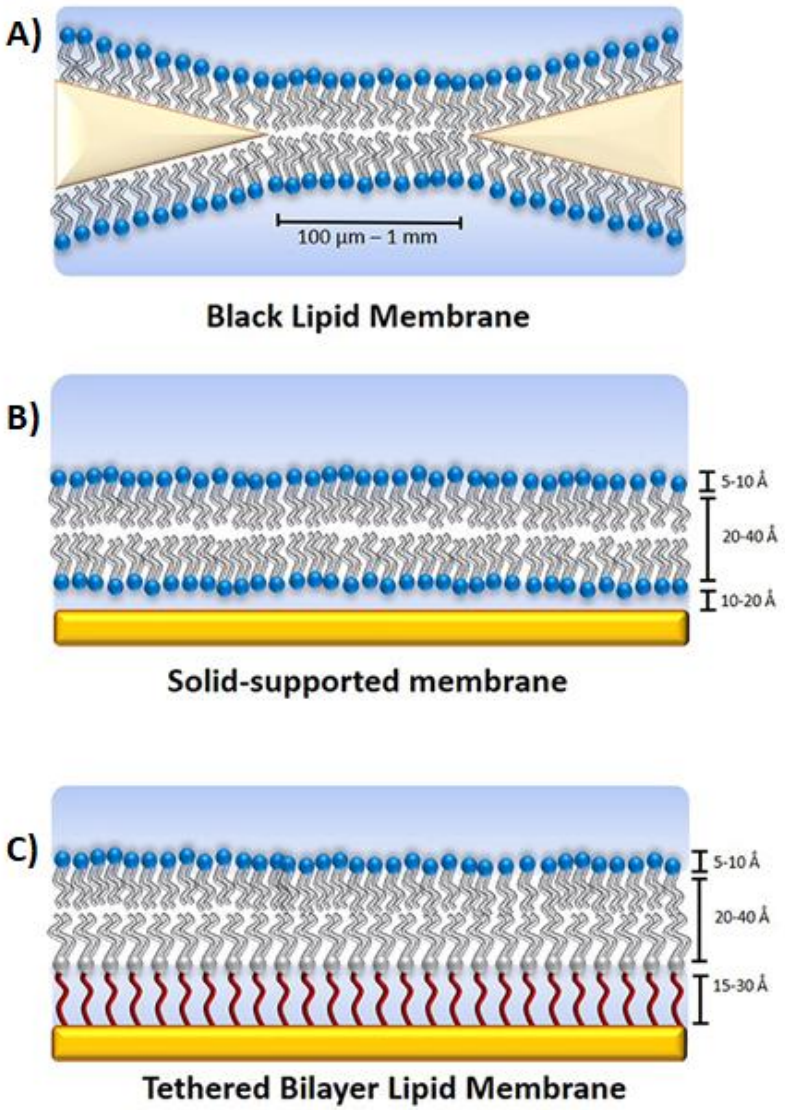

Figure 1.6: The various lipid bilayer membrane model structures. A) The black lipid membrane (BLM) model or free-standing lipid bilayer model, B) the solid support lipid membrane model (SLM) and C) tethered bilayer lipid membrane (tBLM) model. This image is reproduced, with permission, from [165].

1.6.1 Membrane packing

Phospholipids have a hydrophilic head group and hydrophobic tail region. Their tails can also be defined by whether they have a cis-double bond (unsaturated lipid) or are without a cis-double bond (saturated lipid). The number of carbons in the tail or the length and saturation is essential for how the molecules are able to pack against each other [166]. The amphipathic nature of the lipid and the shape can cause spontaneous bilayer formation in an aqueous environment. This spontaneous arrangement can mostly be seen in lipids that take on a cylindrical shape (Figure 1.7B). The most favourable arrangement of conical or wedge-shaped lipids is micelles, Figure 1.7A.

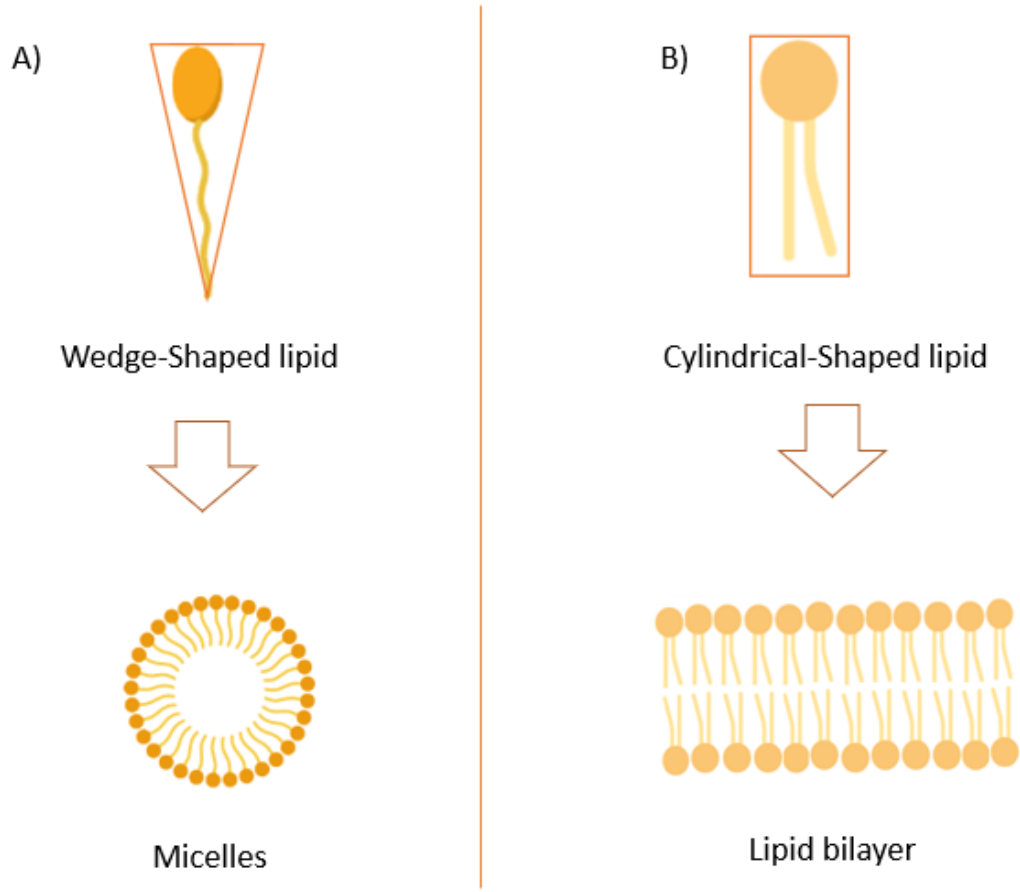

Figure 1.7: The lipid molecules tend to form either micelles or bilayers spontaneously based on the structures in the aqueous phases. (A) The wedge-shaped lipids form micelles, and (B) the cylindrical-shaped lipids form a bilayer.

The *critical packing parameter* (CPP) can be used to determine amphiphilic molecules' self-assembly behaviour [167, 168]. The critical packing parameter can be calculated using the equation of $CPP = \frac{V}{a_0 l}$. In the equation, *V* is the lipid volume, l is the length of the lipid hydrophobic tail(s), and a_0 is the interfacial area occupied by the hydrophilic head group or optimal head group area.

If the surfactants or lipids have a large area in the head group region and a comparatively short tail region, they are cone-shaped and the CPP has a value of ~1/3. A CPP value of less than one would typically lead to lipids to self-assemble into micelles. [169].

The self-assembly of a bilayer or vesicle can form by the lipids with a hydrophilic head group connected to two hydrophobic chains. The CPP value for these types of molecules is ~1. These molecules are more cylindrical in shape and lipids tend to self-assemble into bilayers. On the other hand, when CPP is greater than 1, the surfactant molecules have large tails and small head groups and tend to form inverted micelles [170].

It is suggested that changes in the *overall* membrane morphology, or the *weighted critical packing parameter* (wCPP), can change spontaneous pore diameter in the membranes, which can lead to a change in the membrane conduction as measured using electrical impedance spectroscopy [171-173].

One of the main aims of this research study is to create a new membrane architecture using triglyceride, triolein, to create the tBLMs. It is hoped that by a mixture of fatty acids into triolein, the weighted membrane morphology (wCPP) will change such that lipid packing (area per lipid) will be increased, providing better access to lipases and thus increasing overall hydrolysation.

1.6.2 Electrical Impedance Spectroscopy (EIS).

Most tBLM research uses electrical impedance spectroscopy (EIS) to measure electrical impedance complexes of samples in the AC range. Applying a voltage signal to the sample and measuring the current response as a frequency function to characterise the mimic membranes' structure and functions. The impedance data is represented using polar coordinates, including the impedance magnitude, the absolute value of the impedance, and the phase. To evaluate the impedance spectra, an equivalent circuit model is required, which consists of resistors and capacitors representing the dominant electrical components of the system. The standard equivalent circuit for supporting lipid bilayer membranes includes a series resistor for electrolyte resistance and two RC elements representing the membrane and interfacial properties of the supporting electrode.

While EIS is a valuable technique, it does have some limitations, such as the need for an equivalent circuit model to analyse the impedance data. The choice of the model can affect the accuracy of the derived parameters, and the large number of independent variables associated with complex models can make analysis challenging. Additionally, the accuracy of the derived values of membrane resistance, R_m,, and membrane capacitance,C_m, and other quantities depends on the quality of the data fitting procedure. The relative error can increase close to the lower detection limit of the measurements. However, it generally remains below 15% [174].

EIS can be used for various applications, including developing biosensors [175]. Monitoring changes in the impedance spectrum can provide details about membrane stability, membrane-analyte interactions, permeability, and the effects of various environmental factors.

Mathis T.S. et al. 2019 used the EIS technique to characterise energy storage devices like batteries and supercapacitors [176]. Overall this study shows that EIS can be used to diagnose performance issues and understand degradation mechanisms in energy storage systems.

Furthermore, corrosion studies use EIS to examine corrosion processes, measure polarisation resistance, and assess the protective properties of coatings or inhibitors.

Montemor, M. F. (2007) explains how EIS can provide information about the kinetics of corrosion reactions and the mechanisms of passivation and pitting [177, 178]. The EIS technique's ability to provide insights into complex electrochemical systems makes it a valuable tool for both fundamental research and practical application.

1.7 Aims of this research project

Hypothesis,

That tethered bilayer lipid membranes (tBLM) lipase and phospholipase sensor arrays can be used as a rapid and effective clinical diagnostic of pancreatitis and inflammatory bowel diseases and for lipase detection during lipase production.

Aims,

1. To test the ability of phospholipid tBLMs to act as sensors for phospholipase-A_2 activity in human stool samples as a sensor for inflammatory bowel diseases (IBDs).
2. To identify new tBLM architectures made of triglycerides.
3. To test the ability of these triglyceride tBLMs to act as sensors for pancreatic lipase enzymes dissolved in the blood, potentially as a sensor for acute pancreatitis.
4. To test the ability of triglyceride tBLMs to act as sensors for lipase enzymes produced in bioreactors.

1.7.1 Aim 1

The first aim will be to test the ability of tBLMs to act as sensors for phospholipase-A_2 activity in human stool samples as a sensor for inflammatory bowel diseases (IBDs). The results of this research are detailed in Chapter 2. This part of the project will demonstrate that PLA_2 sensing can be done using stored frozen stool samples provided by collaborators. With that validation, there are a few main things this study hopes to identify:

- Any non-specific actions from frozen stool samples
- The ideal amount of stool sample required in order to be able to test for PLA_2 activity.
- If there is any endogenous PLA or lipase activity from samples.
- If there is any PLA_2 activity in stool samples on negative control tBLMs, such as diether-DOPC tBLMs, or if there is any activity in the absence of Ca^{2+}.
- The range of possible PLA_2 activities in differing stool samples to get baseline responses.
- If there is any activity on triglyceride tBLMs from stool samples.
- Whether PLA_2 activity from stool samples from IBD patients is greater than from healthy population control samples.

1.7.2 Aim 2

The second aim is to identify new tBLM array architectures made of a triglyceride called *triolein* using a long-established solvent exchange technique [179, 180]. The results of this research are detailed in Chapter 3. Electrical impedance spectroscopy is used as a technique to characterise these triolein tBLM architectures. The triolein tBLM morphological structure is explored further in Chapter 4 using neutron reflectometry.

1.7.3 Aim 3

The third aim will be to identify the ability of triolein tBLMs to act as sensors for pancreatic lipase enzymes dissolved in the blood, potentially as a sensor for acute pancreatitis. To create a protocol, porcine pancreatic lipase (PPL) in buffer samples were tested on the triglyceride or triglyceride-containing tBLMs. The sensor was then tested using PPL spiked whole blood or serum. The results of this research are detailed in Chapter 3.

1.7.4 Aim 4

The final aim is to test the ability of triglyceride tBLMs to act as sensors for lipase enzymes produced in bioreactors. This would be an *in-line* enzymatic activity sensor that can detect lipase activity during its production. This part of the study was to create and develop a method to have continuous media flow using a perfusion pump. The results of this research are detailed in Chapter 3. An attempt to improve the triolein tBLM sensitivity was also explored by changing the membrane morphology using oleic acids and different lyso-PC lipids.

2 Detecting PLA_2 in inflammatory bowel disease patients' fecal samples

2.1 Introduction

In this chapter, the effectiveness of the tBLM array impedance sensor to identify the inflammation events from human faeces in order to diagnose IBDs is examined. The marker being identified in faeces is phospholipase A_2 (PLA_2). It is thought that gut bacteria release phospholipase A_2 and this enzyme attacks mucus lipids, removing a natural defence mechanism and facilitating the bacterial invasion of the gut epithelium, leading to inflammation [143]. Therefore, a tBLM sensor capable of quantifying PLA_2 activity in stool samples, by directly measuring membrane destabilisation as a result of lipid hydolysation, could be used as a rapid early diagnostic for IBD conditions. This work builds on a previous study that demonstrated how a tBLM array can identify PLA_2 activity from ant toxins [181].

The gastrointestinal tract can be damaged, which could lead to increased permeability of the mucosa to bowel bacteria and microorganisms are able to trigger an inflammatory response [182, 183]. A protein called calprotectin is then released from the activated neutrophils [184]. This is 36 kDa size and calcium-binding protein [185], which can increase the resistance against inflammation after binding to calcium ions [186]. Calprotectin is an established protein biomarker for inflammatory bowel disease [187], and it is more prominent in Crohn's disease fecal samples than in ulcerative colitis samples [188].

The main aim of this part of the study is to create a protocol to detect phospholipase A_2 activity in human stool samples and then test the ability of the PLA_2 sensor using fecal samples from individuals with and without IBD. Furthermore, this work will compare the PLA_2 sensor with commercially available PLA_2 and fecal calprotectin protein ELISA kits.

2.2 Materials and Methods

2.2.1 Buffers

Analytical graded chemicals have been used in this research project to perform all the experiments. These include pure ethanol (100%), sodium chloride (NaCl), calcium chloride ($CaCl_2$), trisaminomethane (tris), and Ethylenediaminetetraacetic acid (EDTA). All these chemicals were purchased from Sigma-Aldrich Australia. All tethered bilayer lipid membranes (tBLMs) were prepared using 100 mM NaCl and 10 mM tris at pH 7. This buffer is hereafter referred to as *tris buffer*. Calcium ions are known to increase PLA_2 activity. For this reason, an alternative version of the tris buffer containing 1 mM $CaCl_2$ buffer at pH 7 was also used. This buffer is hereafter referred to as the *Ca^{2+} buffer*. An equivalent calcium-free buffer is used as a negative control. Here, the $CaCl_2$ is replaced by 10 mM EDTA, hereafter referred to as *EDTA buffer*.

2.2.2 Phospholipids

1,2-dioleoyl-sn-glycerol-3-phosphocholine (DOPC) lipid powder, and 1-O-hexadecanyl-2-O-(9Z-octadecenyl)-sn-glycero-3-phosphocholine (diether-PC) lipid powder were the lipids used to create the tBLM arrays. All these lipids were purchased from the Avanti polar lipids.Inc, United States. All the powdered lipids are used at a 3 mM concentration dissolved in pure ethanol. All the phospholipids' chemical structures are shown in Figure 2.1 below.

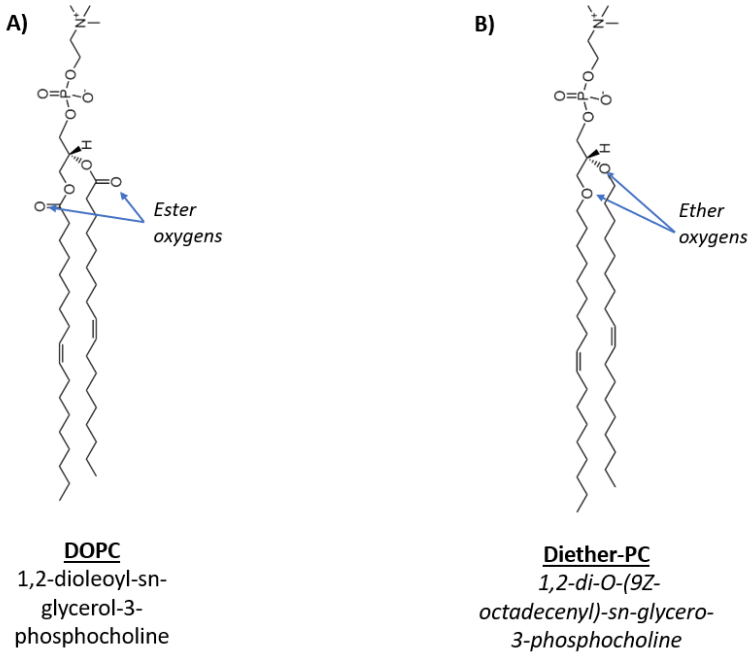

Figure 2.1: Phospholipids used in the tBLM array include A) DOPC, and B) diether-PC. All of these lipids have 18 carbons in their fatty acid tails.

2.2.3 Stool samples

In order to develop a protocol to identify any PLA_2 activity in stool samples, frozen human stool samples were kindly donated by Dr Catherine Burke, University of Technology Sydney. These experiments were approved by the UTS Human Research Ethics Committee, Ref 2015000438 [189]. For comparing PLA_2 activity in stool samples from IBD patients compared to healthy controls, samples from 29 IBD (Ulcerative colitis and Chrohn's disease) patients and 11 samples from healthy volunteers (referred to hereafter as *population control* samples) were received from Prof Georgina Hold of the Microbiome Research Centre, St George and Sutherland Clinical School, University of New South Wales, Sydney. Ethics for the use of these samples is included in the 2019/ETH11443: *Defining the Australian Inflammatory Bowel Disease Microbiome* – The AIM Study. Samples were de-identified, and all experiments were done in a double-blind fashion.

All the samples were stored at -80 °C before the series of experiments started. Solid samples were thawed at room temperature and separated into 100 mg aliquots in small sample containers. To prepare the stock stool solution, each sample was mixed with tris buffer at 100 mg/mL concentration. Using this stock solution, 1 mg/mL and 10 mg/mL concentrations were prepared, as needed, and then stored at -20 °C for further use if required.

The 1mg/mL concentration was used in this study to create the protocol and showed a reliable response. Primarily, this concentration was chosen to ensure that the analyte or targeted enzymatic activity in the stool sample is sufficient to be accurately detected and measured to improve the detection sensitivity. Secondly, experimental standardisation was considered, selecting the 1 mg/mL concentration and less unwanted material in the stool. Furthermore, the enzymatic activity is not dependent on stool sample mass.

2.2.4 Tethered bilayer lipid membrane arrays (tBLMs)

Tethered bilayer lipid membrane arrays (tBLMs) are a specialised type of lipid membrane structure used in various scientific and technological applications. These membranes are constructed by tethering lipid bilayers onto solid supports or substrates, creating a stable and well-defined membrane system.

Lipid bilayers are the basic structure of a tBLM consisting of two lipid bilayers arranged in a back-to-back configuration. Each bilayer comprises amphiphilic lipid molecules with hydrophilic heads and hydrophobic tails. The bilayers provide a barrier between two fluid compartments, mimicking the lipid membranes found in living cells.

The solid substrate is free-standing, and tBLMs are anchored or tethered onto the substrate. This support can be a variety of materials, such as glass, silicon, or gold. The choice of substrate depends on the specific application and experimental requirements.

The tethering molecules are specific and attach the lipid bilayers to the solid support. These molecules typically possess a hydrophobic portion that integrates into the lipid bilayer and a hydrophilic portion that interacts with the solid support. Common tethering molecules include thiolipids for gold surfaces and silane derivatives for silicon-based substrates. The tethering of the lipid bilayers enhances the stability and longevity of the

tBLMs.This prevents the lipid bilayers' detachment or disruption during experiments or when subjected to external stimuli, such as electric fields or mechanical forces.

The tBLMs can be formed in an array configuration, where multiple bilayers are patterned onto a single substrate. This arrangement allows for parallel experiments, high-throughput screening, and simultaneous investigation of multiple samples. There are various applications for tBLMs, particularly in biological and biophysical studies. They are used to study membrane proteins, ion channels, and receptors, providing a controlled and well-defined environment to mimic cellular processes. Additionally, tBLMs are employed in biosensing, drug screening, and membrane-based technologies.

In this study, the tBLMs were prepared using membrane slides from SDx Tethered Membranes Pty Ltd, a biotechnology company in Roseville, Sydney, Australia. These slides contained a gold electrode coated with 10% tethering molecules of hydroxyterminated-bis-tetra-ethyleneglycol and 90% spacer molecules of tethered phytanyl bis-tetra-ethyleneglycol (Figure 2.2). The benzyl disulphide chemically links to the gold substrate and is more stable to oxidisation. The spacer molecules and tether molecules create a reservoir region for ions between the bilayer membrane and the gold electrode.

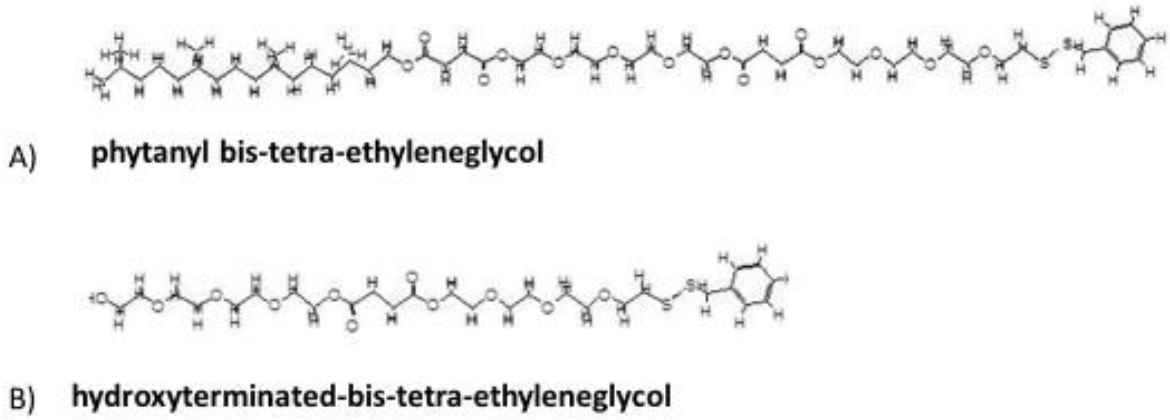

Figure 2.2: The chemistries coated on the gold electrodes A) phytanyl bis-tetra-ethyleneglycol as the membrane ‘tethers’ and B) hydroxyterminated-bis-tetra-ethyleneglycol ‘spacer molecules.

There are six separate gold electrodes on each slide to which a cartridge is attached which has six separate perfusion wells. To the anchoring chemistries, a second layer of the mobile phase lipids in ethanol is added. 8 µL of these desired lipids were added to each well and left to incubate for exactly 2 minutes. Following this, each membrane was washed with 3 x 400 µL tris buffer to enable the lipids to self-assemble into a bilayer [190, 191]. The structure of the DOPC tethered bilayer lipid membrane on the gold electrode is shown in Figure 2.3A. This illustration shows the two separate layers. The second layer contains 100% of phospholipids (DOPC or the diether-PC), which is anchored to the electrode by the first layer containing 10% tethering molecules and 90% of spacer molecules. The DOPC tBLM was used as the *sensor substrate* that is susceptible to PLA_2 hydrolysation, while diether-PC tBLMs, which lack any ester moiety, were used as the negative control substrate [181].

SDx tethaQuick^{tm} software was used in conjunction with a tethaPod^{tm} electrical impedance spectrometer to monitor electrical impedance signals across the membranes. This software is able to collect the data from six sample chambers simultaneously and calculates the membranes' conductance and capacitance by fitting the data to an equivalent circuit. Frequency sweeps were set to 1 s duration with a peak-to-peak amplitude of 50 mV. Complete frequency sweeps were done in the range of 0.1 to 2000 Hz. Unless otherwise mentioned, all experiments were conducted at pH 7 at room temperature.

Figure 2.3B shows the equivalent circuit that is used to measure the impedance measurements of the membrane's conductance (G_m), resistance (R_m) and capacitance (C_m). The gold tethering region was modelled as a *constant phase element* (CPE) which reflects the imperfect capacitance of the reservoir region due to the presence of the first layer chemistries [192-194]. The electrolyte resistance is shown as R_e in the circuit.

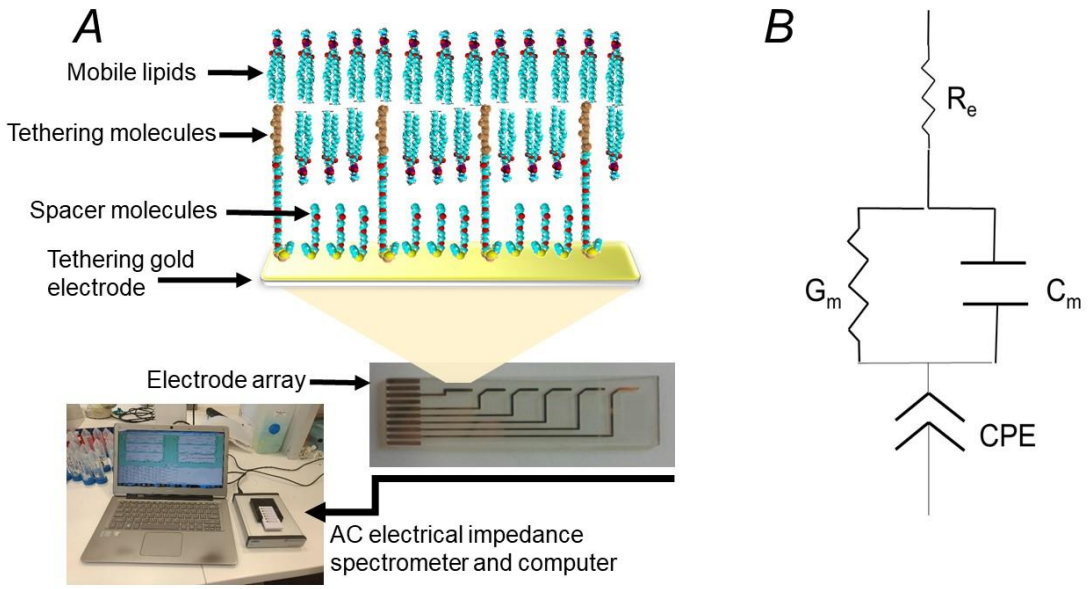

Figure 2.3: A) DOPC tethered bilayer lipid membrane (tBLM) architecture. Spacer and tethering molecules are bound to a gold electrode. Electrical Impedance Spectroscopy (EIS) was then used to determine the actions of lipase enzymes on this model lipid membrane. B) The equivalent circuit is used to fit impedance measures. R_e is the resistance of the bulk electrolyte solution, G_m is the conductance of the lipid membrane, C_m is the capacitance of the lipid membrane, and the CPE (constant phase element) represents the imperfect capacitance of the gold electrode-tether molecule region.

2.2.5 PLA_2 enzyme-linked immunosorbent assay (ELISA)

PLA_2 content of the fecal samples was tested using a commercially available phospholipase A_2 enzyme-linked immunosorbent assay (ELISA). A human PLA2G2A ELISA (product code: EH369RB) was purchased from ThermoFisher Scientific, Australia. This ELISA kit can quantitate the sub-group II human PLA_2 enzymes. This subgroup is used as one of the major markers used in IBD research [195]. The following components were provided with the ELISA kit, the human PLA2G2A antibody-coated 96-well plate, human PLA2G2A biotin conjugate, human secreted PLA2G2A standard, wash buffer, assay diluent, streptavidin-HRP (HRP = horse radish peroxidase), 3,3’,5,5’-Tetramethylbenzidine or TMB ((3,3',5,5'-Tetramethylbenzidine) solution and stop solution.

The frozen 100 mg/mL of stock stool samples were thawed to room temperature, and then the 200 µL of stock samples were transferred into 500 mL of centrifuge tubes for centrifugation. The main purpose of this is to remove any fibres and other extraneous matter from the solution. These samples were centrifuged at 1000 rpm for 15 mins, and the supernatant was then collected. To use in the PLA2G2A ELISA kit, the sample above was diluted 1:100 with the provided assay diluent to prepare the samples.

PLA_2 ELISAs were performed as per protocols provided by the manufacturer (see Appendix A). This involved the creation of a standard curve for the PLA_2 enzyme within the range of 32.7 to 8000 pg/mL. PLA_2 content of each stool sample was measured in duplicate. Measures of the PLA_2 ELISA's absorbance data were read at 450 nm using a Tecan infinite m1000 plate reader.

2.2.6 Calprotectin protein ELISA

The two different calprotectin ELISA kits were tested with the stool samples. The first calprotectin ELISA, EH62RB, was purchased from ThermoFisher Scientific, Australia. This ELISA kit can detect the L1/S100-A8/A9 complex in serum, plasma and supernatant. This ELISA kit is referred to here as the *TheroFisher calprotectin ELISA kit*. The second calprotectin ELISA kit was purchased from Calpro As, Norway. This kit will be referred to as the *CALP0170 ELISA kit*.

2.2.6.1 Thermo-Fisher calprotectin ELISA

This kit contained a human calprotectin L1 antibody-coated 96-well plate, human calprotectin L1 biotin conjugate, human calprotectin L1 standards, wash buffer, assay diluent, TMB substrate, stop solution and adhesive plate covers. The centrifuged stool samples were diluted in assay diluent at 1 in 100 dilutions. This assay has a 32 to 8000 pg/mL range of calprotectin detection. Calprotectin ELISAs were performed as per protocols provided by the manufacturer (see Appendix B). The calprotectin content of each stool sample was measured in duplicate. Measures of the ELISA absorbance data were collected using a Tecan infinite m1000 plate reader at 450 nm.

2.2.6.2 CALP0170 ELISA

This ELISA kit contains affinity-purified monoclonal mouse antibodies specific to calprotectin. The kit contains coated 96 well plates, sample dilution buffer, wash solution, faecal extraction buffer, 6 different calprotectin standards, calprotectin controls (low and high), enzyme conjugate and enzyme-substrate solution (pNPP). The centrifuged stool samples were diluted 1 in 100 in sample dilution buffer, as this is the recommended dilution to give 25 mg/kg to 2500 mg/kg of calprotectin in faeces. These calprotectin ELISAs were also performed as per protocols provided by the manufacturer (see Appendix C). After the incubation, the Tecan infinite m1000 plate reader was read at 405 nm.

2.2.7 Receiver operating characteristic (ROC)

Receiver Operating Characteristic (ROC) is a graphical representation and evaluation widely used in statistics, machine learning, and signal processing to assess the performance of classification models [196]. This data analysis method is beneficial in binary classification tasks, where the outcome can be one of two classes, commonly referred to as positive and negative.

The ROC curve is created by plotting the true positive rate (TPR) against the false positive rate (FPR) at various classification thresholds [197]. The TPR is also known as sensitivity and is the proportion of positive instances correctly classified by the model out of all positive instances. The FPR is the proportion of negative instances incorrectly classified as positive out of all negative instances.

$$FPR = FP / (FP + TN)$$

True negative (TN) is the number of instances correctly classified as negative. False positive (FP) is the number of instances incorrectly classified as positive. False negative (FN) is the number of instances incorrectly classified as negative. True positive (TP) is the number of instances correctly classified as positive.

The ROC curve is generated by plotting the TPR against the FPR as the classification threshold varies from 0 to 1. Each point on the ROC curve represents the trade-off between the model's ability to classify positive instances correctly and its tendency to misclassify negative instances.

A perfect classifier will have a ROC curve that passes through the point (0, 1) with an area under the curve (AUC) of 1.0 [198]. An AUC of 0.5 indicates that the model's performance is similar to random guessing, while an AUC greater than 0.5 indicates that the model performs better than random.

In summary, the ROC curve and AUC provide valuable insights into a binary classification model's overall performance and discriminatory power, allowing researchers and practitioners to select the most appropriate threshold for their specific application.

2.3 Results

2.3.1 Phospholipase A_2 activity in stool samples

Phospholipase A_2 activity was tested in human stool samples to determine if the phospholipase sensor array could test PLA_2 activity on the samples that had been frozen at -80°C. Assays were also done to identify the ideal concentration of the stool samples and any non-specific actions from the stool samples. Phospholipase activity in defrosted stool samples were tested using DOPC membranes in buffer with and without Ca^{2+} ions and on diether-PC tBLMs with Ca^{2+} buffer (Figure 2.4.) Typically, only the DOPC tBLMs with Ca^{2+} buffer showed a membrane conductance increase after the addition of some of the unidentified stool samples, whilst DOPC without Ca^{2+} and diether-PC with Ca^{2+} showed little variation. In these experiments, DOPC without Ca^{2+} and diether-PC are the controls. It was found that a sample as small as 1 mg/mL was able to detect significant enzyme activity. All these initial samples were not centrifuged to remove extraneous matter. This experiment was a validation that the sensor can measure that phospholipase A_2 activity from stool samples that had been frozen for approximately 2 years.

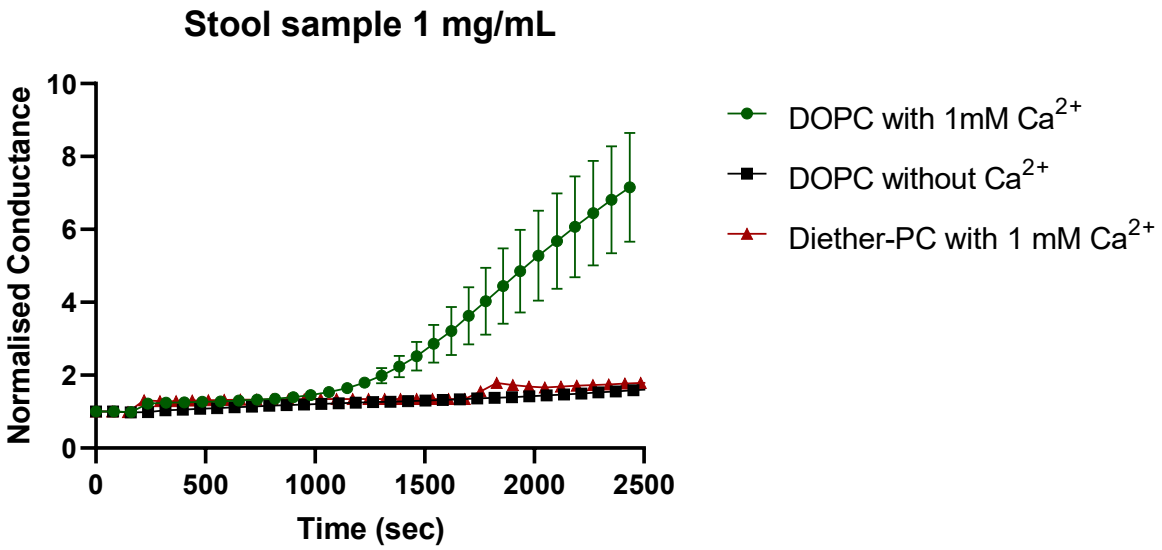

Figure 2.4: Select tBLM array conduction measures using a volunteer stool sample that displayed enzymatic activity at 1mg/mL concentration. Results presented show the sample prepared with Ca^{2+} buffer or with EDTA buffer (without Ca^{2+}) and diether-PC tBLMs with Ca^{2+} buffer.

2.3.2 Sensing phospholipase A_2 from IBD patients

The study was a blind trial to test the IBD sensor to determine how effectively frozen stool samples from patients with and without inflammatory bowel diseases (IBDs) can be tested for their phospholipase A_2 activity using the tethered bilayer lipid membrane (tBLM) sensor array. For this blind trial, 10 samples were identified being from healthy or 'population control' donors, 17 from patients diagnosed with ulcerative colitis and 12 from those diagnosed with Crohn's disease.

Depending on the patient's inflammation and the spread, IBD data can be separated into low, medium and high inflammatory levels based on patient-reported disease activity. Of these, 15 UC samples were recorded from patients with low activity, one with medium and one with high activity. 11 of the Crohn's stool samples were reported from periods of low activity and one from a patient experiencing high flare activity. Figure 2.5 shows the results of percentage conductance changes over 20 min after adding the stool samples

to the tBLMs. All these experiments were conducted at room temperature and the samples were not centrifuged or treated any differently.

DOPC membranes with Ca^{2+} present show the strongest conductance increase in samples from UC and Crohn's disease patients over healthy volunteer control samples (Figure 2.5A). There are relatively lower conductance increases in DOPC tBLMs without Ca^{2+} ions compared to Ca^{2+} ions present in the membranes (Figure 2.5B). Figure 2.5C shows the stool sample effect on the diether-PC membranes. There are barely detectable conductance percentage changes on the diether-PC tBLMs with any stool sample. These experiments indicate that there are minimal non-specific activities from stool samples.

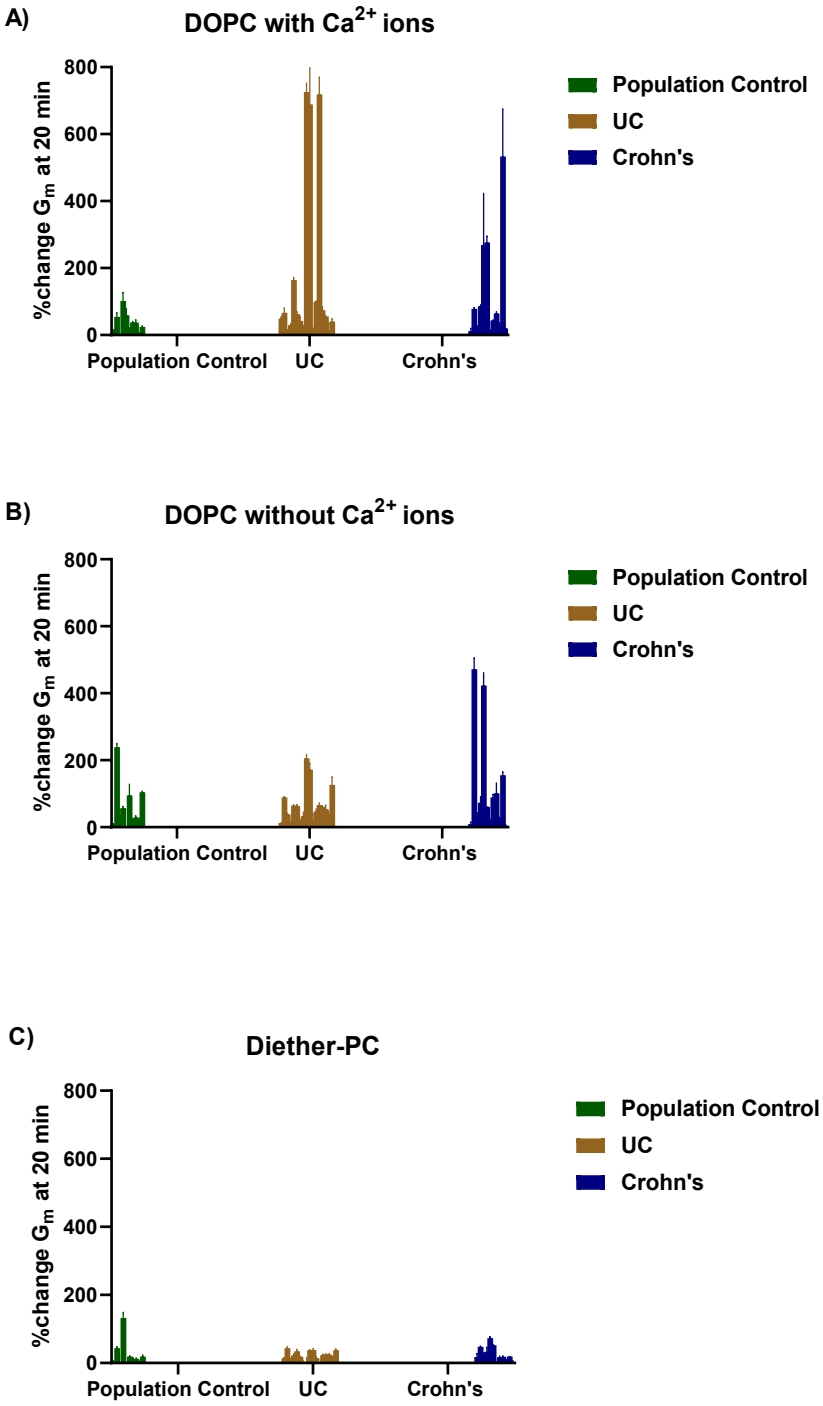

Figure 2.5: IBD and non-IBD stool samples measuring the change in conductance over 20 min. The UC, Crohn's and population control1 mg/mL stool samples were tested on A) DOPC with Ca^{2+} B) DOPC without Ca^{2+} C) diether-PC tBLMs. All the stool sample data represent the mean of n = 2 tBLMs at room temperature.

2.3.3 PLA_2 sensor incubation time optimisation

This part of the study confirms the best time to analyse the stool sample data for the sensor. The conductance changes in DOPC tBLMs with Ca^{2+} ions at 10, 20, 30 and 40 minutes were recorded as shown in Figure 2.6 A, B, C and D. Each UC and Crohn's patient's percentage change values were analysed against the population control values using the GraphPad Prism 8 software.

These data show that membrane conductance plateaus within 30 minutes. After 20 mins the conductance change percentage increased up to 800% compared to the initial starting time and 16 times more than the conductance at 10 mins. Between times 20 to 30 mins, the changes are 1.5 times. When it comes to the point-of-care sensor, less time is more desirable, so the earliest and best suitable time is considered to be 20 minutes after adding the stool samples.

The Wilson and Brown receiver operating characteristic (ROC) method was used to analyse the utility of using tBLMs as a sensor for IBDs [199]. ROC curves are used to show the graphical connection between clinical sensitivity and specificity for diagnostic tests. In these curves, the true positive rate vs false positive rate is used to test a diagnostic's overall ability. The best clinical test or sample should have the highest true positive rate with the lowest false positive rate. The *area under the curve* (AUC) in ROC plots represents the probability that a randomly selected patient will have a higher test result than a randomly selected control.

Figure 2.7 A, B, C and D show the analysed data in the form of receiver operating characteristic (ROC) curves (see 2.3.4 below) at 10, 20, 30, and 40 minutes, respectively. The UC samples' ROC values for the 10, 20, 30 and 40 minutes are 0.67, 0.76, 0.74 and 0.71, respectively. The values for Crohn's disease were 0.68, 0.73, 0.68 and 0.66 at 10, 20, 30 and 40 minutes, respectively. The highest ROC value reported was at 20 minutes in UC and Crohn's disease samples. This further confirms that 20 mins were the best time to test for PLA_2 activity using this sensor.

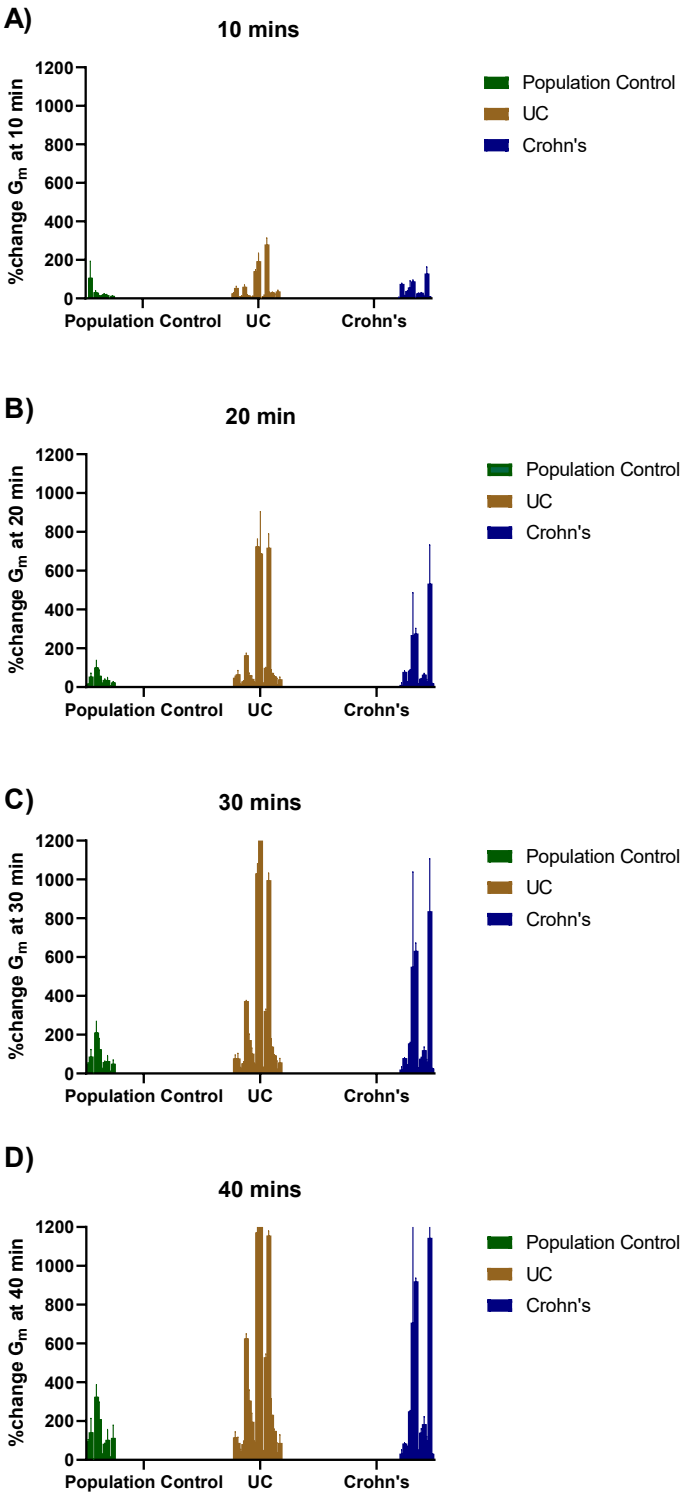

Figure 2.6: Results for IBD and non-IBD stool samples measuring the change in conductance as a percentage change in conductance on the DOPC tBLMs in the presence of Ca^{2+} ions at A) 10 minutes, B) 20 minutes, C) 30 minutes, and D) 40 minutes.

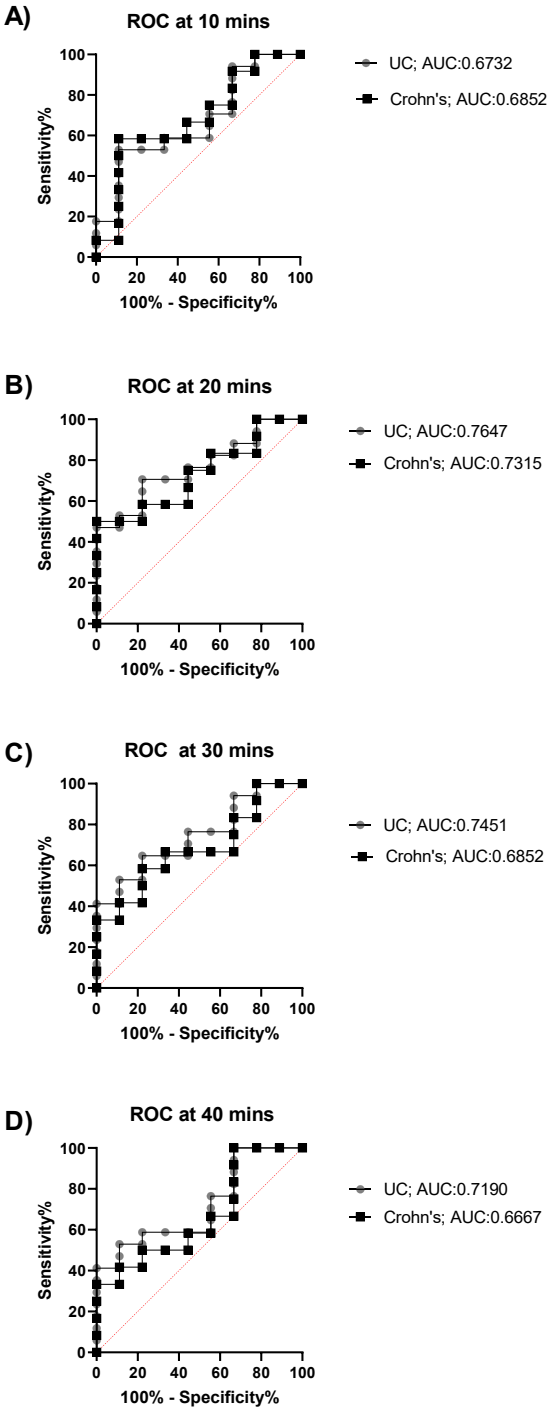

Figure 2.7: The corresponding ROC curves at A) 10 minutes, B) 20 minutes, C) 30 minutes, and D) 40 minutes points. All the stool sample data represent the mean of n = 2 tBLMs at room temperature.

2.3.4 DOPC memebranes with Ca^{2+} ions with Receiver operating characteristic (ROC) curve.

The higher the AUC, the better the reliability of the sensor [200]. An AUC of 0.5 is akin to having a 50:50 chance, so not effective as a diagnostic at all. The enzyme activity data (as measured using a percentage change in conductance over 20 min) from the stool samples of population control volunteers were compared to samples from UC and Crohn's disease patients. The AUC values for DOPC tBLMs in the presence of Ca^{2+} are 0.76 and 0.73 for UC and Crohn's, respectively (Figure 2.8).

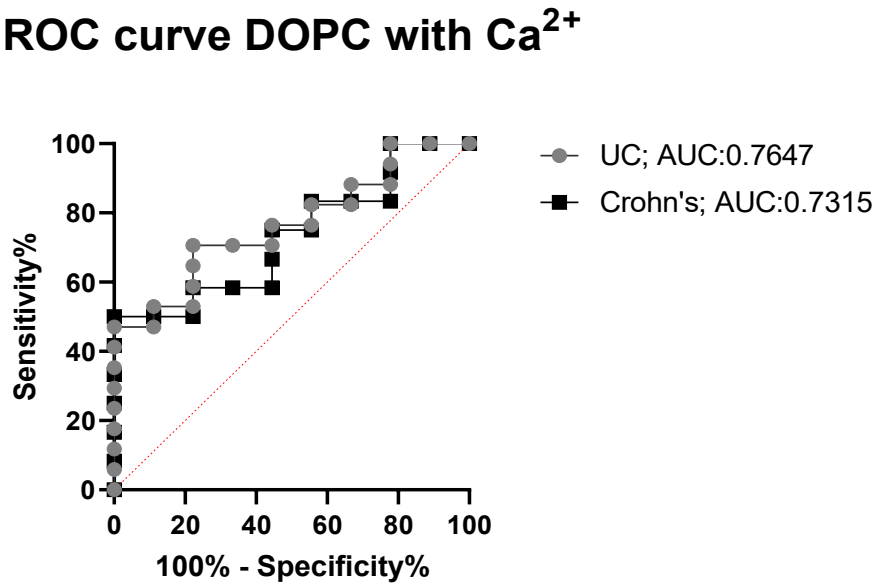

Figure 2.8: Room temperature trial data analysed using the receiver operating characteristic (ROC) for Crohn's and UC samples compared to the healthy or non-IBD stool samples. All the stool sample data represent the mean of n = 2 tBLMs at room temperature.

2.3.5 Temperature dependence

This part of the study was designed to compare the phospholipase A_2 activity and IBD sensor accuracy at normal human body temperature. Stool samples were tested in DOPC tBLMs with Ca^{2+} ions at a healthy human body temperature of 37°C. The tBLMs were prepared at room temperature as described in the method section, then kept at 37°C in incubators before starting the test. All the buffers and 1 mg/mL stool sample solutions were at 37°C before being added to the membranes. These tests with the electrical impedance sensor showed higher starting membrane conductance than room-temperature membrane conductance. This is as expected due to increased membrane fluidity. Figure 2.9 shows the ROC curves of the DOPC membrane for UC and Crohn's disease at 37°C. ROC curve analyses give an AUC of 0.6 for ulcerative colitis and 0.61 for Crohn's disease. This result shows that the sensitivity of the sensor is reduced at 37°C. Overall, room temperature would seem to be the better condition for using this sensor.

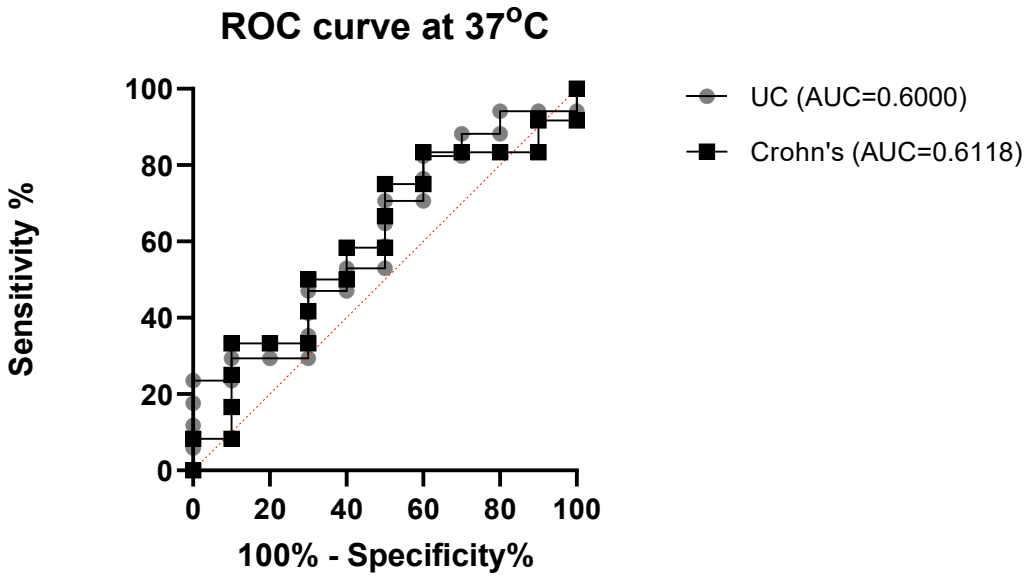

Figure 2.9: Receiver operating characteristic (ROC) curves of DOPC tBLMs with stool samples at 37°C. All the stool sample data represent the mean of n = 2 tBLMs.

2.3.6 Removal of extraneous fecal matter

All the stool sample experiments mentioned above were conducted without the removal of extraneous fecal matter. Therefore, this part of the experiment was designed to compare the difference between centrifuged supernatant and complete fecal matter samples' activity on the DOPC tBLMs with Ca^{2+} ions present.

1 mg/mL of Crohn's (SGH66) and UC (SGH125, and SGH134) samples were centrifuged at 10,000 and 1000 rpm for 15 mins. The supernatant was collected without disturbing the pellet. Figure 2.10 shows the normalised conductance data of three IBD patients' stool samples and suggests that the most rapidly centrifugated samples (10,000 rpm) consistently show reduced enzymatic activity compared to non-centrifuged and slowly centrifuged samples. Therefore, this suggests that 10,000 rpm is not suitable for the IBD samples as this speed is forcing the PLA_2 into the pellet or denaturing the protein.

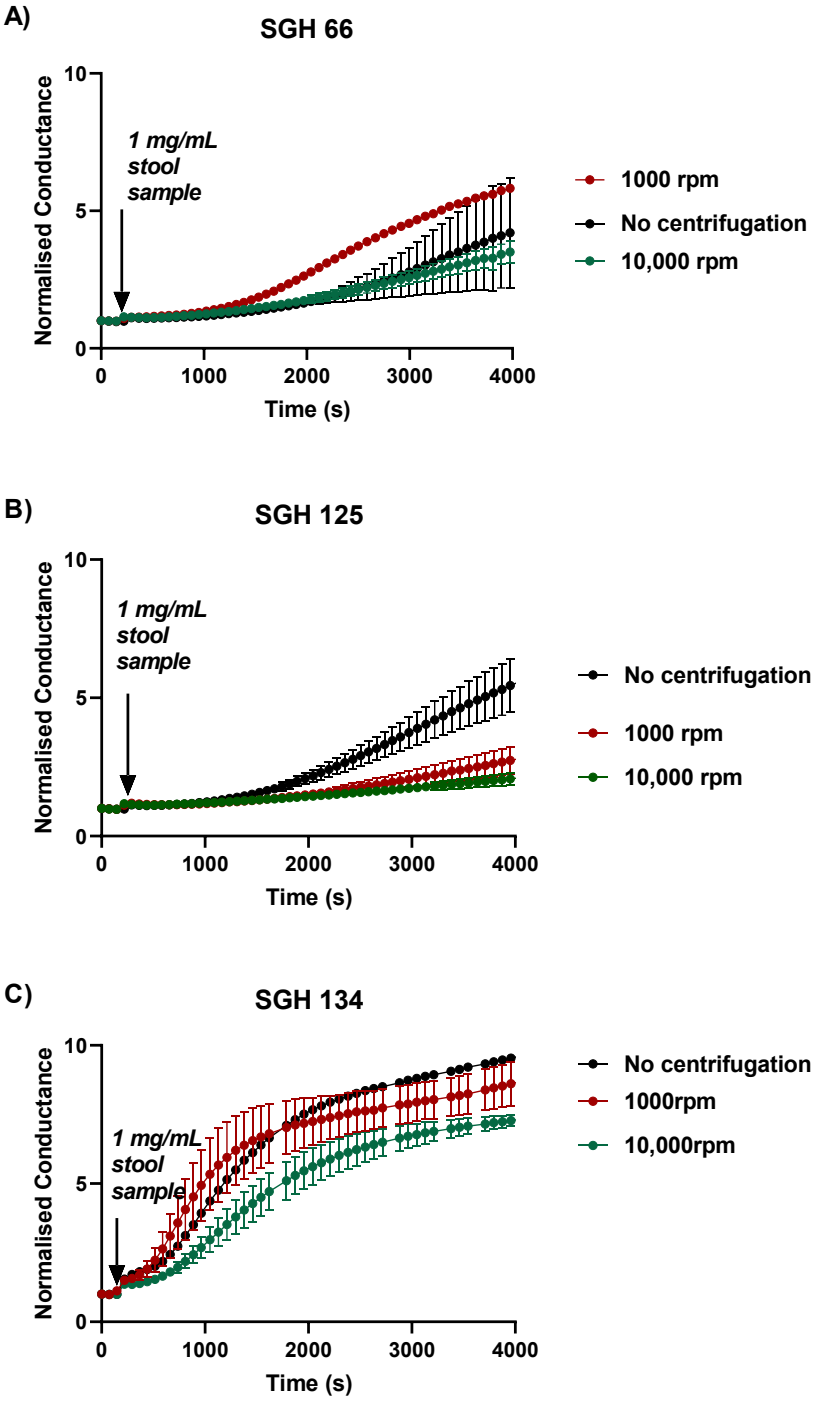

Figure 2.10: Three separate high-activity IBD stool samples of Crohn's A) SGH66, and UC samples of B) SGH125, and C) SGH134 showing PLA_2 activity on the DOPC tBLMs with Ca^{2+} with and without centrifugation at two different speeds. All the stool sample data represent the mean of n = 2 tBLMs at room temperature.

2.3.7 PLA_2 enzyme-linked immunosorbent assay (ELISA)

The PLA_2 concentrations in the 1 mg/mL stool samples are shown in Figure 2.11B. UC and Crohn's stool samples have high PLA_2 concentrations compared to the healthy population control samples. Most of the healthy population samples showed less PLA_2 concentration, except for one outlier sample. Figure 2.11C shows the ROC curves for the human PLA_2 ELISA kit. The area under the curve for Crohn's and UC is 0.66 and 0.59, respectively. This suggests that ELISA is able to detect the presence of PLA_2 in both healthy and IBD samples.

Figure 2.11C shows the linear correlation of PLA_2 *activity* as measured using EIS and *concentration* as measured using an ELISA in the stool samples. The R^2 value shows as 0.00533 and that shows there is no linear correlation between activity and concentration.

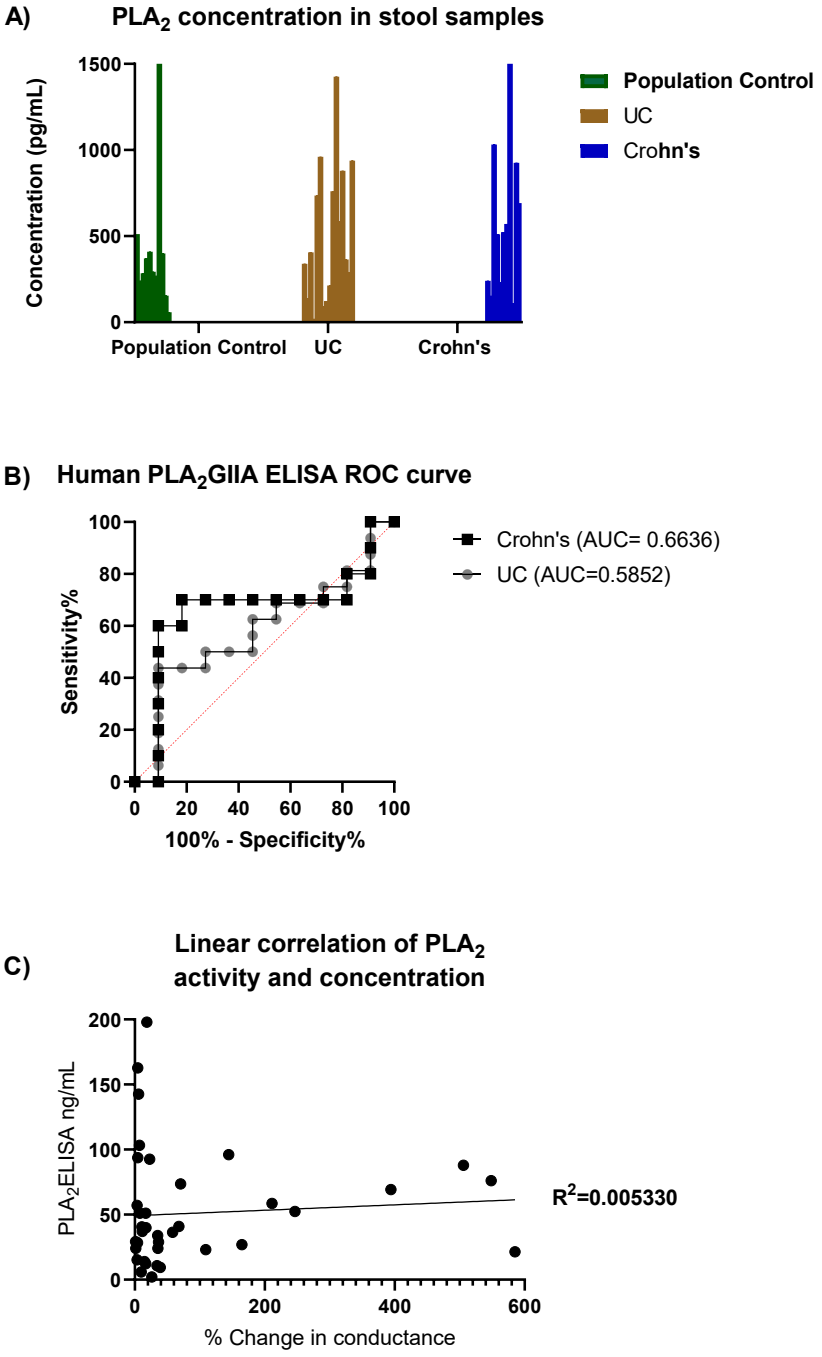

Figure 2.11: The UC, Crohn's and population control 1 mg/mL centrifuged samples were tested using a human PLA_2GIIA enzyme-linked immunosorbent assay (ELISA). A) The PLA_2GIIA concentrations according to the standard curve. B) The ROC curves of the Crohn's and UC samples compared to the population control samples (all 1mg/mL). C) The linear correlation of PLA_2 activity and concentration. All the stool sample data represent the mean of n = 2 at room temperature.

2.3.8 Calprotectin protein ELISA

The 38 stool samples were analysed using two different available calprotectin protein ELISA kits. During both experiments, the plate was read right after adding the stop solution while controlling the minimum exposure to the light. GraphPad Prism 8 software was used to generate the best standard curve and interpolated using four-parameter algorithms to provide the best standard curve fit.

2.3.8.1 Thermo-Fisher calprotectin ELISA

The Calprotectin L1/S100-A8/A9 ELISA kit was used to measure calprotectin concentration in 38 stool samples as shown in Figure 2.12. This is designed to measure calprotectin from serum and plasma samples. The healthy population control stool samples showed minimum detection of the calprotectin proteins except for one outlier sample. All the Crohn's and Ulcerative Colitis stool samples were able to detect the calprotectin proteins, Figure 2.12A. This ELISA kit has 35 – 8,000 pg/mL of analytical sensitivity.

The UC and Crohn's disease stool samples were analysed using the ROC curve compared to the healthy population's stool samples. The ROC curve analysis gives an AUC of 0.83 for the ability to detect Crohn's disease and 0.74 for ulcerative colitis detection, Figure 2.12B. This suggests that the calprotectin L1/S100-A8/A9 Complex's ELISA kit is better at detecting Crohn's disease over UC.

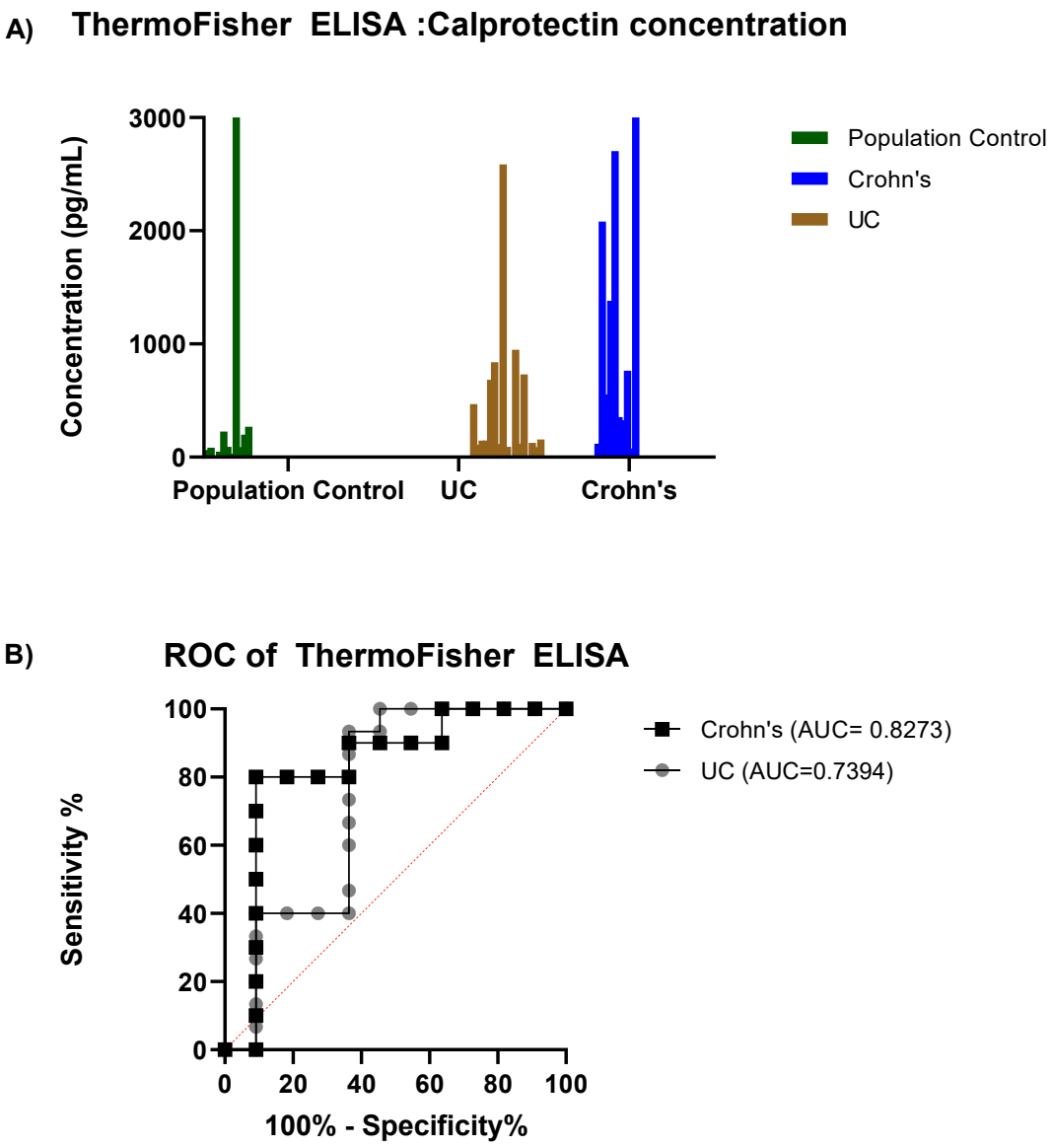

Figure 2.12: The UC, Crohn's and population control 1 mg/mL centrifuged samples were tested for human calprotectin using a L1/S100-A8/A9 complex enzyme-linked immunosorbent assay (ELISA). A) The human Calprotectin L1/S100-A8/A9 complex concentrations according to the standard curve. B) The ROC curves of Crohn's and UC compare to the population control. All the stool sample data represent the mean of n = 2 at room temperature.

2.3.8.2 CALP0170 ELISA

CALP0170 is an ELISA test to specifically detect calprotectin in active chronic inflammatory bowel disease patients' stool samples. This ELISA kit is sensitive to the concentration range is 0 to 500 ng/mL.

The calprotectin concentration in population control samples, ulcerative colitis and Crohn's disease patient stool samples is shown in Figure 2.13A. Most of the population control samples did not show any calprotectin protein concentration except for two samples. On the other hand, all the IBD samples show calprotectin protein.

The UC and Crohn's disease patient stool samples were analysed using a ROC curve compared to population control samples, Figure 2.13B. The area under the curve for Crohn's is 0.73 and 0.63 for UC. Overall, the data shows that the CALP0170 ELISA kit is more sensitive to identifying Crohn's disease than ulcerative colitis.

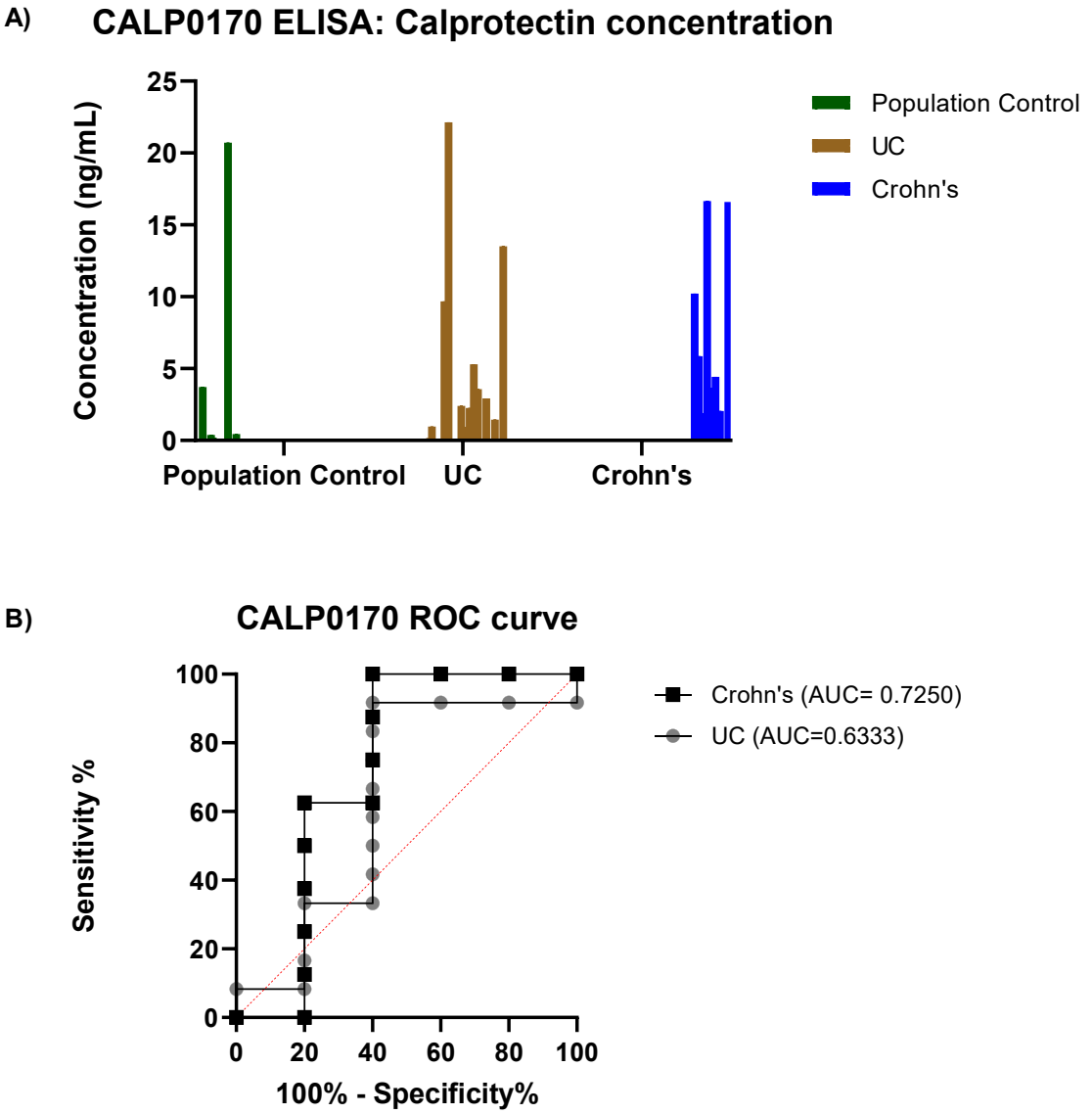

Figure 2.13: The UC, Crohn's and population control 1 mg/mL centrifuged samples were tested using a human calprotectin protein enzyme-linked immunosorbent assay (ELISA). The ROC curves of Crohn's and UC compared to population controls. All the stool sample data represent the mean of n = 2 at room temperature.

2.3.9 Comparison of receiver operating characteristics

The summarised ROC data for UC and Crohn's disease samples' ELISA and PLA_2 sensor results are shown in Table 2.1 below. The PLA_2 activity sensor shows better diagnostic ability than the commercially available PLA_2 ELISA. However, the PLA_2 ELISA is not optimised for measuring fecal samples and so could have significant non-specific binding. The ELISA can measure the denatured PLA_2 while tBLMs are able to measure the functioning PLA_2.

Receiver operating characteristic	**PLA_2 sensor (enzyme activity)**	**PLA_2 ELISA**	***TheroFisher* calprotectin ELISA**	***CALP0170* ELISA**
AUC for Crohn's disease	0.73	0.66	0.82	0.72
AUC for ulcerative colitis	0.76	0.58	0.73	0.63

Table 2.1: The ROC's area under the curves of Crohn's and UC compared to the population control for all the ELISAs used and tethered PLA_2 tBLM sensor.

2.4 Discussion

The experiments here were designed to test the capability of the PLA_2 tBLM sensor array in testing PLA_2 enzyme activity in frozen stool samples. There were three samples that showed similar conductance changes with and without Ca^{2+} ions present in the DOPC tBLMs. This suggests that these three IBD samples may have contained Ca^{2+} independent PLA_2 group. This PLA_2 group enzymes do not rely on calcium ions for their activity. Instead, they can catalyse the hydrolysis of phospholipids and release fatty acids and lysophospholipids, even in the absence of calcium ions.

If a percentage change in conductance threshold of >100% is applied for this PLA_2 activity sensor, then only eight of the 40 tested samples have 'high' percentage conductance changes after 20 min and all of them were from IBD patients. Furthermore, if the cut-off mark is a 50% change in conductance, then 17 of the 40 samples fit into this category and only two of those samples were from population control samples. This suggests that a reasonable cut-off level for this sensor could be a 50% increase in conductance changes.

To further statistically validate the change in the conduction threshold, Figure 2.14 shows the positive and negative predictive values for the PLA_2 activity sensor. The analysed data for change in Gm > 50% shows 17 IBD and 2 population control samples. For the change in Gm < 50 %, there were 12 IBD and 21 population control samples. A two-tailed *Fisher's exact test* supports the hypothesis that the proportion of samples that have increased in Gm > 50% over 20 min is greater in IBD samples than in the population control samples with a P value of 0.0341 (as calculated using Graphpad Prism).

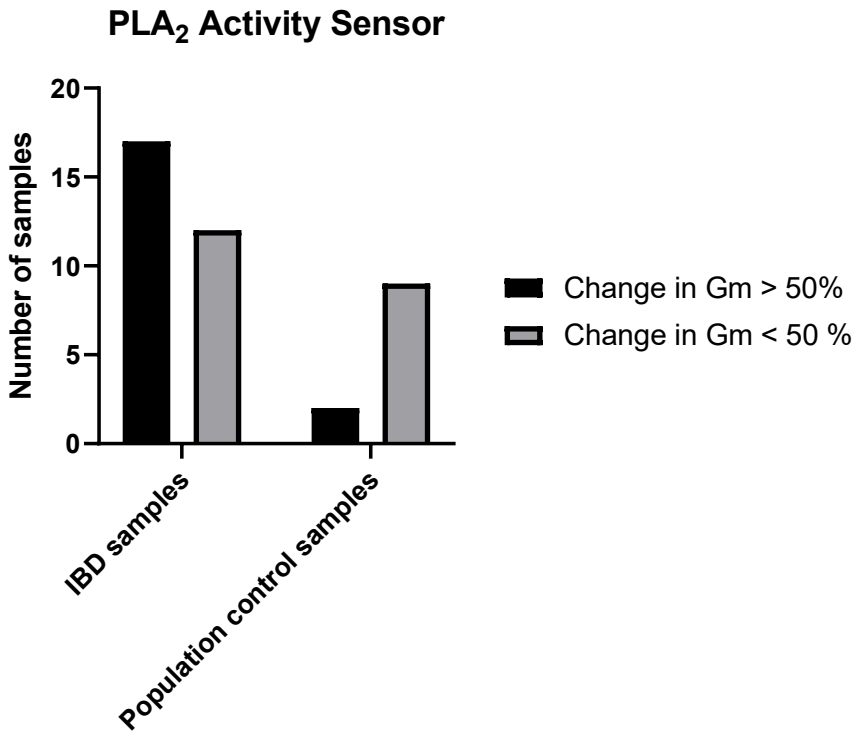

Figure 2.14: The positive and negative predictive values for the PLA_2 activity sensor.

The sample SGH13 was one of the population control samples showing significantly increased conductance changes on the negative control diether-PC tBLMs. Upon closer inspection, it is thought that the lipids were incorrectly assigned to each well when testing this sample, and so this sample was excluded from the study (only one sample in this study). Any activity detected in the diether-PC samples might indicate conductance changes due to the presence of other enzymes such as phospholipase C (PLC) [201, 202] and D (PLD) could also be in there. Also, there could be microbial peptides that can affect PC lipid membranes. Alternative reasons the DOPC without Ca^{2+} negative controls may have shown activity could be the samples contained sufficient Ca^{2+} ions already, not sequestered by the EDTA or they can contain different PLA isotopes which are Ca^{2+} independent [203-205].

The exact cause for IBDs is still unknown and also the aetiology of the PLA_2 activity recorded by the sensor is still unknown. This measured PLA_2 activity can be a result of human-secreted PLA_2 or perhaps, as mentioned previously, it could be due to gut bacterial secretions. To determine this, a microbiome bioinformatics study could be conducted and the activity data correlated with known PLA_2-secreting microbes. Alternatively, extracting PLA_2 from the stool samples and utilising mass-spectroscopy techniques might also be a way of determining the aetiology of the PLA_2 source. These experiments are beyond the scope of this project currently.

The sensing time is a very important factor when it comes to performance. Chapter 2.3.3 shows the membrane conductance changes over a period of 40 minutes. In the first 10 minutes, the conductance rapidly changed and by 20 minutes, it had started to plateau. The ROC curve data gives the best detection at 20 minutes. Burack, W.R. et al. (1994) have observed the fluorescence intensity that changes with the PLA_2 hydrolysation over the period of 0 to 1500 seconds (25 min) [206]. In contrast, this study typically shows low initial activity until 500 seconds is reached, and this low activity period ends abruptly with a sudden increase in membrane conductance. At 1000 seconds (~16 min) the PLA_2 typically reaches its highest activity level which justifies the PLA_2 sensors' time optimisation in this project.

The normal human body temperature range is 36.5 to 37°C [207] and human enzymatic isoforms are expected to be more active at body temperatures [208]. All the tBLMs, however, show higher membrane conductance than at room temperature, as expected as they are more fluid at higher temperatures [209]. This could lead to membranes having less dynamic range due to their already increased leakiness.

The improved performance of the membrane biosensor measurements at room temperature over 37°C could be attributed to several factors such as the improved structural stability of the enzyme proteins. If measuring at even lower temperatures like 4°C, several important considerations, such as reduced enzyme kinetics and reaction rates need to be considered. At lower temperatures, the rate of specific biological processes may significantly decrease, leading to delays in response times or reduced biosensor

sensitivity. Further, at low temperatures, the properties of the membrane may become less flexible, affecting the diffusion of analytes and, ultimately, the sensor's sensitivity.

Fecal samples can be centrifuged 3 to 5 times to remove the parasites, fibres, etc. and to increase the sensitivity of the ELISA tests [210, 211]. However, the data presented here suggest that the 10,000 rpm is not reliable as it removes some enzymes from the supernatant or denatures them (see Chapter 2.3.6). Lower centrifugation speed can be beneficial when separating specific biological components sensitive to high forces, such as enzymes. The lower centrifugation speeds reduce the magnitude of the forces acting on the enzymes, which can help preserve their structural integrity and enzymatic activity. Also, reducing the centrifugation time may be helpful when a rapid separation is needed or when dealing with delicate components that settle quickly. The shorter exposure of enzymes to high forces may mitigate denaturation and other adverse effects. The longer centrifugation times may be necessary when substances requiring extended centrifugation fully precipitate. When using the un-centrifuged samples, it might be expected that the presence of extraneous matter would lower the sensitivity. However, this PLA_2 sensor seemed capable of quantifying the enzymatic activity without any special sample treatment. In point-of-care sensors, less sample preparation and less use of advanced equipment are really important.

The fecal calprotectin and PLA_2 ELISA data suggest that they are more prominent in the Crohn's disease samples than the ulcerative colitis samples. However, the PLA_2 tBLMs sensor data shows that this sensor is more sensitive to ulcerative colitis than Crohn's disease and so is potentially better than fecal calprotectin ELISAs in diagnosing ulcerative colitis.

Figure 2.14 show data shows that there appears to be no linear correlation between PLA_2 activity and PLA_2 concentration. It should be noted, however, that the PLA_2 ELISA used is specific for the G2A subgroup and the PLA_2 tBLM sensor is capable of detecting any phospholipase A activity. This could be a telling reason that, according to the ROC data, the PLA_2 activity sensor has better sensitivity for IBDs than the PLA_2 ELISA used.

The PLA_2 activity sensor seems more sensitive to enzymes in UC samples than in Crohn's samples. Crohn's can occurs anywhere in the digestive tract, while UC is confined to the

colon and rectal regions of the gut. This could suggest that PLA_2 activity is more readily detected when the stool sample has less distance to travel through the gut.

2.5 Conclusion

During the blind trial, 40 stool samples were tested on the DOPC membranes with and without Ca^{2+} ion presence and on diether-PC membranes using electrical impedance spectroscopy. This sensor's sensitivity was been analysed in stool samples with and without centrifugation, at different temperatures and at various incubation times to develop the best protocol.

Overall, the data suggest that tBLM arrays can detect PLA_2 activity in fecal samples, and this research finding indicates the potential for developing a point-of-care diagnostic tool for inflammatory bowel diseases. Diagnosing IBDs currently involves a combination of clinical evaluation, endoscopy, imaging studies, and laboratory tests. A point-of-care diagnostic test would offer several advantages, such as faster and more convenient detection, potentially leading to early intervention and improved patient outcomes. Using tBLM arrays in this context suggests a novel approach to detecting PLA_2 activity. The PLA_2 activity has been observed in the intestines of individuals with IBDs, making it a potential biomarker for these conditions.

3 Triolein tethered membrane characterisation with electrical impedance spectroscopy

3.1 Introduction

For more than two decades *phospholipid* tBLMs have been well-characterised in terms of their stability, the impact of pH [212], the membrane thickness and their water content [213]. However, of the use triglyceride membranes has not been reported yet to the best of our knowledge. Therefore, this part of this research is to create and characterise triglyceride tethered membranes. Most triglycerides contain an asymmetry making their packing into a tethered membrane problematic. However, the commonly used triglyceride *triolein* is symmetrical and unsaturated [214]. Therefore, triolein was used as the triglyceride of choice for this study to create a new tethered membrane architecture. The successfully created triolein tethered membranes were characterised using electrical impedance spectroscopy (EIS).

The main objective of this part of the study was to develop this new membrane architecture and to characterise their functionality compared to phospholipid tBLMs with differing pH environments [171] and in the presence of Ca^{2+} ions which would typically condense phospholipid tBLMs [215]. The potential of these triglyceride tethered membranes to act as sensors for pancreatic lipase enzymes dissolved in the blood, as a possible diagnostic device for acute pancreatitis was also tested.

Also, this chapter will assess this triglyceride-tethered membrane architecture as a sensor for lipase enzymes produced in bioreactors. The four lipases that have been used in this project are lipase from *Aspergillus Niger (ANL), Candida Rugosa (CRL),* wheat germ (WGL) and *Rhizopus Oryzae (ROL).* The idea behind this research is to eventually create a device that acts as an in-line sensor with bioreactors that will identify that sufficient lipases have been successfully produced in the reactor before cultivation.

Finally, by altering membrane packing by incorporating fatty acids alongside triolein in these tethered membranes it is hoped the sensitivity of the triolein triglyceride tethered

membrane to lipases can be improved. The mixture of triolein with wedge-shaped fatty acids should be able to change the overall membrane morphology and perhaps decrease the *area per lipid* giving improved access for the lipases to the lipid substrate. Alternatively, this change in lipid packing might alter the tethered membrane such that it destabilises more readily upon triglyceride hydrolysis.

Overall, this chapter shows the combination of experiments that tested the new architecture of triolein tBLMs to characterise EIS and its possible applications. This experiment's two potential applications are acute pancreatitis detection and industrial lipase activity detection sensors. Pancreatic lipase activity has been tested on serum, whole blood and stool samples, showing better serum detection. Therefore, in further development, the serum can use as the primary sample type while eliminating the rest. Most of the mimic membrane researchers are involved in medical-related research. This research data shows the attempt to create an industrial application of an in-line sensor to detect industrial lipase activity during production. Finally, this new triolein membrane characterisation details future research on triolein membranes.

3.2 Materials and Methods

3.2.1 Chemicals

Analytical graded chemicals have been used in this research project to perform all the experiments. Chemicals used include pure ethanol (100%), sodium chloride (NaCl), calcium chloride ($CaCl_2$), trisaminomethane (tris) and 2-(N-morpholino) ethanesulfonic acid (MES). All these chemicals were purchased from Sigma-Aldrich Australia.

3.2.2 Buffers

The tris buffer and Ca^{2+} buffer preparation are discussed in Chapter 2.2.1.

For determining lipase activity at low pH, a 10 mM MES buffer prepared with 100 mM NaCl at pH 5 was used. This buffer is henceforth referred to as the *MES buffer*. Depending on the experiment, $CaCl_2$ is added to this buffer at a 1 mM concentration.

3.2.3 Phospholipids and triglycerides

DOPC and diether-PC lipid preparation are discussed in Chapter 2.2.2

Triolein (Figure 3.1A) 18:1 lyso-PC (Figure 3.1B), and 17:1 lyso-PC (Figure 3.1C) were each used at a 3 mM concentration dissolved in pure ethanol and stored under -20 °C. All of these lipids and triglycerides were purchased from Avanti Polar Lipids in the United States.

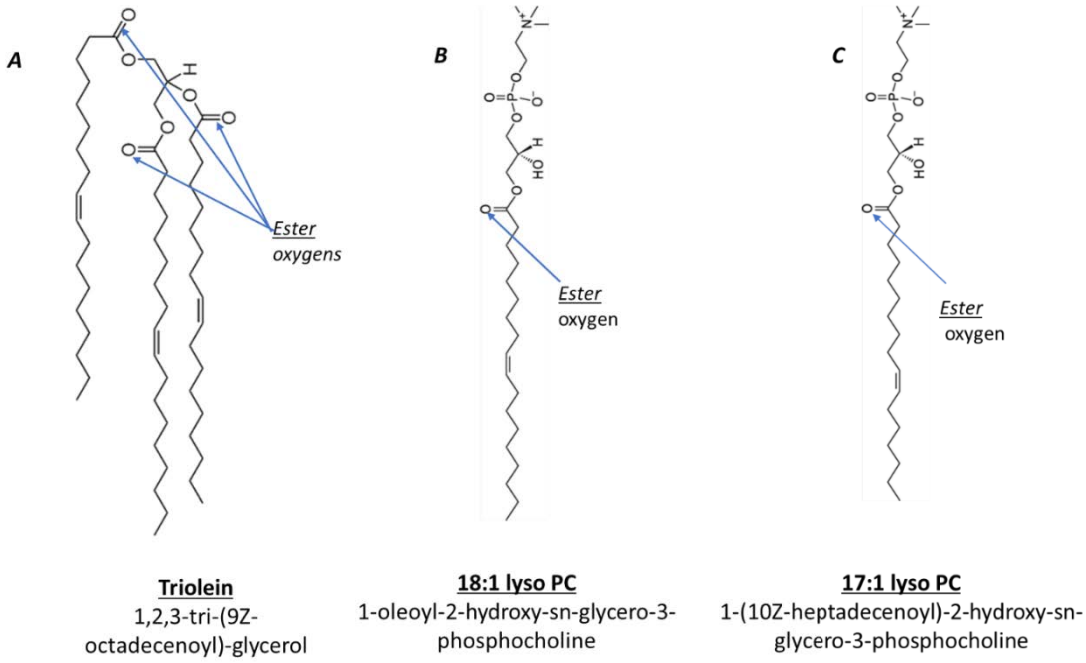

Figure 3.1: Chemical structures of lipids used to create tethered membranes. A) The triglyceride, triolein, has three esters moieties in each fatty acid chain which can be hydrolysed by the lipases. Lysophospholipids such as B) 18:1 lyso-PC and c) 17:1 lyso-PC are small bioactive lipid molecules with a single hydrocarbon chain.

3.2.4 Pancreatic lipase

Analytical grade lipase from porcine pancreases was purchased from Sigma-Aldrich Australia. This is type VI-S lyophilised powder with ≥ 20,000 U/mg protein. One unit is defined as being able to hydrolyse 1 micro equivalent of fatty acid of triglyceride in 1 hr at pH 7.7 at 37 °C [216]. The enzyme's catalytic activity is measured in the enzyme unit (U or IU). A 1 U of the enzyme can convert 1 micromole (µmole) of substrate per minute

under specific assay conditions, such as temperature, pH, and substrate concentration. The ordered pack size was 100 kU of protein. This protein powder was diluted in 1 mL of tris buffer to make 100 kU/mL stock solution. This was then diluted further in buffer to prepare a 1 kU/mL sample for addition to the tBLMs.. When used, the stock sample was diluted 1 in 100 to an activity of 10 U/mL. Each stock sample was separated into a few different sample tubes to reduce thawing and re-freezing. All of the porcine pancreatic lipase (PPL) samples were stored at -20 °C.

3.2.5 Horse blood

The 50 mL of horse blood serum was purchased from ThermoFisher Scientific Australia. This product is prepared by collecting the blood from the donor horse directly into sterile blood bags. The blood is defibrinated by vigorous agitation for 8 minutes, then filtered to remove the fibrin aggregates. [217]. According to the supplier, Serum Australia, this product will maintain its properties for 28 days under 4 °C. All whole blood experiments were conducted within a week of the sample being received at room temperature.

For the experiments, PPL in blood was prepared in a few different ways. Firstly, stock PPL was diluted in whole blood to create 10, 100, 1000 and 10000 U/mL activities. To test PPL-in serum, whole horse blood was centrifuged for 10 mins at 1000 rmp at 4°C and the serum supernatant was collected. Alternatively, the serum from the whole blood was collected and then PPL was added to that. Both of these sera samples, one with lipase added to the whole blood prior to centrifugation, and one with PPL added subsequently, were tested on triolein tethered membranes.

3.2.6 Stool samples

The activity of any lipases in stool samples was tested. The preparation of these samples was as per Chapter 2.2.3.

3.2.7 Industrial lipases

Lipases from *Aspergillus niger (ANL), Candida rugosa (CRL), Rhizopus oryzae (ROL)* and wheat germ lipases (WGL) were ordered from Sigma-Aldrich Australia. All the lipases were in powder form, and the stock concentration was prepared depending on the

activity per gram of the ordered sample. Samples were prepared in the tris buffer and Ca^{2+} buffer.

3.2.8 Tethered membranes and electrical impedance spectroscopy

Triolein tethered membranes were prepared with the same solvent exchange technique described for phospholipid tBLMs in Chapter 2.2.4. Impedance measures were also done using the same hardware settings and the data was modelled using the same equivalent circuit.

3.3 Results

3.3.1 Triolein tethered membrane preparation with DOPC

The attempt to create a membrane that includes triolein molecules is shown in Figure 3.2. The DOPC and triolein were mixed in a few different ratios and then tested with 10 U/mL of PPL and conductance changes across the membrane with EIS were measured. Conductance changes in response to PPL are evident for the DOPC: triolein, 1:8 and 1:4 ratio membranes, while the other two membranes that were predominantly DOPC in content did not show any sign of hydrolysation.

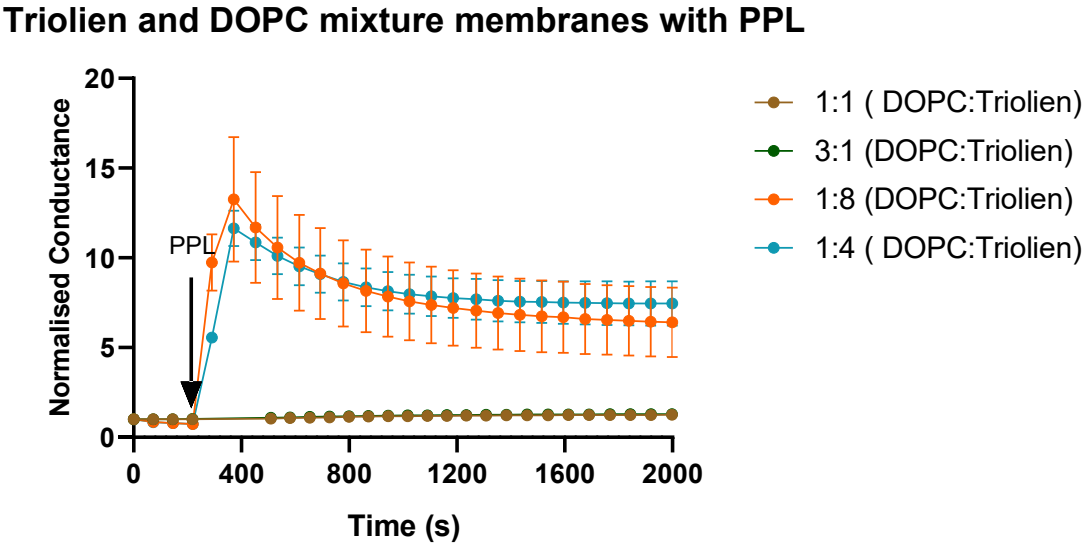

Figure 3.2: The electrical impedance spectroscopy data for triolein and DOPC mixture membranes with PPL.

3.3.1.1 Bode plots for triolein, DOPC and diether-PC membranes

The impedance magnitude and the angle of the phase shift between the excitation signal and the measured response were both measured. These results are compiled into what is known as *Bode plots*. These plots display the impedance and phase angle shifts at various measurement frequencies.

Frequency (x-axis) shows the rate at which an alternating current (AC) signal oscillates, measured in Hertz (Hz). The frequency represents on a logarithmic scale, ranging from very low to very high frequencies [218]. As the frequency increases along the x-axis, the AC signal alternates faster. Physically, the frequency in Bode plots is relevant because it provides information on how the electrical properties of the PC membrane respond to different rates of applied AC signals. Different frequencies can affect various processes in the membrane, such as the charging and discharging of capacitance or the opening and closing of ion channels, thus revealing the membrane's electrical behaviour at different time scales.

The impedance magnitude (y-axis) shows the absolute value of the impedance of the PC membrane at a given frequency. Impedance is the complex resistance that includes both resistance and reactance. Physically, the impedance magnitude gives an understanding of the overall electrical resistance and capacitance properties of the PC membrane at different frequencies. At certain frequencies, the impedance magnitude may be higher, indicating stronger resistance or capacitance, while at other frequencies, it may be lower, suggesting lower resistance or capacitance.

Phase (y-axis) shows the phase shift between the AC circuit's voltage and current. It is measured in degrees and indicates the time delay between the AC voltage applied to the membrane and the resulting AC current flow. Physically, the phase provides insights into the time relationship between the voltage and current response of the PC membrane. A phase shift can occur due to the capacitive or inductive nature of the membrane. For example, a capacitive phase shift of -90 degrees indicates that the current leads the voltage by 90 degrees, while an inductive phase shift of +90 degrees means that the current lags the voltage by 90 degrees.

Typical Bode plots for triolein, DOPC, diether-PC and a mixture of triolein to DOPC membranes are shown in Figure 3.3. DOPC, diether-PC, 1:1 and 3:1 DOPC to triolein membranes show similar impedance magnitude and a similar frequency-at-minimum-phase of ~ 1Hz. The triolein membrane, and DOPC: triolein mixtures at 1:4 and 1:8 show a frequency-at-minimum-phase at a higher frequency, ~5Hz. This indicates the triolein containing membranes have a higher conductance compared to the PC membranes.

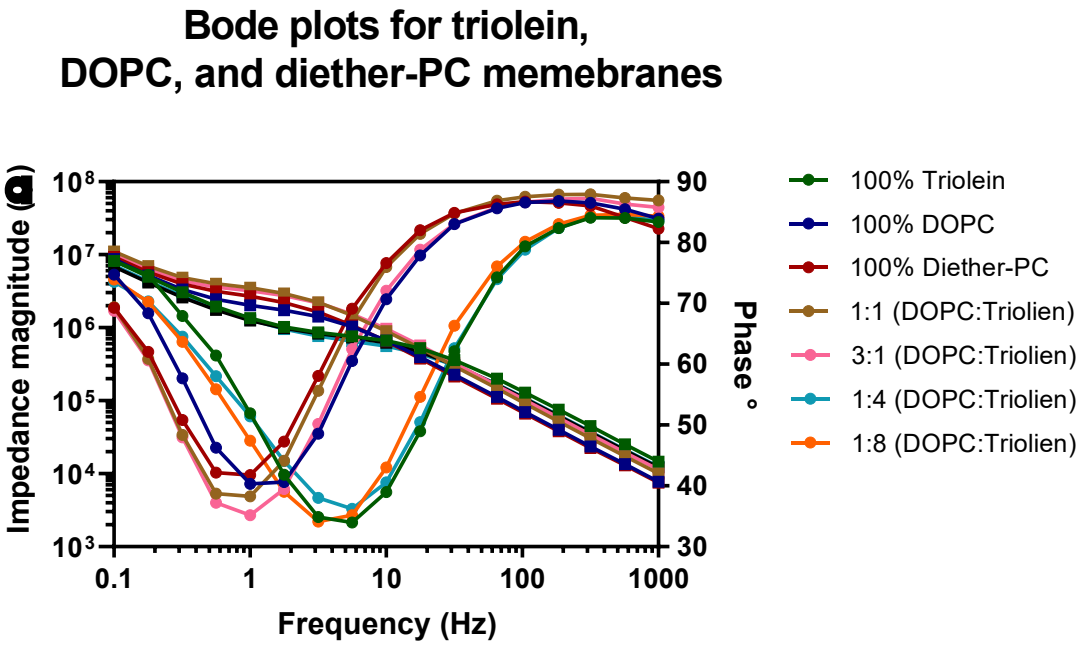

Figure 3.3: The Bode plot for triolein, DOPC and diether-PC membranes.

That the phase-at-minimum-phase for triolein is lower than the PC membranes suggests that either the capacitance at the tethering electrode is lower and/or the capacitance of the membrane is higher than the PC membranes [219]. The tethering region and the gold electrode is modelled as a *constant phase element* (CPE) (see Figure 2.3, Chapter 2) [193]. Whilst triolein and the PC membranes show similar capacitive terms (Q_s), this is related to the electrical capacitance of the system. The membranes can store electric charge in response to an applied voltage or an electric field. The similarity in Q_s between triolein and PC membranes suggests that they both have comparable electrical charges in response to an applied voltage. This similarity suggests that the two types of membranes

have similar electrical capacitance properties. The dimensional constant ($\propto_s$) is lower in the triolein tethered membranes. The $\propto_s$ can give an indication of the contribution of the restricted diffusion in the reservoir region [219].

The comparison between triolein and PC membranes in terms of Q_s and $\propto_s$ suggests that they might have different properties in interacting with their surroundings and responding to electrical fields, likely due to differences in their chemical compositions or molecular arrangements.

One might speculate this could be due to excess triolein molecules in the reservoir following self-assembly Table 3.1. The R_e represents the effective resistance of the electrolyte solution surrounding the tBLM. When an electric current applies to the system, it encounters resistance as it flows through the surrounding electrolyte medium. The effective resistance considers the electrolyte's resistive properties and any other factors that might affect the flow of current through the system. Table 3.1 shows the highest R_e in the triolein membrane, followed by DOPC and Dieter-PC membranes, while all the mixtures of membranes have low R_e values. Furthermore, the data shows that triolein, DOPC, and Diether-PC membranes have similar Q_s values. Triolien membrane shows the lowest $\propto_s$ in Table 3.1. A lower $\propto_s$ suggests that restricted diffusion contributes more significantly in the reservoir region of the triolein tethered membranes than in the PC membranes. G_m is the membrane conductance that measures the ability of the lipid bilayer membrane to conduct ions or electric current. The lipid bilayer's permeability to ions affects the conductance and the presence of ion channels. Table 3.1 shows the lowest G_m values when more PC lipids are present in the membrane than triolein lipids. The membrane capacitance (C_m) shows the ability of the lipid bilayer membrane to store electric charge per unit of applied voltage. The physical properties and arrangement of the lipid molecules within the membrane influence the capacitance. Table 3.1 shows that the 100% triolein membrane has the lowest C_m compared to the PC membranes. Overall, these findings show valuable insights into the electrical properties of different tBLMs, which are essential for understanding when designing biosensor applications.

Membranes	**R_e** **Ω**	**Q_s** **nF**	**$\propto_s$**	**G_m,** **µS**	**C_m,** **nF**
Triolein	980	186	0.66	1.55	13.22
DOPC	571	188	0.93	0.66	26.34
Diether-PC	629	180	0.89	0.47	29.62
DOPC:triolien (1:1)	260	152	0.93	0.34	19.94
DOPC:triolien (3:1)	405	167	0.91	0.39	17.84
DOPC:triolien (1:4)	483	214	0.838	1.92	17.12
DOPC:triolien (1:8)	448	227	0.855	1.58	16.77

Table 3.1: Summarised electrical impedance spectroscopy data for DOPC, diether-PC, triolein and DOPC-triolein mixture tethered membranes. R_e is the resistance of the electrolyte solution, Q_s is the imperfect capacitance of the electrode-reservoir region as modelled by a constant phase element (CPE), $\propto s$ is the dimensional constant of the CPE, G_m is the membrane conductance and C_m) is the membrane capacitance.

3.3.2 Pancreatic lipase activity on triolein and phospholipid tethered membranes

3 mM Triolein tethered membranes, DOPC and diether-PC tBLMs were prepared using the solvent exchange method. These tethered membranes were first tested with 10 U/mL PPL with and without 1 mM of Ca^{2+}. Figure 3.4A shows a conductance increase in the presence and absence of Ca^{2+} on triolein tethered membranes. This result indicates that the PPL activity is improved in the presence of Ca^{2+}.

Phospholipase A_1 and the A_2 activity on the triolein membranes were also tested, Figure 3.4B. The ester bond in glycerophospholipids at the sn-1 and sn-2 positions is hydrolysed by PLA_1 and PLA_2, respectively. Because PLA_1 only targets and hydrolyses the ester bond at the sn-1 position of phospholipids, leaving the sn-2 position unaffected, therefore PLA_1 shows no activity. The fatty acid and a lysophospholipid are released when PLA_2 hydrolyses the ester bond at the sn-2 position. Interestingly, PLA_1 shows activity on triolein-tethered membranes, whereas PLA_2 did not display any activity. This result has been proved in previous studies [220, 221]. The activity of both these phospholipases was measured in the presence of 1 mM Ca^{2+}.

The activity of the pancreatic lipases was further tested on DOPC and the diether-PC tBLMs, Figure 3.4C. There was little enzymatic activity of the 10 U/mL pancreatic lipases on tBLMs composed of ester or ether phospholipids, as expected. The activity of PLA_2 is evident in ester phospholipid tBLMS but not ether phospholipid tBLMs, as predicted (Figure 3.4D) [181].

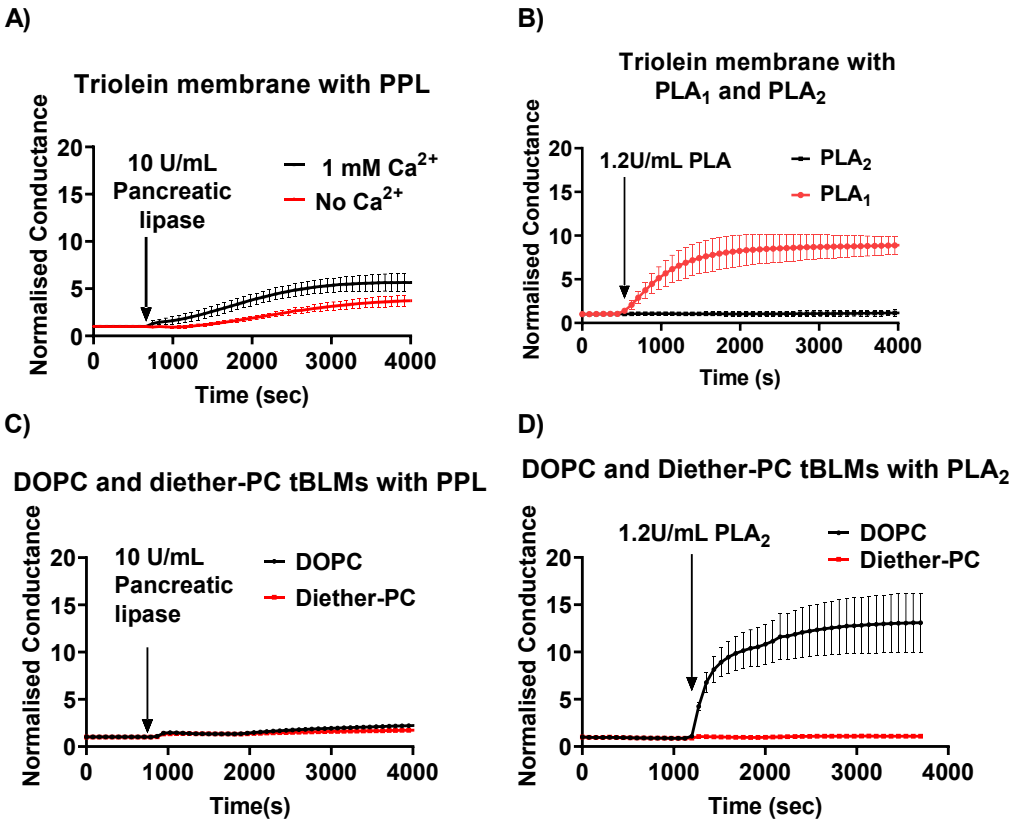

Figure 3.4: (A) Response of triolein tethered membranes to PPL in the presence and absence of Ca^{2+}; B) phospholipase A_1 and A_2 activity on triolein tethered membrane. C) PPL fails to hydrolyse phospholipids (DOPC and diether-PC) tBLMs. D) In comparison with C) PLA_2 does have activity on DOPC tBLMs but not diether-PC tBLMs. In all panels, data represent the mean ± standard error of the mean of n = 3 experiments.

3.3.3 Pancreatic lipase activity on the triolein tethered membrane with and without inhibitor

The triolein tethered membrane was tested with and without the PPL inhibitor, *orlistat*, Figure 3.5. The enzyme sample with orlistat did not show any conductance changes on triolein membranes. The other sample shows a typical response to membrane hydrolysation. Overall, these data show that the orlistat inhibited the PPL and that the orlistat itself did not affect the triolein membranes.

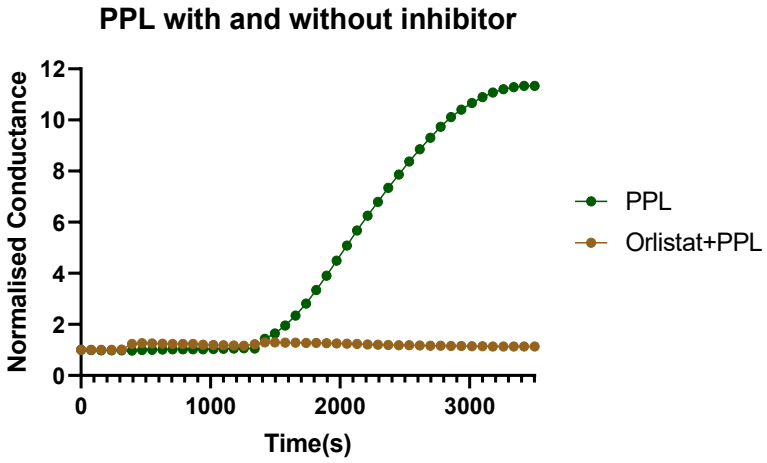

Figure 3.5: The pancreatic lipase effect with and without PPL inhibitor 3.3 µg/mL orlistat on 3mM triolein tethered membrane. In all panels, data represent the mean ± standard error of the mean of n = 3 experiments.

3.3.4 Triolein with different pH

This experiment was designed to analyse the pancreatic lipase activity on the triolein tethered membranes at different pHs, with and without Ca^{2+} ions. Tris and MES buffers were used in this experiment. Slightly acidic (pH 5.5), neutral (pH 7), and slightly base (pH 9) buffers were tested to test the stability of triolein tethered membranes. All these membranes were prepared with tris buffer with and without Ca^{2+} ions at pH 7, then the surrounding buffer was exchanged with the relevant pH buffers and left for at least 15 mins before adding 1000 U/mL PPL.

Figure 3.6A shows the triolein tethered membrane prepared with tris buffer (without Ca^{2+} ions in the buffers). The conductance slightly drops at pH 5.5, increases at pH 9 and remains the same at pH 7. All these membranes' conductance was increased after adding 10 U/mL PPL to the membranes. The highest normalised conductance was at pH 7, and the lowest was at pH 9.

Triolein tethered membranes were then prepared with 1 mM Ca^{2+} ion-containing tris buffer. They were subsequently washed with different pH buffers, also containing Ca^{2+}. The conductance did not markedly change, unlike with the tris buffer without Ca^{2+}, Figure 3.6B. 10 U/mL PPL was then added to the membranes at these different pH values. Tris buffer at pH 7 showed a conductance increase with the PPL, while tBLMs at pH 5 and pH 9 did not show any effects with the PPL. These data confirm that the pancreatic lipases are pH-dependent [222] and enzymatic reaction is better at pH 7 compared to the other two pH values.

It also shows that the PPL has a better enzymatic reaction when the Ca^{2+} ion is absent. Model PC membranes are commonly prepared with buffer without Ca^{2+} ions (see Chapter 2.2.4 for tBLM preparation). This set of experiments was designed to see if the triolein membranes are more sealed when Ca^{2+} is present in the membranes' preparation buffer. The results in Figure 3.6A show that the triolein membranes are less conductive and have a reduced response to enzymatic activity when the membranes were prepared with Ca^{2+} at pH 7 (see Figure 3.6).

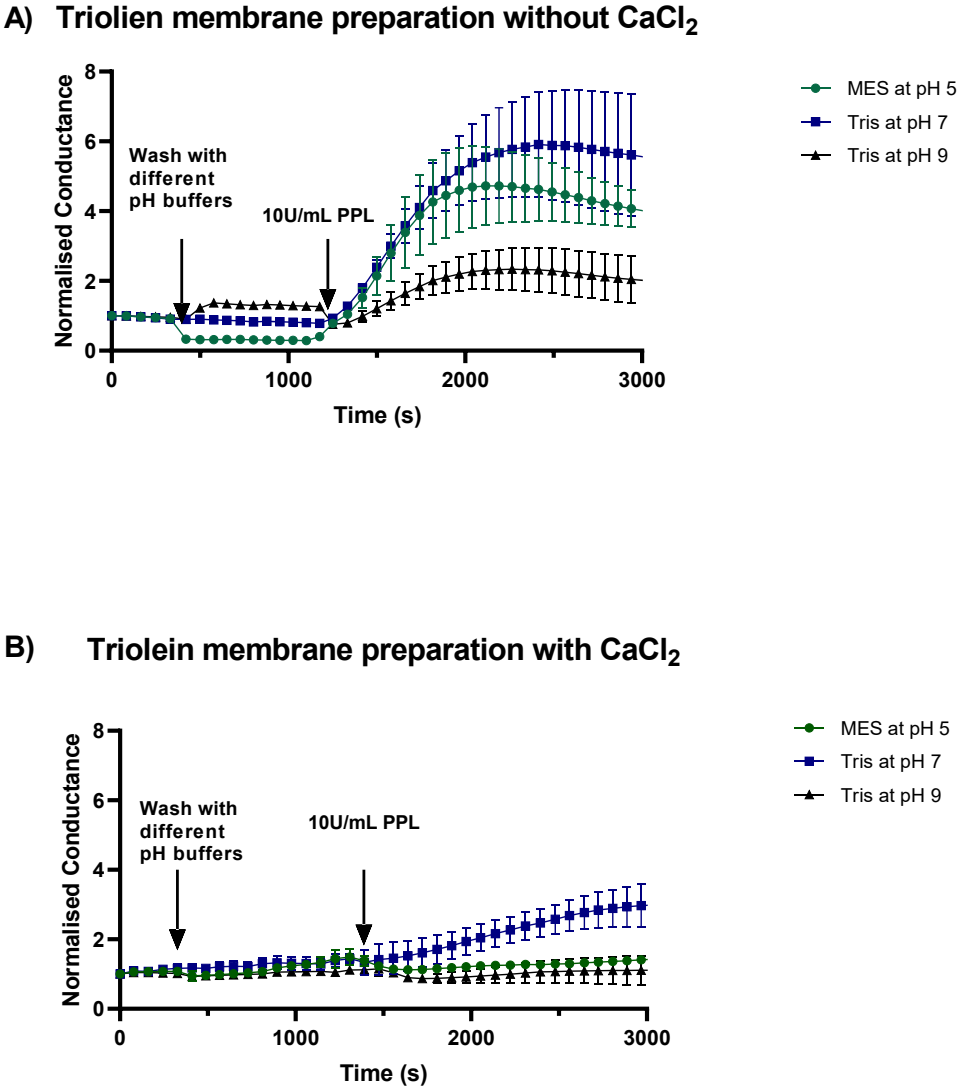

Figure 3.6: Triolein membrane prepared with (A) and without (B) Ca^{2+} ions at pH 5, 7 and 9. 10 U/mL of pancreatic lipase was then added to each membrane. In all panels, error bars represent the ± standard error of n = 2 experiments.

3.3.5 Lipase in horse blood

Horse blood spiked with PPL, PLA_1 and PLA_2 were tested on DOPC, diether-PC and triolein tethered membranes (Figure 3.7). All the membranes were prepared with tris buffer and exchanged with Ca^{2+} buffer before adding whole horse blood to the membranes.

Once blood samples were introduced to the membranes, DOPC and diether-PC tBLM conductance started to increase, while triolein conductance displayed little change. This suggested that the DOPC and diether-PC membranes' conductance is unstable with whole horse blood.

The PLA_1 (Figure 3.7A) and PLA_2 (Figure 3.7B) contained in whole blood were added to the DOPC, dither-PC and triolein membranes. The DOPC and diether-PC membranes show some conductance increase with these two phospholipids, while the triolein membrane remains the same. Figure 3.7C shows the mentioned three membranes with whole blood containing PPL. The data shows that the DOPC membrane's conductance changes while triolein and diether-PC membrane conductance remains the same. These results are comparatively different to when lipases are in a buffer solution.

Overall, these experiments show that the triolein membranes are stable and do not change the membrane or fall apart with whole blood. On the other hand, using DOPC and diether-PC with whole blood shows the conductance changes and therefore is not reliable.

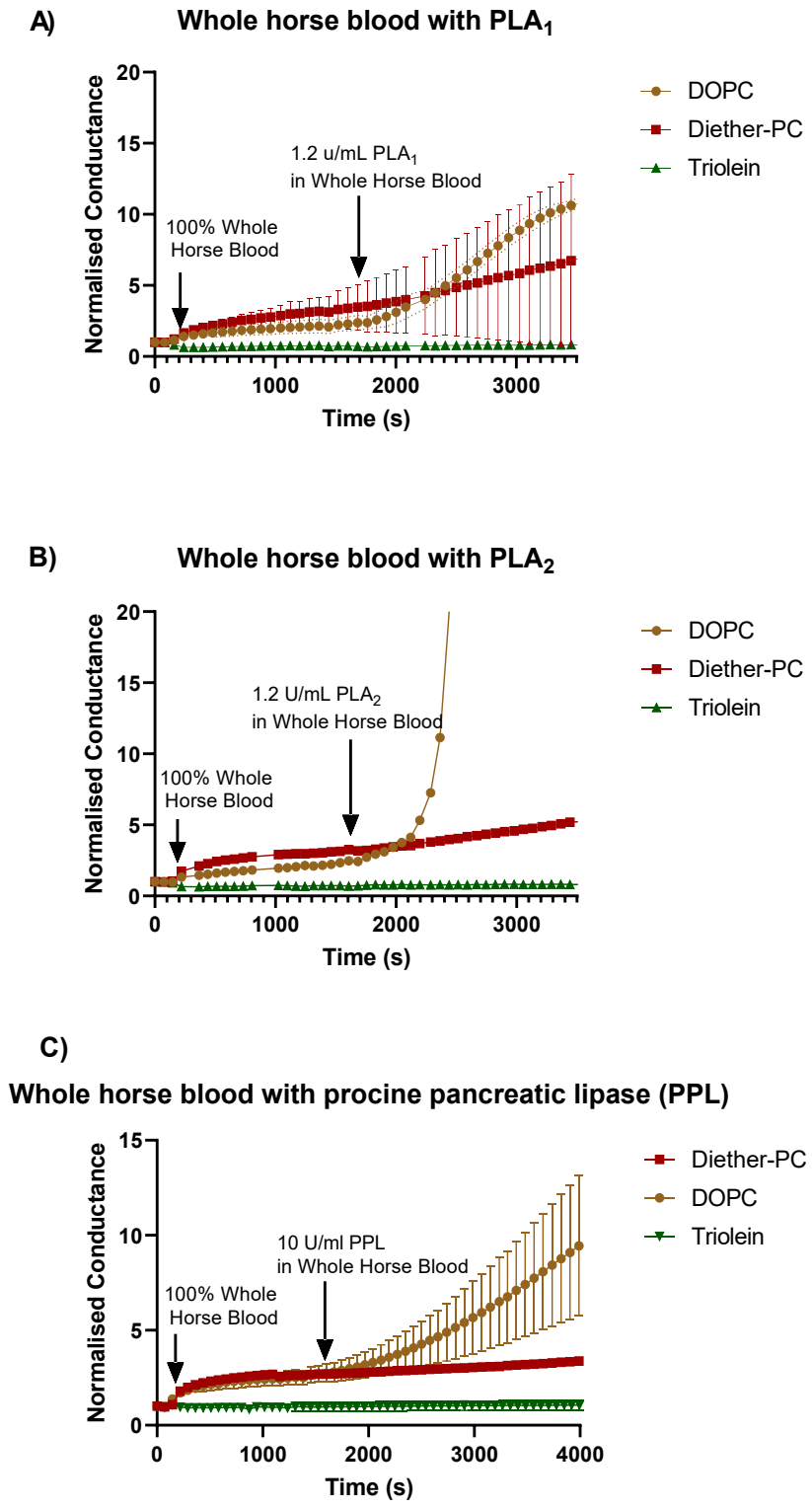

Figure 3.7: Horse blood activity with A) phospholipase A_1 B) phospholipase A_2, and C) Porcine pancreatic lipase. In all plots, data represent the ± standard error of n = 2 experiments.

Figure 3.7 shows the whole horse blood activity with PLA_1, PLA_2, and porcine pancreatic lipase. The data shows the DOPC and diether-PC membranes' instability with whole blood. Based on the results in Figure 3.7 C, the following experiments were conducted with different concentrations of pancreatic lipase-spiked whole blood on triolein tethered membranes. These experiments were designed to find if serum with PPL is better than whole blood in detecting PPL activity.

Figure 3.8A shows the 100, 1000 and 10,000 U/mL activities of PPL in whole blood. 1000 and 10,000 U/mL show slight conductance increases, while 100 U/mL did not show any changes on the triolein membranes. This suggested that only an activity above 100 U/mL can be detected in whole blood.

PPL experiments were then done using serum spiked with PPL to see if the membrane conductance changes would be different compared to the whole blood. Figure 3.8B shows conductance increases with PPL in sera at 100, 1000 and 10000 U/mL. To show that sera can be harvested from whole blood and still show lipase activity, PPL was added to whole blood and then centrifuged and the supernatant was collected to test with triolein tethered membranes, Figure 3.8C. The conductance increased in 1000 and 10,000 U/mL PPL samples, while 100 U/mL samples did not show any changes. Overall, these data show that this sensor can detect pancreatic lipase in the blood and serum when the activity is higher than 100 U/mL.

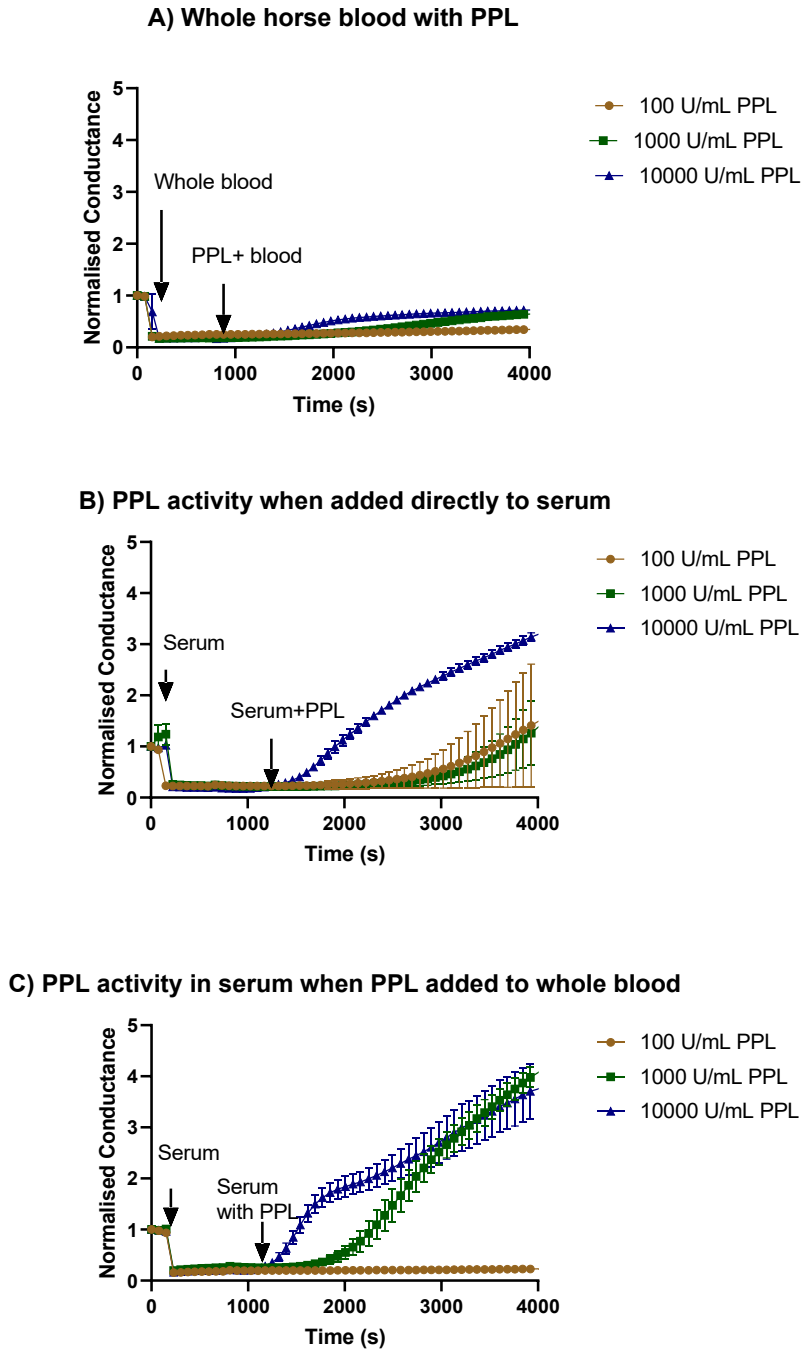

Figure 3.8: The 100, 1000 and 10,000 U/mL porcine pancreatic lipases were prepared in whole blood (A) and (B) sera. (C)The same activity of PPL was added to the whole blood and then centrifuged to see if the lipases' activity could still be detected in the serum. In all panels, data represent the mean ± standard error of the mean of n =2 experiments.

3.3.6 Pancreatic lipase activity checks on stool samples

In this experiment, stool samples were tested using the triolein tethered membranes to determine if they contained any pancreatic lipase activity. Figure 3.9 shows two different stool sample tests on 3 mM of DOPC, ether-ester PC and triolein membranes. Sample SGH 66 is from a Crohn's disease patient, and sample SGH125 is from an ulcerative colitis patient's stool sample.

1 mg/mL stool samples were prepared in the calcium buffer and then added to the triolein-tethered membranes. The SGH 66 shows the conductance increase in the DOPC tBLMs while ester-ether PC and triolein membranes conductance showed little change compared to the DOPC membranes, Figure 3.9A. The sample of SGH 125 showed little change in any of the membranes tested, Figure 3.9B.

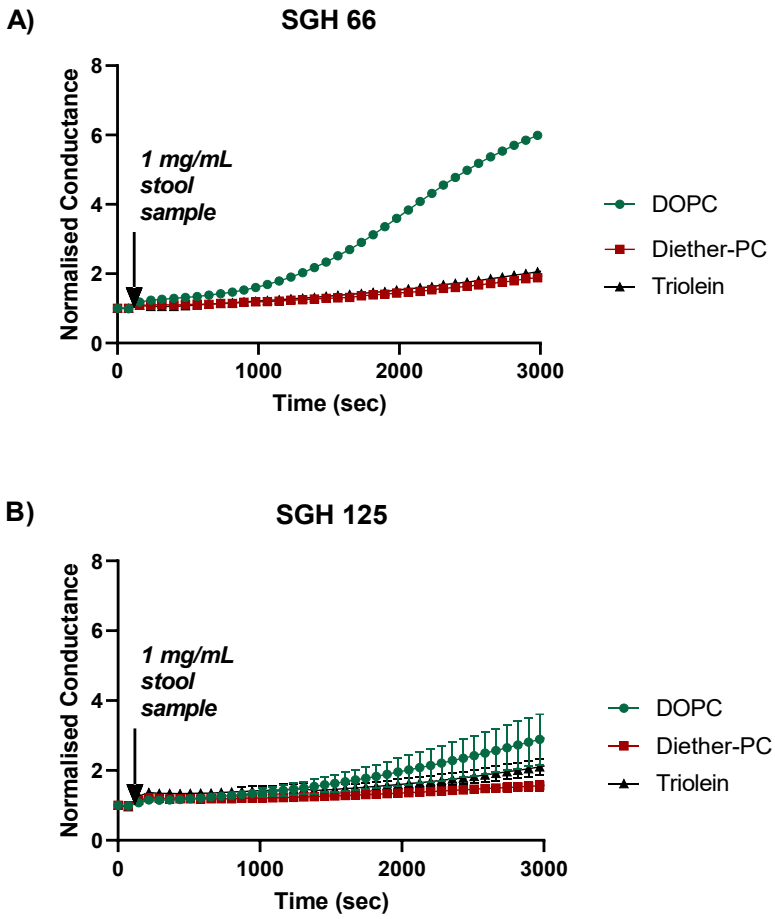

Figure 3.9: Pancreatic lipase activity test on the stool samples from Crohn's and ulcerative colitis patients of A) SGH 66 is from a Crohn's disease patient, and B) SGH 125 is from an ulcerative colitis patient. In all panels, data represent the ± standard error of the mean of n = 2 experiments.

3.3.7 Industrial lipases with triolein tBLMs

Figure 3.10 shows the triolein tethered membranes with and without Ca^{2+} ions to these were added commercially produced lipases. This part of the study is to test if these industrial lipases need Ca^{2+} ions to activate the enzymatic reaction. The ANL (Figure 3.10D) and CRL (Figure 3.10A) show how increased activity when Ca^{2+} ions are present in the buffer. While ROL (Figure 3.10B) shows the enzymatic reaction is inhibited when Ca^{2+} ions are present. The WGL (Figure 3.10C) lipase did not show any activity with or without Ca^{2+} ions on the triolein membrane.

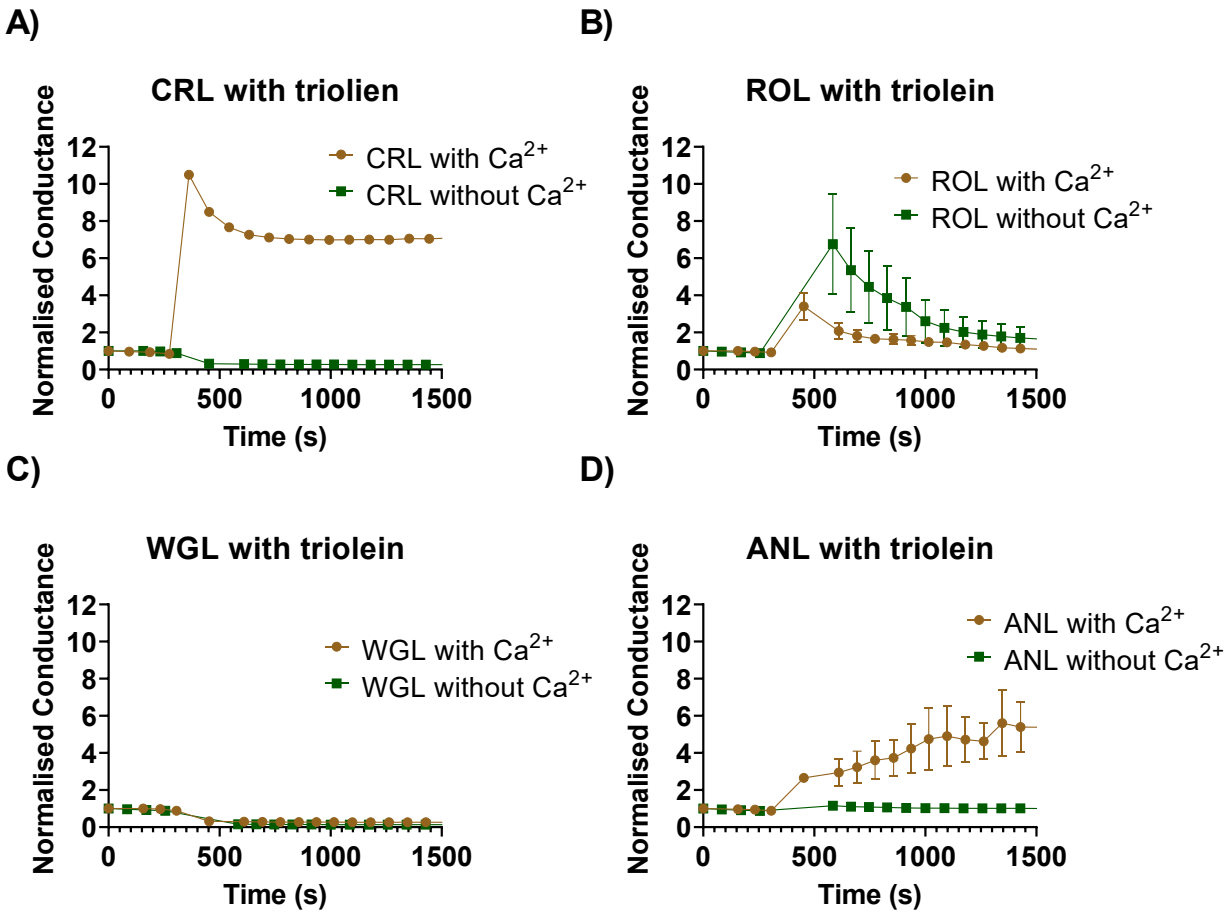

Figure 3.10: Selected industrial lipase activity on triolein membranes with and without Ca^{2+} ions present with A) CRL, B) ROL, C) WGL and D) ANL. The data represent the mean ± standard error of the mean of n = 3 experiments.

3.3.8 The tethered membrane of triolein and the oleic acid mixtures

Oleic acid is an unsaturated fatty acid with 18 C in the tail. Triolein and oleic acid have the same number of carbons in their tail groups. It was thought that by creating tethered membranes that were a mixture of oleic acid and triolein, the overall membrane morphology would be altered in such a way that would support lipase interaction at the lipid-water interface and permit greater hydrolysation of the triglyceride substrate, thus increasing the dynamic range of the triolein sensor. Figure 3.11 shows the 100% triolein, 100% oleic acid and four different ratios of the mixture of triolein and oleic acid

membranes tested with the CRL. The ability of single-chained fatty acids to form tBLMs has been reported previously [223]. The data shows that the 100% triolein membranes with CRL show the highest conductance increase while the triolein: oleic acid 5:1 and 8:1 ratio shows the next best conductance increases with the least error bars. When triolein and oleic acid were mixed 1:1 ratio, the CRL was not detected. This suggests that mixing triolein with oleic acid does not improve the sensing capability of these triglyceride-tethered membranes.

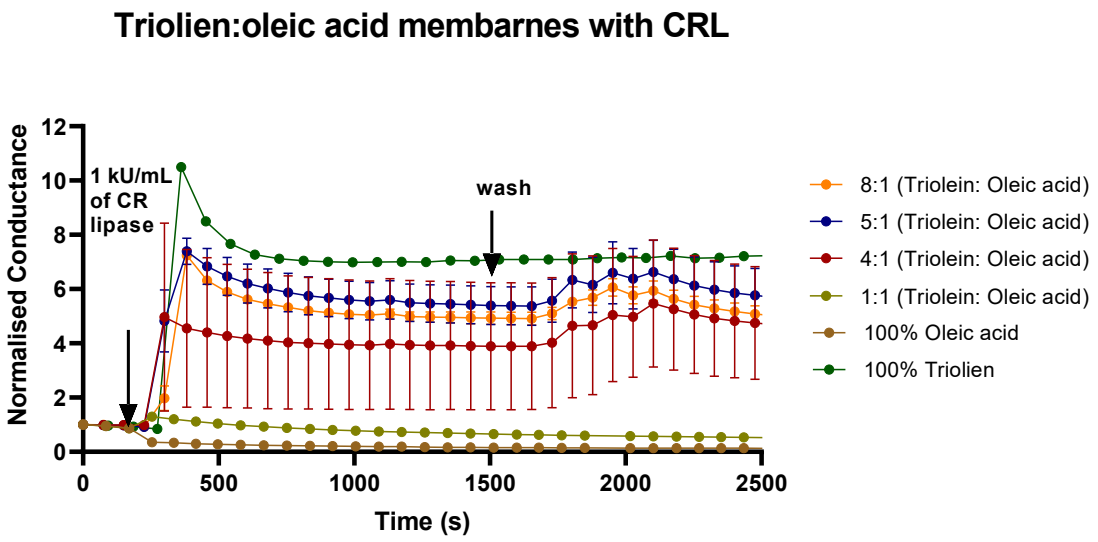

Figure 3.11: The triolein and oleic acid different ratios mixture and 100% triolein, 100% oleic acid membranes test with CRL. The data represent the mean ± standard error of the mean of n = 2 experiments.

3.3.8.1 Bode plots for triolein and the oleic acid mixtures

Figure 3.12 shows the Bode plot for the membranes that were created using oleic acids. All the different ratios of triolein and oleic acid membranes show similar phase and impedance magnitudes. Only the 100% oleic acid membrane has a distinct Bode spectra.

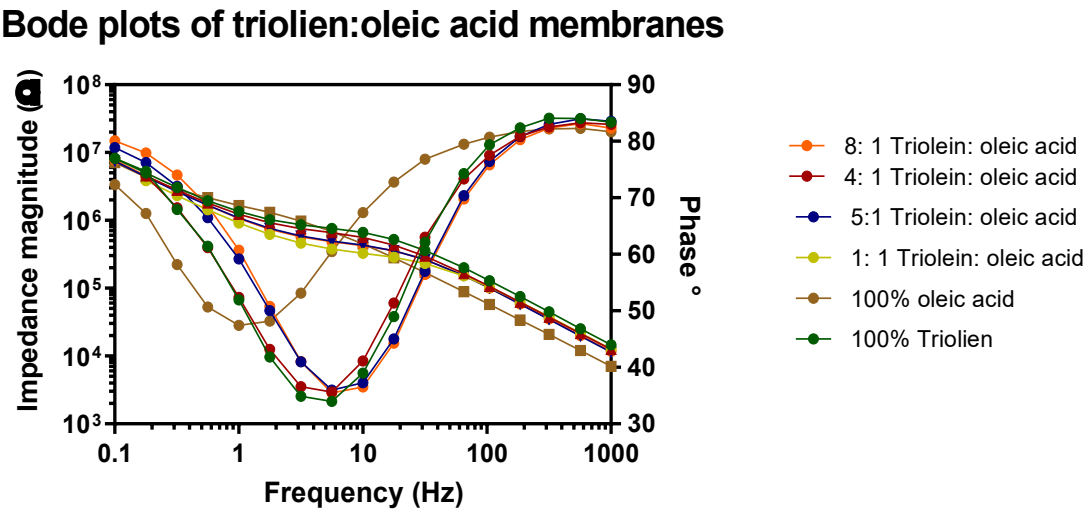

Figure 3.12: Bode plots for membranes composed of triolein-oleic acid mixtures.

Table 3.2 shows the summarised electrical properties of all the different triolein and oleic acid mixture membranes. The very high membrane capacitance of the 100% oleic acid membrane indicates the membrane is either very thin and/or has high water content.

Triolein:oleic acid membranes	R_e Ω	Q_s nF	$\propto_s$	G_m, µS	C_m, nF
8:1	943	201	0.91	2.64	16.64
4:1	740	205	0.87	1.89	16.55
5:1	662	208	0.89	2.62	17.28
1:1	917	238	0.88	3.723	15.25
100% oleic acid	12	218	0.81	1.28	47.53
100% Triolein	980	186	0.66	1.55	13.22

Table 3.2: Bode plots for triolein and the oleic acid mixture of membranes. This table included the values of electrolyte solution (R_e), similar capacitive terms (Q_s), the dimensional constant ($\propto s$), membrane conductance (G_m), and capacitance (C_m).

3.3.9 Tethered membranes of triolein and 17:1 lyso-PC mixtures

17:1 lyso-PC has an unsaturated 17 C chain and, unlike oleic acid, has a phosphocholine head group. Figure 3.13 shows different ratio mixtures of triolein to 17:1 lyso-PC lipids and their response to CRL. The results show the best conductance increase in the 100% triolein membranes, closely followed by all the triolein to 17:1 lyso-PC ratios. Even after washes post hydrolysation, membranes do not seem to show any increased conductance as a result of irreparable membrane disruption.

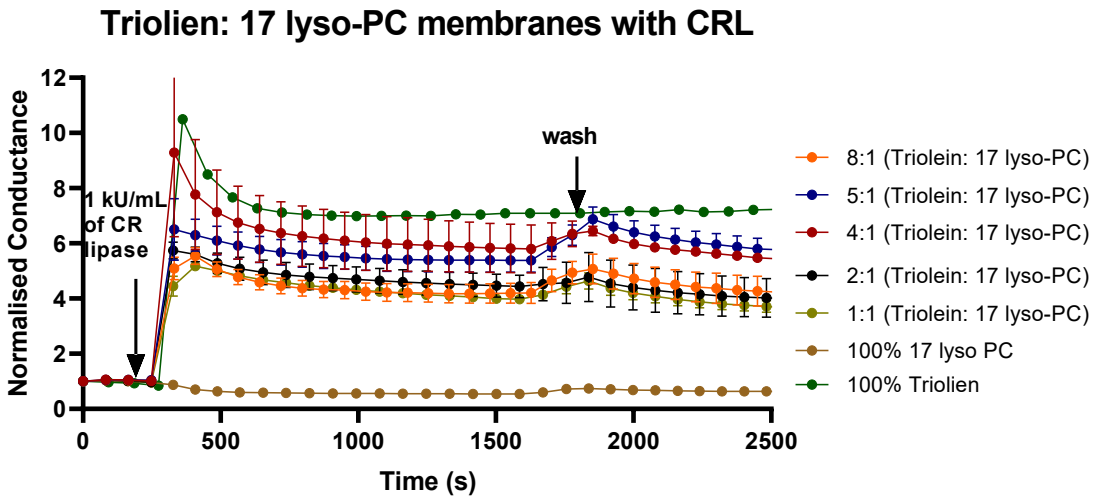

Figure 3.13: The triolein and 17 lyso-PC at different ratios mixture and 100% triolein, 100% oleic acid membranes test with CRL. The data represent the mean ± standard error of the mean of n = 2 experiments.

3.3.9.1 Bode plots for triolein and the 17:1 lyso-PC mixtures

Figure 3.14 shows the Bode plot for triolein and 17 lyso-PC lipid mixture tethered membranes. No clear changes are showing in the impedance magnitude, however, the phase change happened around 10 Hz. The main difference in these data is the angle of phase changes in 100% membranes, triolein around 35^0 and 17 lyso-PC is around 43^0.

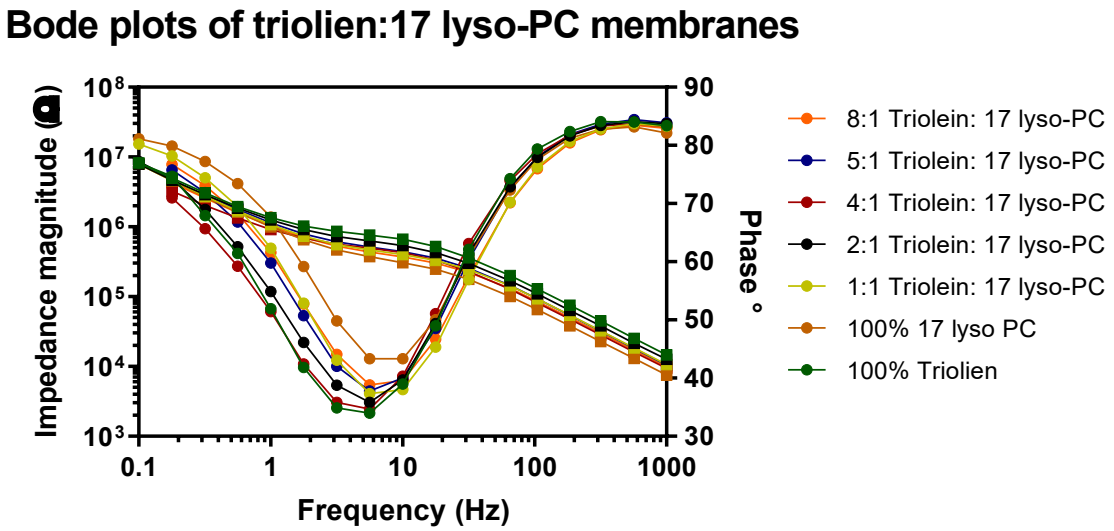

Figure 3.14: The bode plot for triolein and 17 lyso-PC mixture of membranes.

The EIS data for triolein and 17 lyso-PC lipid mixture membranes are shown in Table 3.3. Membrane conduction and capacitance of the triolein:lyso-PC membranes are all very similar.

Triolein:17 lyso-PC Membranes	**R_e Ω**	**Q_s nF**	**$\propto_s$**	**G_m, µS**	**C_m, nF**
8:1	629	215	0.88	3.19	20.94
5:1	532	198	0.89	2.56	19.36
4:1	483	290	0.85	2.49	22.01
2:1	621	196	0.87	2.02	16.27
1:1	690	198	0.90	2.86	18.45
100% 17 lyso-PC	621	200	0.91	3.96	28.13
100% Triolein	980	186	0.66	1.55	13.22

Table 3.3: Bode plots for triolein and the 17 lyso-PC membrane mixtures. R_e is the resistance of the electrolyte solution, Q_s is the imperfect capacitance of the electrode-reservoir region as modelled by a constant phase element (CPE), $\propto s$ is the dimensional constant of the CPE, G_m is the membrane conductance and C_m) is the membrane capacitance.

3.3.10 Tethered membranes of triolein and 18:1 lyso-PC mixtures

Finally, tethered membranes containing a lyso-PC with an equivalent chain length to triolein were tested. Varying ratios of triolein to 18:1 lyso-PC mixtures were tested with CRL, as shown in Figure 3.15. As with oleic acid and 17:1 lyso-PC, the highest conductance changes are shown with the 100% triolein tethered membranes.

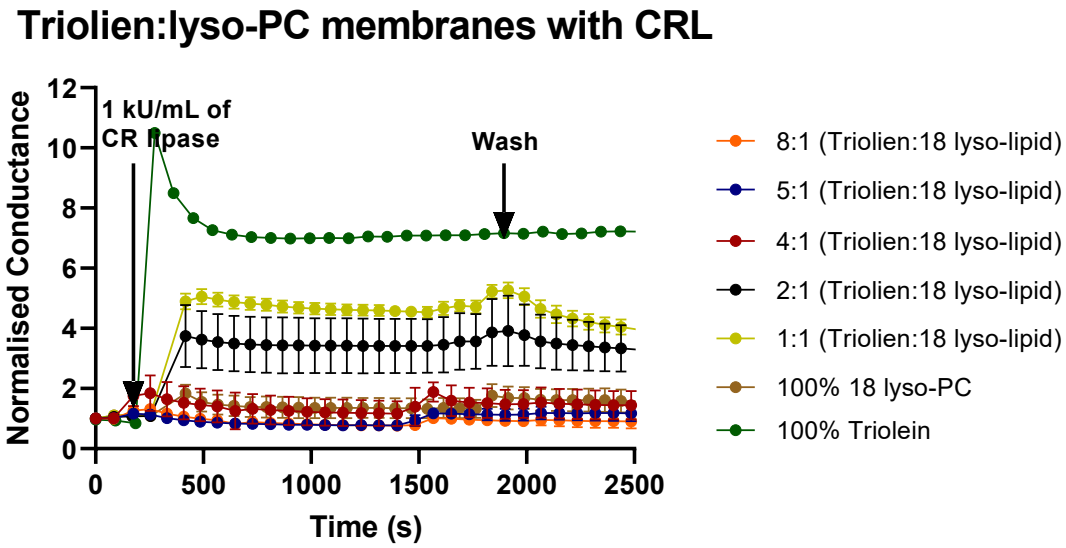

Figure 3.15: The triolein and 18 lyso-PC at different ratios mixture and 100% triolein, 100% oleic acid membranes test with CRL. The data represent the mean ± standard error of the mean of n = 2 experiments.

3.3.10.1 Bode plots for triolein and the 18:1 lyso-PC mixtures

Figure 15 shows the phase and impedance magnitude changes in a mixture of triolein and 18 lyso-PC lipid membranes. The triolein to 18 lyso-PC 8: 1 and 5: 1 show the phase change at 20 Hz while all the other membrane phase changes happened around 10 Hz. This data suggests that 8:1 and 5:1 mixtures of membranes are much leakier than triolein membranes.

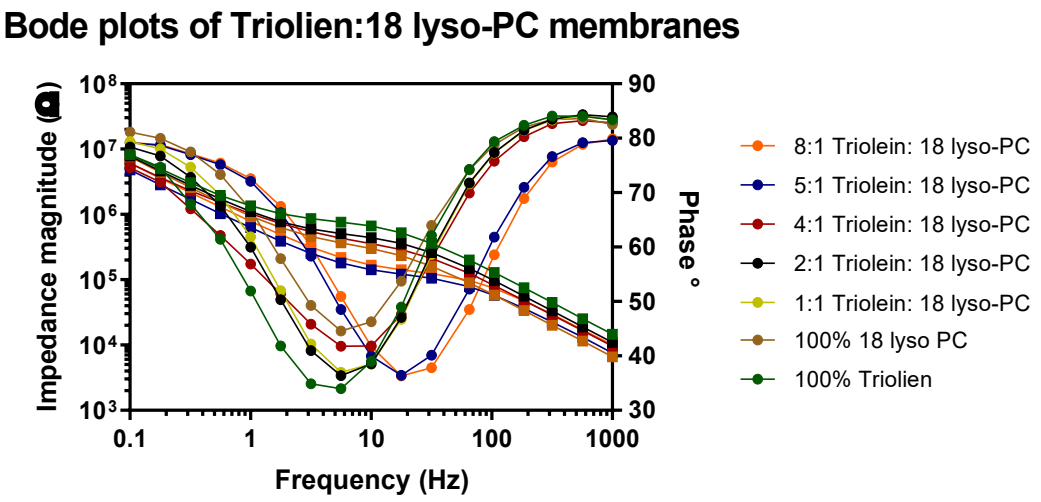

Figure 3.16: Bode plots for triolein and 18 lyso-PC tethered membrane mixtures.

The summarised Bode plots data for triolein and 18 PC lipid mixture of membranes are shown in Table 3.4.

Triolein: 18lyso-PC membranes	**R_e Ω**	**Q_s nF**	**$\propto_s$**	**G_m, µS**	**C_m, nF**
8:1	787	253	0.89	9.15	19.45
5:1	685	320	0.89	10.4	26.03
4:1	258	249	0.81	3.57	24.36
2:1	588	199	0.90	2.53	18.05
1:1	704	190	0.91	2.61	18.22

100% 18 lyso-PC	524	209	0.92	3.93	32.65
100% Triolein	980	186	0.66	1.55	13.22

Table 3.4: Bode plots for triolein and the 18 lyso-PC mixture of membranes. R_e is the resistance of the electrolyte solution, Q_s is the imperfect capacitance of the electrode-reservoir region as modelled by a constant phase element (CPE), $\propto s$ is the dimensional constant of the CPE, G_m is the membrane conductance and C_m) is the membrane capacitance

3.3.11 Triolein membrane with perfusion pump

This part of the study is to demonstrate that triolein tethered membranes can be used as a sensor *in-line,* as would be the case when connected to a lipase-producing bioreactor. Figure 3.17 shows the triolein membranes with and without a perfusion pump with tris buffers. The MINIPULS 3 pump with four channels (Gilson, USA) was used in these experiments.

The 100 U/mL CRL and ROL enzymes were tested on the triolein membranes to compare the differences. The CRL in tris buffer without the pump showed a higher conductance increase compared to when the pump was operating (Figure 3.17A). ROL also shows similar responses with and without the pump operating (Figure 3.17B). This pump operated at 50 µL/min speed, and this is the best speed that the perfusion pump operated without creating air bubbles or giving the least disturbance in the membrane.

Overall, the attempt to create continuous flow through the triolein membrane is not efficient compared to without the pump. When it comes to creating a sensor it also can be an on-and-off sensor still in-line with the bioreactor.

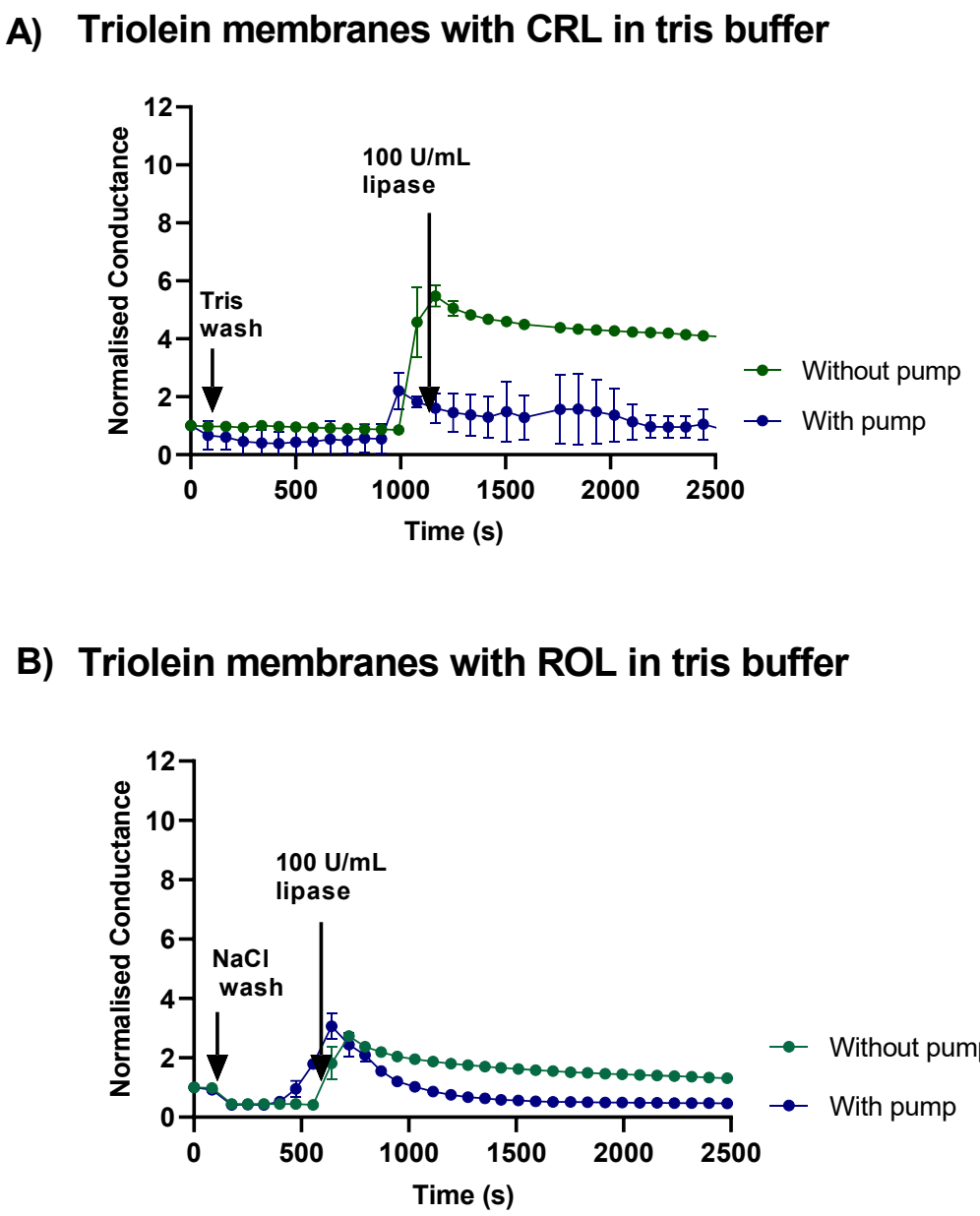

Figure 3.17: Triolein membrane with A) *Candida rugosa* lipase (CRL) with and without a perfusion pump operating with lipase in tris buffer and B) *Rhizopus oryzae* (ROL) with and without a perfusion pump operating with lipase in tris buffer. The data represent the mean ± standard error of the mean of n = 3 experiments.

3.4 Discussion

The data presented indicates it is possible to create a triolein tethered membrane architecture. The Bode plots of the triolein membrane suggest that triolein can create a membrane that can be fitted with a simple equivalent circuit, as depicted in Chapter 2.2.4. That this model fits so well suggests that a homogenous membrane has been formed rather than just triolein micelles forming around the tethers, Figure 3.2. Further, the response to PPL and Bode plot data in Chapter 3.3.1 indicates that when the triolein is mixed with DOPC, the self-assembly process typically incorporates one lipid in preference to the other. Which lipid gets priority is dependent on the relative amounts of each lipid.

Some phospholipase A_2 isotopes require the presence of Ca^{2+} ions to upregulate enzymatic hydrolysis [224, 225] and can hydrolyse the lipids with the ester group in the sn-2 chain. This was demonstrated in the previous chapter, Figure 3.4. On the other hand, this is less evident with the pancreatic lipases tested on the triolein tethered membranes, Figure 3.4A. Pancreatic lipase from the pancreas is released as an active enzyme; however, in the activation of pancreatic lipase, Ca^{2+} ion and colipase are sometimes required [226]. This study shows that the PPL enzymatic reaction is slightly higher when Ca^{2+} ions are present in the enzymatic buffer. Furthermore, this suggests that triolein membranes can detect the PPL activity without the presence of the colipase. Human pancreatic lipase shows maximum activity at pH 7.5 to 8.5 [227] and the results in Figure 3.6 indicate that at pH 7 the porcine pancreatic lipase also shows the highest conductance on triolein membranes. Figure 3.6 would suggest that lipid packing can be altered by the pH and the presence of divalent cations in the surrounding buffer solution. This has also been shown in tBLMs EIS study by Lowe, L.A. et al. 2022 [223]. In this work they demonstrated a similar impact of pH-induced changes in lipid packing on oleic acid-single chain fatty acid bilayers.

Chapter 3.3.5 showed the results of testing the enzymes when delivered in whole horse blood. The DOPC and diether-PC membranes both showed conductance increases in horse blood without the presence of added enzymes. However, triolein membranes do not show any marked conductance increase as a result of being in horse blood. Healthy horse blood is known to contain phospholipase A [228, 229]. This could be the main reason the

conductance increases in the DOPC tBLMs with whole blood. On the other hand, the conductance increases also occurred in diether-PC tBLMs when immersed in whole blood. This could be a result of the presence of phospholipase C, which catalyses the cleavage of phospholipids at the phosphate of the head group region [230, 231]. This would suggest that DOPC and diether-PC tBLMs are not suited to sensing enzymatic abnormalities using samples of whole blood.

Pancreatic lipase activity increases with Ca^{2+} ions [232], which is reflected in the results presented here (see Figure 3.4A). Furthermore, triolein-tethered membranes do not respond to PLA_2. Therefore, in a biosensor, triolein tethered membranes could feasibly be used for pancreatic lipase detection and potentially as negative controls for inflammatory bowel disease diagnostics that rely on sensing PLA_2. However, when whole horse blood was used in this research to determine if the triolein-tethered membranes can be used as an acute pancreatitis sensor, the porcine pancreatic lipase seemed to lose its activity.

When pure blood or serum is added to the membranes, the conductance drops slightly (Figure 3.7). This is a similar change that can be seen with the Ca^{2+} ion buffer wash on the membrane. This calcium response is likely as a result of the ion intercalating with the polar oxygens of the lipids [215]. This is expected, as the whole blood Ca^{2+} ion levels are 1.45-1.75 mmol/L in healthy horses [233]. Triolein tethered membranes show the similar effects to PC tBLMs which might be as a result of Ca^{2+} induced lipid condensation due to the presence of ester oxygens in the triglyceride fatty acid chains.

There are a few reasons why the blood shows near zero activity; one of the reasons that the whole blood experiment is not able to detect the PPL could be that red blood cells also act as a substrate and absorb all the PPL. Also, pancreatic lipase inhibition from other blood components might be another reason. However, Figure 3.8B, shows that when PPL is added directly into serum there is evidence of membrane hydrolysis occurring. There was also evidence of membrane hydrolysis when the PPL was present in whole blood that the serum that had been separated from. This suggests the sensor should be able to detect pancreatic lipase in a patient's serum, just not whole blood. What the component(s) of whole blood are that might be inhibiting PPL activity remains to be determined.

The experiments detailed in Chapter 3.3.6 were exploratory experiments to identify if pancreatic lipase activity could also be detected from frozen stool samples. The results show that there was no conductance increase on triolein membranes in these two patient samples, unlike for DOPC tBLMs. However, this data does indicate that triolein tethered membranes can be used with stool samples as there did not appear to be any non-specific activity.

The next aim of this study was to create a sensor that can detect lipase activity during enzyme production in bioreactors. Triolein membranes with industrial lipases seem to show membrane rearrangement after hydrolysation. Therefore, attempts were made to create triolein-fatty acid mixture membranes to improve the sensing ability in response to lipase hydrolysation. The hypothesis for this part of the study was that the membrane *critical packing parameter* (CPP) changes when shorter or longer fatty acid tails were incorporated into the triolein membrane. However, the data in Figure 3.11, Figure 3.13, and Figure 3.15, show that any mixture of lyso-PC lipids or oleic acid does not have better conductance changes in response to enzymatic hydrolysation than 100% triolein membranes.

The triolein membrane with perfusion pump experiments shows that the best hydrolysation is detectable in buffer without the pump functioning. The experimental results (Figure 3.17) suggest that the flow prevents lipases from binding with the triolein substrate. Even though the conduction increases when the pump was running was reduced, hydrolysis was still detected. This suggests that the industrial lipase detection sensor can be used *in-line* with a bioreactor. Alternatively, the sensor could simply be used to monitor lipase production *off-line*.

3.5 Conclusion

In conclusion, triolein can form a tethered membrane and is able to be used to test the activity of lipases using electrical impedance spectroscopy. Triolein tethered membranes show similar effects in response to Ca^{2+} ions in that the presence of the divalent cations can reduce membrane conduction. The same is true with reducing the pH, albeit to a lesser degree in triolein tethered membranes than with phospholipid tBLMs.

The electrical impedance spectroscopy experiments with triolein tethered membranes that incorporate different ratios of oleic acid, 17 lyso-PC or 18 lyso-PC molecules suggested that hydrolysation detection is best when 100% triolein in used. This observation indicates that the enzymes do indeed penetrate the 100% triolein substrate. What is also interesting is that the triolein tethered membranes show signs of membrane recovery after hydrolysation. This, and other unknown factors with the triolein tethered membrane, such as its thickness, water content, and structure (monolayer, bilayer or multilayered) are explored using neutron reflectometry in Chapter 4.

4 Neutron reflectometry characterisation of tethered membrane phospholipase and lipase sensors

4.1 Introduction

Chapter 3 presented electrical impedance spectroscopy (EIS) data around a new tethered membrane architecture using *triolein*. The EIS data deduced that these triglyceride membranes form tethered membranes that are slightly leakier than the well-established phospholipid membranes. For these measures, a lower capacitance is suggestive of a thicker membrane. As water is dielectric, it can increase the capacitance of the membrane. This might suggest that these triglyceride membranes appear thinner than they are. However, the multilamellar and unilamellar properties of tethered membranes are not to be readily observable using EIS techniques. In this chapter, the thickness and water-containing properties of these unique substrate-anchored triglyceride membranes are characterised using neutron reflectometry (NR).

4.1.1 Neutron Reflectometry (NR)

Neutron reflectometry (NR) is a diffraction technique that can measure a thin film's chemical composition, roughness and thickness. The neutron scattering technique is used to determine a material's structure and composition and is widely employed in engineering, scientific research, medicine, transportation, mining and building [234].

NR is similar to ellipsometry or X-ray reflectivity. Fermi and Zinn first demonstrated a mirror reflection of neutrons in 1944 [235-237]. A neutron is scattered with the matter in two ways; with nuclei via the strong nuclear force or as a result of magnetic moments produced by unpaired electrons [238]. However, most neutrons directed into a thin layer of matter pass through without any interaction.

There are two main sources of neutrons, either from fission or spallation sources. Some nuclei can undergo fission spontaneously; however, uranium 233, 235 and 239 can fission from a chain reaction due to neutron emissions This reaction happens when nuclei break apart and more neutrons are released. Alternatively, a spallation source is a high-flux neutron source in which protons that have been accelerated to high energies hit a heavy target material like mercury and tantalum. The individual nuclei are sent into a highly excited state, causing the emission of neutrons. Each proton delivered to the target results in approximately 15-20 neutrons.

When the neutrons are incident on the sample, they can be scattered, absorbed or transmitted by the samples. During neutron reflectometry, it is the scattered and/or transmitted beam that is measured to obtain sample information.

4.1.2 Principles of neutron reflectivity

Neutrons are treated as wave particles, and therefore, the scattering from the material can be modelled according to Bragg's law, where $2d \sin\theta = n\lambda$.

Where d is the distance, θ is the scattering angle, λ is the wavelength, and n is an integer to determine the scattering order. Here the assumption is the neutron beam is reflecting from an infinite flat surface. In Figure 4.1, k_f is the final scattering vector, and k_i is the incident momentum vector. The scattering vector is known as Q, such that with *elastic scattering*:

$$|k_i| = |k_f| = |k| = \frac{2\pi}{\lambda}$$

and

$$Q = 2\,sin\theta.|\,k| = \frac{4\pi\,sin\theta}{\lambda}$$ [239].

Neutron reflectometry data of elastically scattered neutrons are typically plotted as intensity (or reflectivity) vs Q per Angstrom distance.

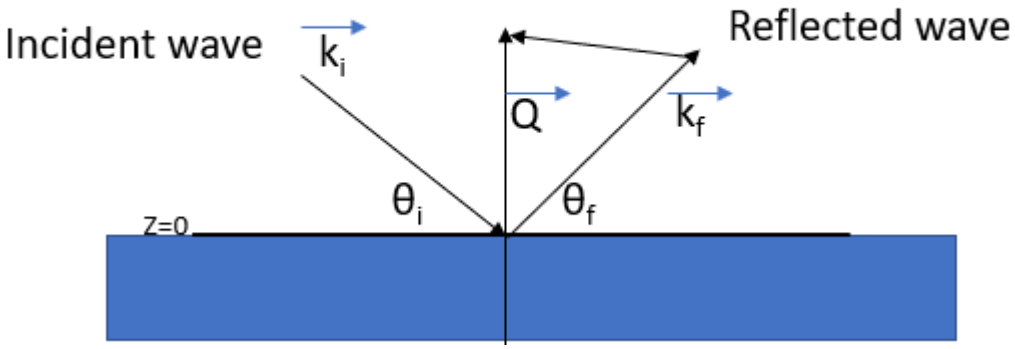

Figure 4.1: The sketch of the Incident neutrons and scattered neutrons. The wave vectors of the incident (k_i) neutrons and the scattered neutrons (k_f) are depicted along with the momentum-transfer vector (Q).

If a single homogenous layer (such as a lipid bilayer) of thickness *d* is deposited on the surface of a perfectly flat substrate of what can be considered to be infinite thickness, then the system contains three different media such as air, the single homogenous layer and the substrate. The refractive indices change between each layer creates two interfaces: an air-layer interface and a layer-substrate interface. An incident neutron beam comes from the air and is partially reflected at the first surface and partially transmitted through the layer, where it can then be partially reflected at the second surface. The two reflected beams can interfere constructively or destructively depending on the relative thickness of the deposited layer. The reflectivity curves will then exhibit interference fringes that can be used to measure the thickness of the layer [239], Figure 4.2.

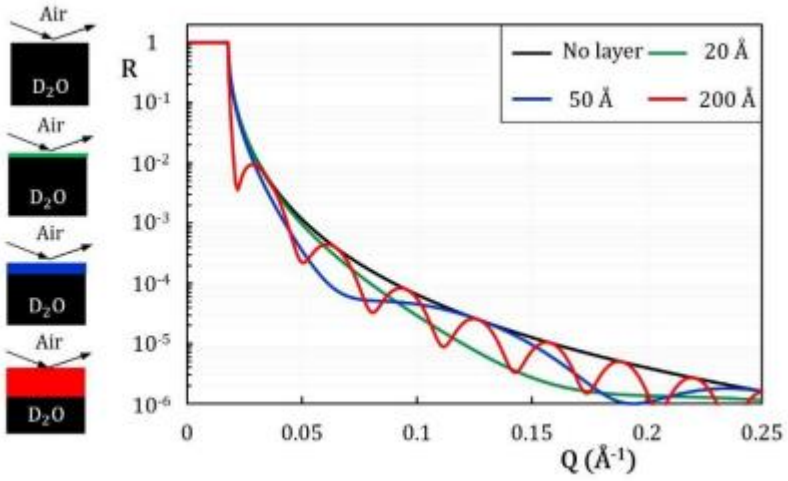

Figure 4.2: The single layer reflectivity at the air/D_2O interface at thicknesses of 20, 50, 200 Å and without a layer are shown by green, blue, red and black, respectively. This figure is sourced from [239] *EPJ Web Conf. Volume 236, 2020, An introduction to neutron reflectometry, Fabrice Cousin and Giulia Fadda, This is an Open Access article distributed under the terms of the Creative Commons Attribution License 4.0, which permits unrestricted use, distribution, and reproduction in any medium, provided the original work is properly cited:* With kind permission of The European Physical Journal (EPJ).

The curves in Figure 4.2 shows the single later reflectivity at the air/D_2O interface at thicknesses of 20, 50, and 200 Å and without a layer are shown by green, blue, red and black, respectively. The green curve shows the reflectivity of a thin layer with a thickness of 20 Å. The layer interacts with the D_2O interface at this thickness, leading to a specific pattern of reflected neutrons. The blue curve indicates the thicker layer with a thickness of 50 Å at the same air/D_2O interface. The position and shape of the peak in the reflectivity curve reveal information about the structural characteristics of the layer, such as its density, roughness, and thickness.As the thickness of the layer increases, the reflectivity pattern changes and additional features might appear in the curve. The peak position and intensity can provide insights into the changes in the layer's structure and properties compared to the 20 Å thickness.The red curve shows the reflectivity of an even thicker layer with a thickness of 200 Å. The reflectivity curve will further differ from the previous two cases as the layer becomes thicker. It might show additional oscillations and variations, indicating more complex interactions and structural changes within the layer.The black curve represents the reflectivity measurement taken without any layer at

the air/D_2O interface. This serves as a reference or baseline measurement, allowing researchers to distinguish the contributions of the layer from the underlying D_2O interface. In summary, the curves in Figure 4.2 shows the single layer reflectivity at the air/D_2O interface changes with varying thicknesses of the layer. These reflectivity patterns provide valuable information about the structural and compositional characteristics of the thin film.

4.1.3 Scattering length density (SLD)

Scattering length density (SLD) is the measure of the scattering power of a material. It is the ratio of the scattering length to the density of the material. The SLD for a material can be calculated by fitting the scattering data to a model of its proposed structure. The scattering length density for water is -0.5 $Å^{-2}$, and for D_2O, it is 6.35 $Å^{-2}$ [240]. Because deuterated molecules have a very different SLD than hydrogenated molecules, they can be used to create contrast in neutron scattering experiments. Table 4.1 shows the calculated SLD values for all the layers used in the tethered membrane NR experimental setups.

	Molecular formula	Density (g/cc)	Neutron SLD ($Å^{-2}$)
Cr		7.19	3.03
Au		19.35	4.67
Thiol 100%			0.87 [171]
Space 100%	Benzyldisulphide-TEG-OH		0.98 [171]
Tethered	$C_8H_{18}O_5$	1.125	0.6
Tether and spacer			0.94
h-triolein	$C_{57}H_{104}O_6$	0.9078	0.15
d-triolein	$C_{57}D_{104}O_6$	1.107	7.46
DOPC	$C_{44}H_{84}NO_8P$		0. 30
D_2O		1.04	6.3
H_2O		1	-0.56
Mixture of H_2O (25%) and D_2O (75%)			4.5

Table 4.1: Theoretical or calculated neutron scattering length density for all the structural layers in the experiment.

4.1.4 Membrane measurements with the Platypus Neutron Reflectometer

Platypus is a neutron reflectometer at the OPAL reactor in Lucas Height, Sydney, Australia. Platypus is a time-of-flight spectrometer. Time-of-flight spectrometers have many advantages, such as they allow simultaneous measurement of a large region of energy and wavevector space, giving a good overview of the excitations which allow unexpected phenomena to be observed.

The first chopper in the instrument spins and lets neutrons through once per revolution. The second chopper spins at the same rate and is phased so that it opens at a specific time later. The phase is chosen to let through only neutrons of a specific velocity and energy. All these choppers are made with neutron-absorbing material of boron-10 to absorb the unwanted neutrons. Platypus contains four different slits to select the beams and provides the neutron bandwidth range from 2.5 to 18 Å. The selected beam scattered through the sample is measured with the helium (He) detector. This determines the time of arrival of the scattered as well as the number of neutrons.

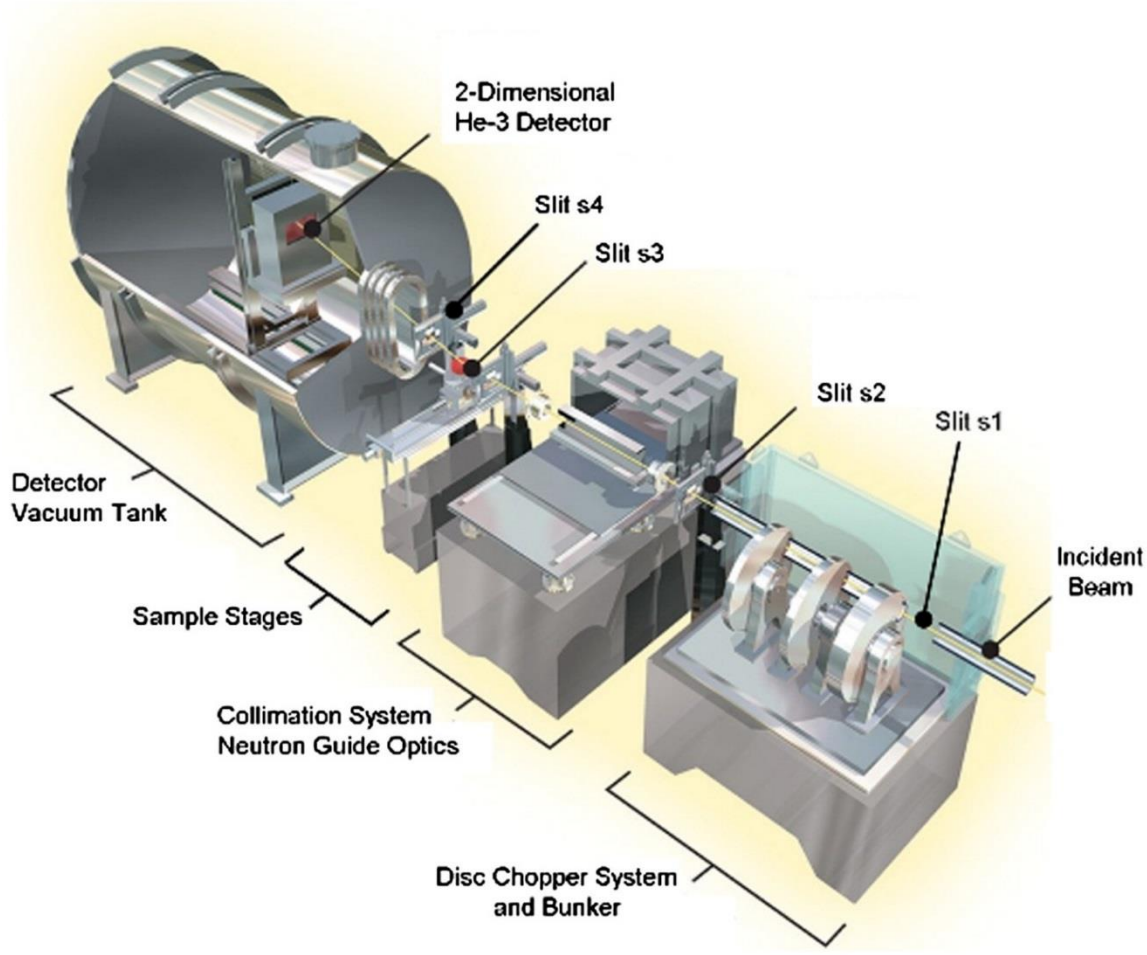

Figure 4.3: The Platypus neutron refractometer at OPAL reactor in Sydney, Australia. The figure was used with permission from James, M., et al. (2011) [241].

The Platypus Neutron Reflectometer is a flexible and multipurpose instrument that can measure soft and hard materials at air/liquid interfaces, solid/liquid and solid/air interfaces [241]. Therefore, this instrument can give the data for this project which gives the thickness and the water volume fraction of triolein tethered membranes. This data can provide information on whether the membranes are single layer, bilayer or multilayers.

4.2 Material and Method

4.2.1 Lipids and Triglycerides

Unless mentioned below, the lipids used in these experiments have been previously described in Chapter 2.2.2 and Chapter 3.2.3. The analytical grade d-triolein powder was supplied from the National Deuteration Facility at ANSTO, Figure 4.4. All the lipids were dissolved in 100% ethanol to prepare a 12 mM concentration. All these lipids and triglycerides were stored at -20 ºC.

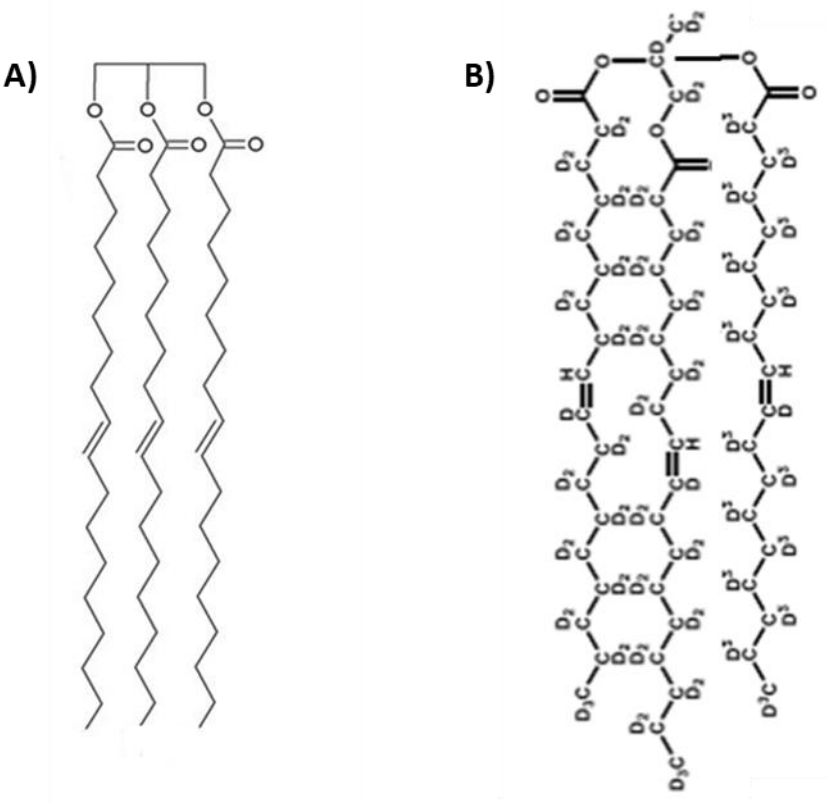

Figure 4.4: The structure of A) hydrogenated-triolein and B) deuterated-triolein.

4.2.1.1 Buffers

Tris buffer and Ca^{2+} buffer (see Chapter 2.2.1 for more details) were used for neutron scattering experiments. Three different contrasts were made, one using ultrapure water, one using D_2O (National Deuteration Facility, ANSTO) and a gold-matched version incorporating 75% D_2O with 25% H_2O. In NR, "gold-matched" means a gold layer is employed to calibrate the experimental setup and accurately determine the sample's reflectivity. Gold is commonly chosen as the matching material due to its well-known neutron scattering properties and relatively high neutron scattering length density.

4.2.1.2 Phospholipase and lipases

10 U/mL of porcine pancreatic lipase (PPL), phospholipase A_2 (PLA_2), and *Aspergillus niger* lipase (ANL) were prepared in calcium buffer at pH 7. Phospholipase A_2 was used in the DOPC membranes with the 1.2 U/mL activity, which was prepared with calcium buffer. All these chemicals were ordered from Sigma-Aldrich Australia, and D_2O was supplied from the National Deuteration Facility, ANSTO.

4.2.1.3 Sample cell and preparation

The silicon wafer is used to prepare the membranes, and it has two additional layers. The first is a chromium layer $\sim 6\ to\ 9\ nm$ and the second layer is a thin gold layer $\sim 30\ nm$ except for one sample that was 16 nm. Figure 4.5 shows the cell which was used to create the lipid layers. Shown are the top view (Figure 4.5A) and the side view (Figure 4.5B). All the experiments were conducted at the Australian Nuclear Science and Technology Organisation (ANSTO) at Lucas Heights, New South Wales, Australia.

All the samples were prepared as follows: newly coated silicon wafer was cleaned with ultra-pure water, ethanol, and isopropanol, then dried with nitrogen gas, and finally, the silicon wafer was ozone cleaned. The 1st step is to coat the tethered layer on the wafer; to do that, cleaned silicon waters were soaked in the T10 solution (mentioned in Chapter

2.2.4) for 1 to 2 hrs at 4 ºC. The 2nd step is to form a lipid layer around the tethering molecules whereby 1 mL of relevant lipid or triglyceride ethanolic solutions (depending on the experiment) were injected into the closed cells shown in Figure 4.5.

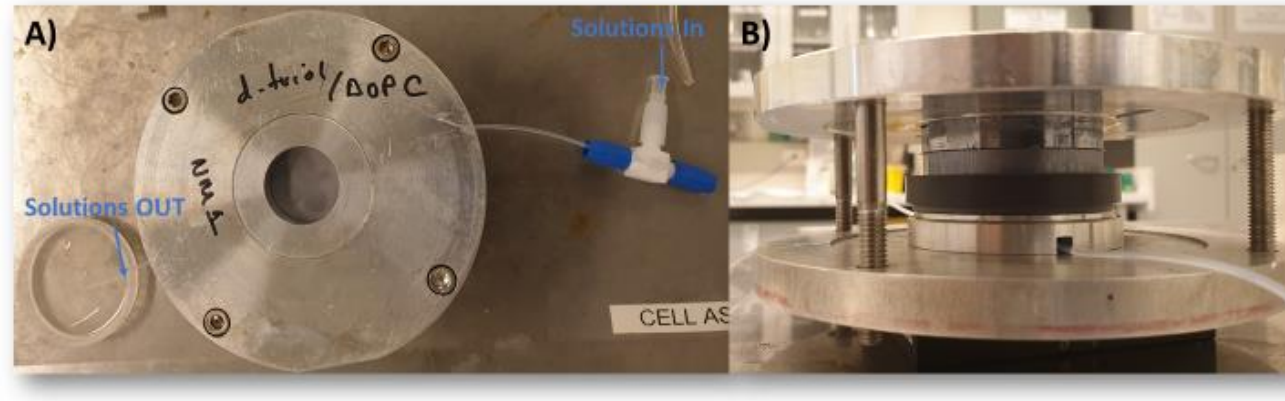

Figure 4.5: The sample cell preparation for the neutron reflectometry experiments of A) top view, where you can see the solution in and out and B) side view of the cell, where can see the different hard visible layers.

Once adequately sealed, the bilayer was formed through rapid solvent exchange after 20 mins incubation. This was achieved by quickly flushing the cell with 20 mL of buffer solution. Then the samples were first tested in the presence of the D_2O, H_2O and the mixture of D_2O, H_2O contrast solutions (see Table 4.1) using the Platypus neutron reflectometer. To collect the NR data after the hydrolysation, 1 mL of lipase or phospholipases were injected into the cell and left for 20 mins before washing with the relevant buffer.

Figure 4.6A shows a schematic diagram of the sample setup for neutron reflectometry and the pathway of the neutron beam to the sample and from the sample. Figure 4.6B and C show an illustration of triolein (if it forms a bilayer) and phospholipid bilayers on the silicon wafer, respectively.

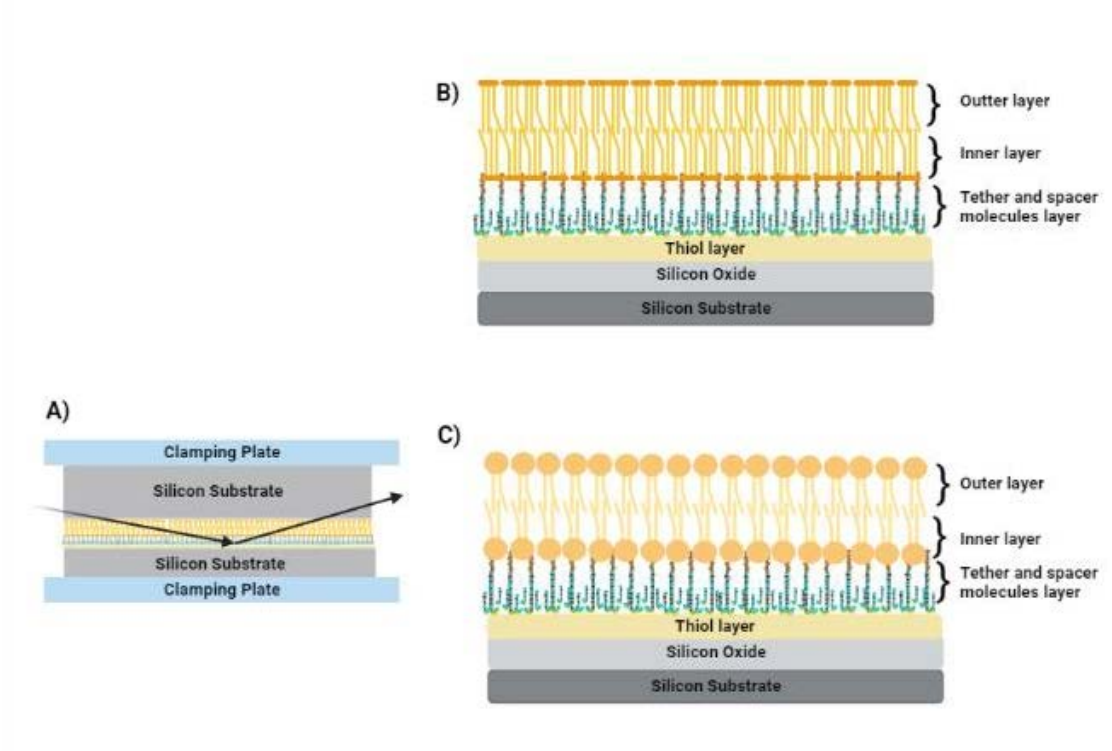

Figure 4.6: A) This is a schematic diagram of the sample setup for the neutron reflectometer measurements from the solid-liquid interface. The illustration of B) triolein as a purported bilayer and C) phospholipid bilayers on the silicon wafer.

4.2.1.4 Software

Neutron reflectometry data were fitted in the *refnx* environment with the simultaneous refinement of multiple contrast datasets employing H_2O, mixture of 25% H_2O and 75% D_2O, and D_2O bulk solutions. The *refnx* is a python package for generalised curving fitting analysis for x-ray and neutron reflectometry data. NR data were fitted using "slabs" with four main parameters for all the layers, namely scattering length density (SLD), thickness, roughness and water volume fraction.

In each layer, the SLD was either fixed based on the known materials present in the layer or permitted to vary in order to provide the best fit to the data. Using the architecture described in Figure 4.6, the data were fitted to Si, Cr (on the silicon wafer), Au, thiol, tether region, and inner and/or outer lipid layers. Gold-thiol interactions play a vital role in electrochemical impedance spectroscopy (EIS) because they enable immobilization of

biomolecules and functional molecules onto gold surfaces. This coordination interaction firmly sulphur atoms in thiol groups to the gold atoms on the surface.

4.3 Results

There were four different sample data sets collected using neutron reflectometry. The 1st experiment is DOPC before and after the addition of phospholipase A_2. The 2nd experiment is the deuterated triolein (d-triolein) membrane before and after the addition of porcine pancreatic lipase. The 3rd experiment is of a d-triolein and DOPC mixture 80:20, respectively. The 4th experiment is hydrogenated triolein before and after the addition of *Aspergillus niger* lipase.

4.3.1.1 DOPC with phospholipase A_2

This experiment was set up to compare a triolein with a DOPC membrane's neutron reflectometry data. Figure 4.7A shows the reflectivity data profiles for a DOPC tBLM with D_2O, H_2O and gold-matched buffer contrasts before adding phospholipase A_2. These data were then fitted with the following structural layers; Au, spacer, tethered, inner leaflet, outer leaflet and backing (surrounding buffer).

Figure 4.7B shows the SLD versus distance data for a DOPC tBLM before and after adding 1.2 U/mL PLA_2. Figure This figure shows the difference in the SLD for the D_2O solution before and after PLA_2. This is an indication of the membrane hydrolysation with PLA2. An *indicative-only* fitting was done where, like the gold and backing buffer, the spacer and tether layers had predetermined fixed SLD, thickness and water content values. In these fits, the SLD value in the inner and outer layers was reduced after adding the PLA_2. The inner and outer layers' thicknesses were calculated to be 1.85 and 2.07 nm, respectively, before adding the lipases. After adding the PLA_2, the inner and outer layers' thicknesses were calculated to be 2.35 and 1.81, respectively. Therefore, the indicative bilayer thickness before adding PLA_2 was 3.92 nm and 4.16 nm after the addition of the enzyme.

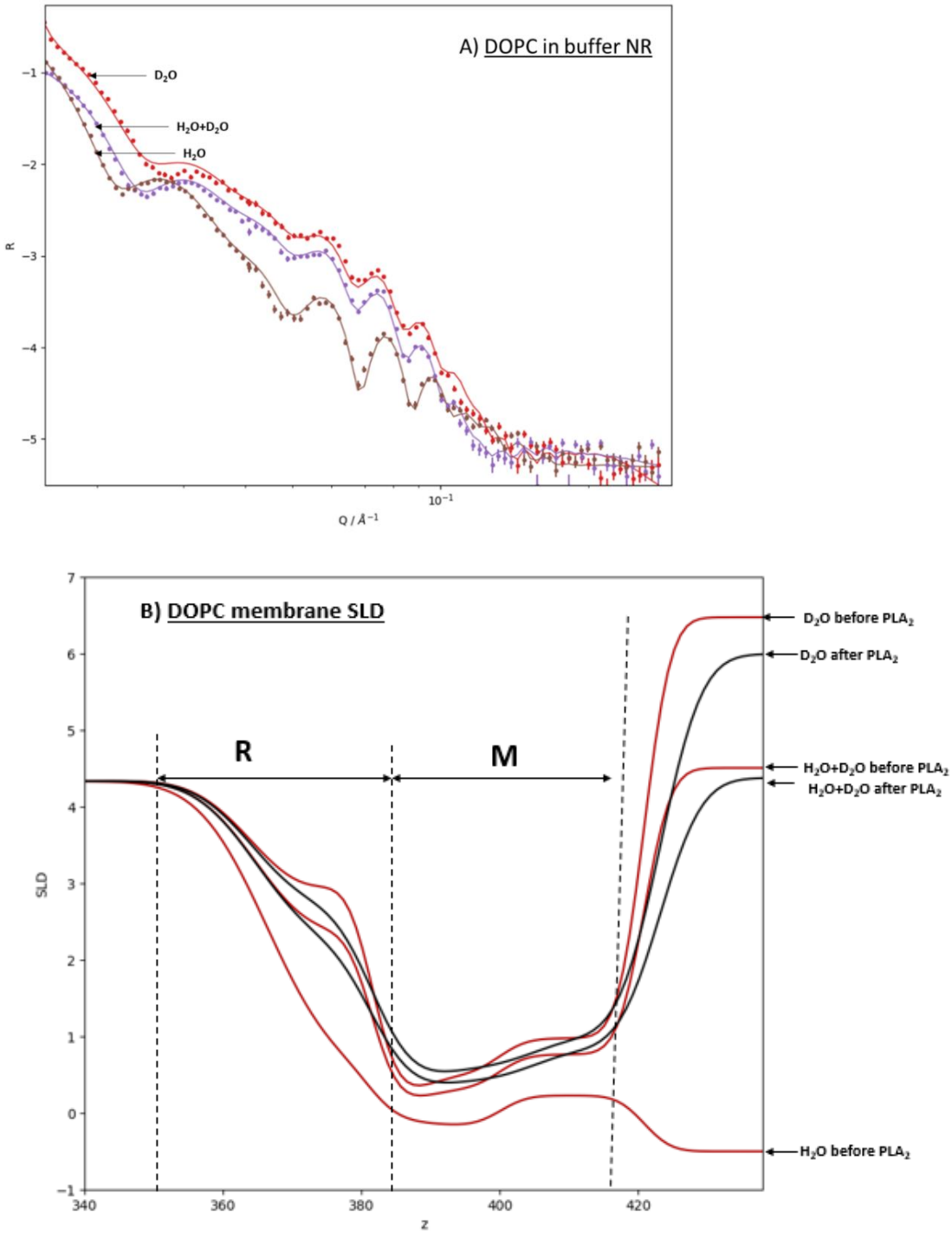

Figure 4.7: DOPC membrane with H_2O, D_2O and a gold-matched mixture of H_2O and D_2O A) neutron reflectometry data and B) scattering length density (SLD) versus distance (z) before and after adding PLA_2. NB, due to equipment failure, no H_2O contrast data after the addition of PLA_2 was available. *R* represents the reservoir region between the gold substrate and the membrane, and *M* represents the membrane.

The water volume fraction of the bilayer showed little difference before or after the addition of PLA_2. Table 4.2 summarised the data for DOPC tBLMs' inner and outer layers before and after adding the PLA_2.

	Thickness (nm)	**SLD**	**Water volume fraction**
Spacer	0.75*	0.98*	0.002*
Tether	0.80*	1.21*	0.50*
Inner layer before PLA_2	1.85	-0.14	0.10
Outer layer before PLA_2	2.07	0.12	0.10
Inner layer after PLA_2	2.35	-0.03	0.11
Outer layer after PLA_2	1.81	0.43	0.10

Table 4.2: Summarised data for DOPC tBLMs' inner and outer layers before and after adding the PLA_2.The * indicate the values that are fixed during the fitting.

4.3.1.2 D-triolein tethered membranes with pancreatic lipase

Figure 4.8A shows the indicative bilayer-fitted neutron reflectometry data for the d-triolein membranes. All these data were fitted with structural layers; Au, spacer, tethered, inner leaflet and backing (buffer region).

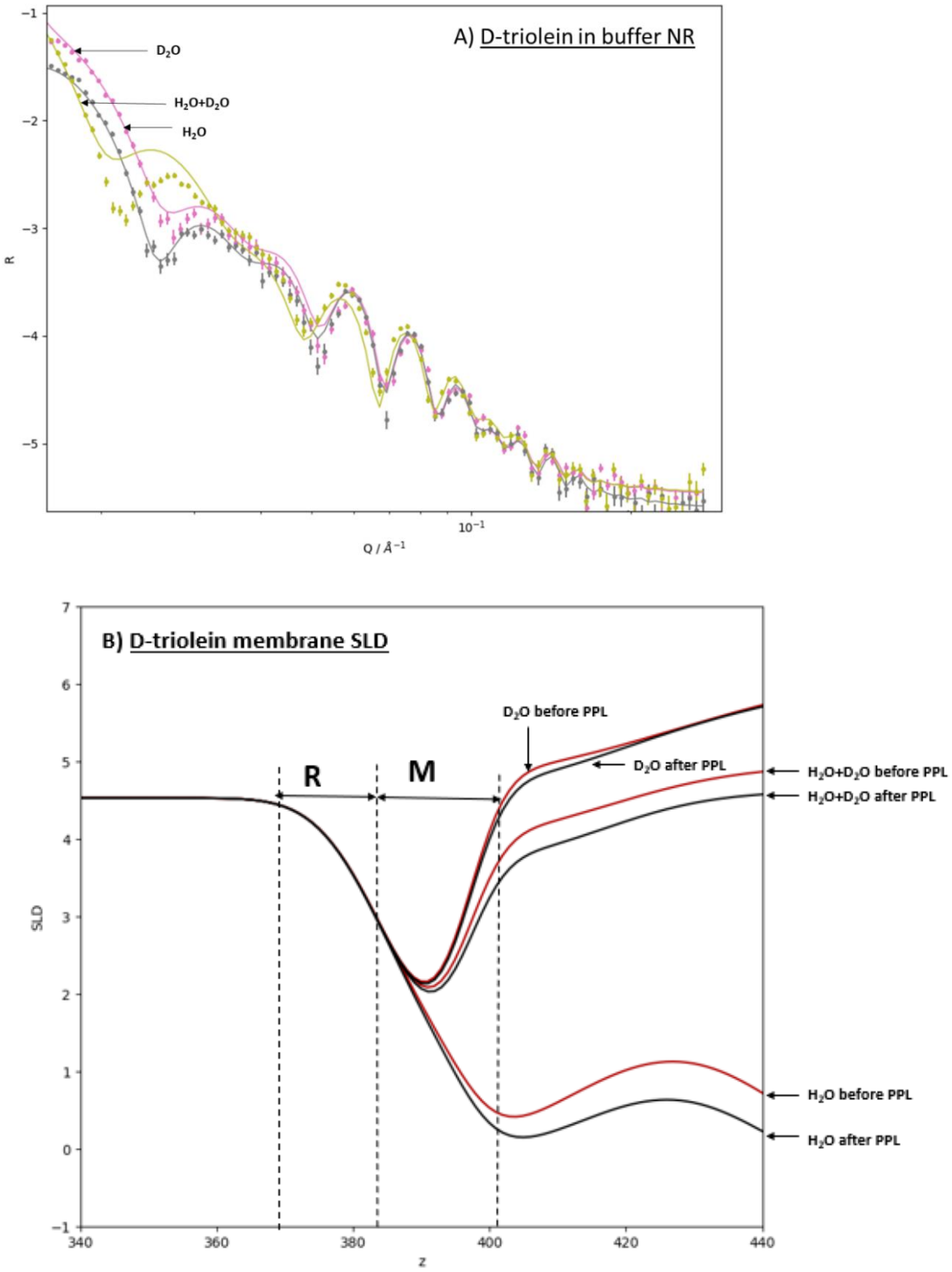

Figure 4.8: d-triolein membrane with H_2O, D_2O and mixture of H_2O and D_2O A) neutron reflectometry data versus Q vector and B) scattering length density versus distance before adding PPL and after adding PPL. *R* represents the reservoir region between the gold substrate and the membrane, and *M* represents the membrane.

Figure 4.8B shows the SLD data for the d-triolein membrane before adding PPL and after adding PPL. As with the DOPC tBLM, indicative-only fitting was done where, like the gold and backing buffer, the spacer and tether layers had predetermined fixed SLD, thickness and water content values. In these fits, the SLD after adding the PPL has slightly reduced compared to the membrane in the buffer solution alone. The lowest Q value shows the background noise and the data in lowest Q is not reliable. Table 4.3 shows the summarised data for d-triolein before and after the addition of PPL. The membrane thickness was calculated to be 2.37 nm prior to the addition of PPL and 2.27 nm after. The water volume fraction in the membrane increased by 17% following the addition of PPL. Overall, the NR data would seem to suggest that d-triolein forms a monolayer; however, caution is needed given the very high water volume fraction. This would suggest there is poor membrane coverage.

	Thickness (nm)	**SLD**	**Water volume fraction**
Spacer	1.20*	0.98*	0.002*
Tether	1.98*	1.02*	0.74*
Membrane before PPL	2.37	4.82	0.50
Membrane after PPL	2.27	4.44	0.67

Table 4.3: Summarised data for d-triolein inner and outer layers before and after adding the PPL. The * indicate the values that are fixed during the fitting.

4.3.1.3 D-triolein and DOPC mixture tethered membranes with PPL

This experiment was designed to see if tethered membranes can be formed with a mixture of triolein and phospholipids. The membrane was prepared with d-triolein and DOPC mixture in a 4:1 ratio, respectively. EIS data indicated that it was possible to create tBLMs using this mixture (Chapter 3.3.1). The first attempt to fit this NR data was to the bilayer model. However, the data was difficult to fit. Therefore, the data shown below are single-layer fitted values to the d-triolein and DOPC mixture membrane. Figure 4.9A shows the d-triolein membrane's NR data in the buffer with three different contrasts (these data for the membrane were before adding the pancreatic lipase).

The SLD profile for the soft material region is shown in Figure 4.9B, and the summarised data is shown in Table 4.4. The thickness of the monolayer before adding the PPL is 2 nm and after adding the PPL is 2.38 nm. This could be due to lipases interacting with the membrane. The water volume fraction remained the same, even after adding PPL. Overall, this data fitting shows that when triolein is mixed with the phospholipids, it will most likely form a monolayer rather than a bilayer.

	Thickness (nm)	**SLD**	**Water volume fraction**
Spacer	0.99*	0.98*	0.03*
Tether	1.64*	1.94*	0.50*
Membrane before PPL	2.00	0.81	0.10
Membrane after PPL	2.38	1.20	0.10

Table 4.4: Summarised data for a mixture of d-triolein and DOPC tBLMs' inner and outer layers before and after adding the PPL. The * indicate the values that are fixed during the fitting.

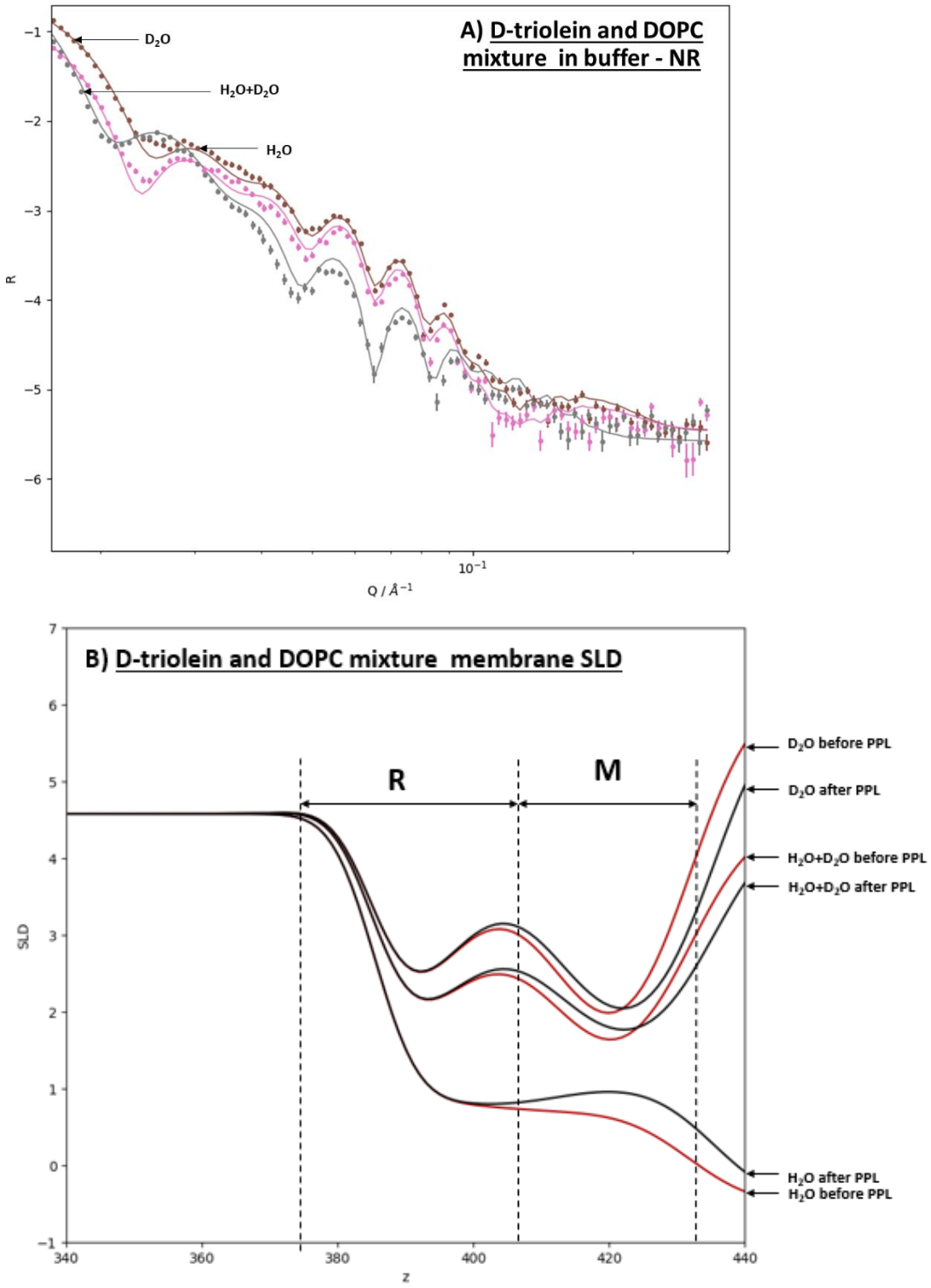

Figure 4.9: The mixture of d -triolein and DOPC membrane with H_2O, D_2O and mixture of H_2O and D_2O A) neutron reflectometry data and B) scattering length density before and after adding PPL. *R* represents the reservoir region between the gold substrate and the membrane, and *M* represents the membrane.

4.3.1.4 H-triolein membrane with *Aspergillus niger* lipase

Deuterium is an isotope of hydrogen, and deuterium has a similar geometric structure to hydrogen but contains an extra neutron in the nucleus. The mass of the atoms can affect the bond strength. Therefore, the heavier isotope can form stronger bonds. Stronger bonds cause bond-cleavage reactions to proceed more slowly, leading to the *kinetic isotope effect*, a well-studied concept in physical chemistry [242].

This part of the experiment was set up to analyse how hydrogenated triolein membrane properties compared to the aforementioned DOPC membranes and d-triolein membranes before and after adding a lipase. The reservoir region is a small gap or space between the solid substrate and the lipid bilayer. This gap allows for the presence of a solution. Figure 4.10 shows the well-separated reservoir region in the H-triolein membrane.

In this case, lipase from *Aspergillus niger (AN)* was used as it seemed to work better, based on EIS data (see Chapter 3.3.7). Hydrogenated data in Figure 4.10A shows the neutron reflectometry data for the h-triolein membrane in buffer using the three different contrasts. Figure 4.10B shows the calculated SLD for the soft matter region in the experimental setup before and after adding the AN lipase. An indicative-only measure of triolein membrane thickness was calculated to be 1.02 nm before and 3.16 nm after adding the AN lipase. Table 4.5 shows the summarised data.

	Thickness (nm)	**SLD**	**Water volume fraction**
Spacer	0.57*	0.98*	0.003*
Tether	0.82*	1.07*	0.71*
Membrane before AN lipase	1.02	-0.53	0.10
Membrane after AN lipase	3.16	-0.13	0.15

Table 4.5: Summarised data for an h-triolein membrane's inner and outer layers before and after adding the *Aspergillus niger* lipase. The * indicate the values that are fixed during the fitting.

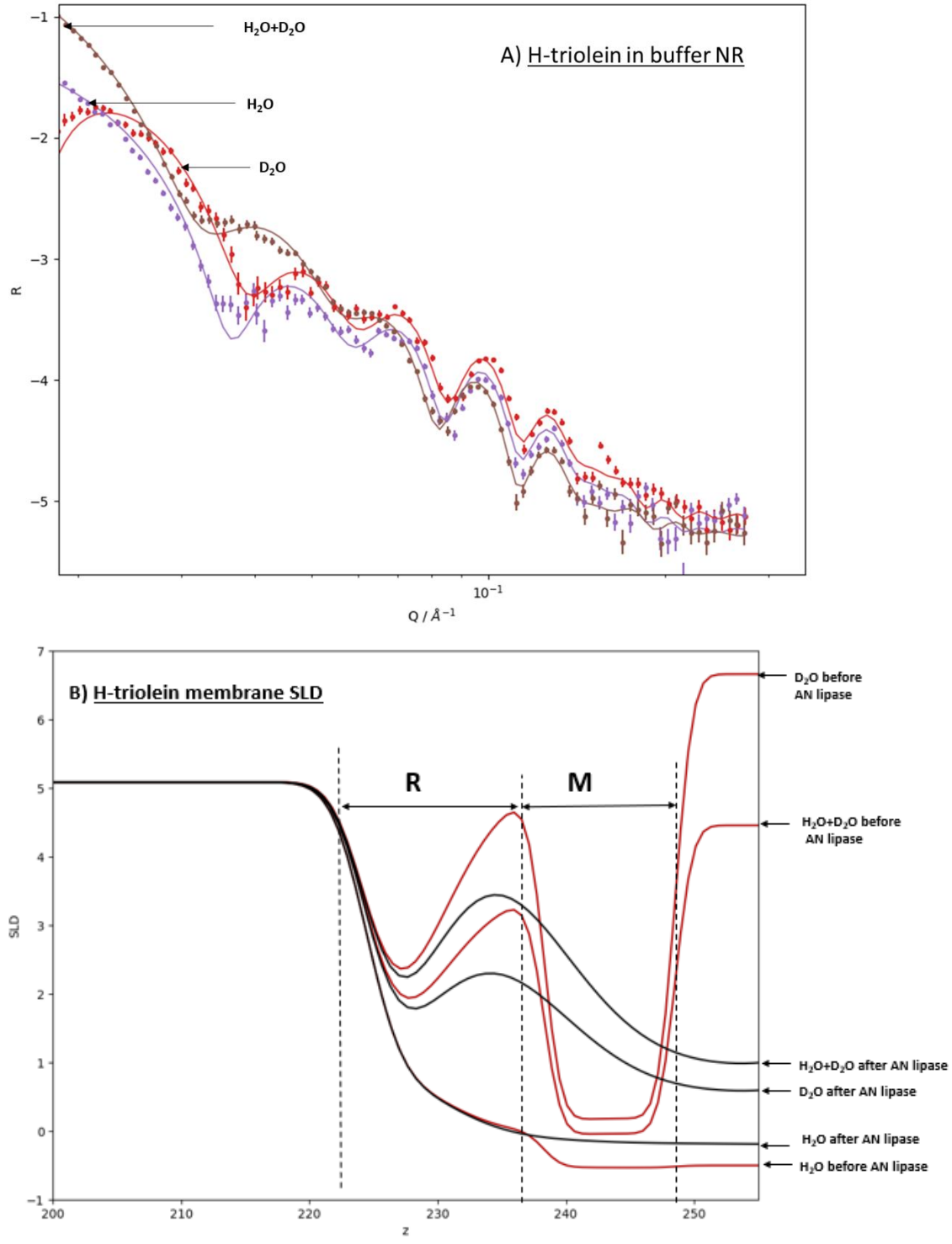

Figure 4.10: H-triolein membrane with H_2O, D_2O and mixture of H_2O and D_2O A) neutron reflectometry data and B) scattering length density before and after adding *Aspergillus niger* lipase. *R* represents the reservoir region between the gold substrate and the membrane, and *M* represents the membrane.

4.4 Discussion

Electrical impedance spectroscopy showed it was possible to create triglyceride-tethered membranes (see Chapter 3). However, the EIS data cannot confirm if triolein membranes were single-layer, bilayers or multilayers. Neutron reflectometry data was thus employed to provide structural information by measuring the scattering length density through the membrane normal [243].

The fitted data shows each experiment's various SLD values for the spacer and tether molecules. Therefore the thickness changes in each sample; thickness is not a variable directly controlled or influenced by experimental designs. It depends on how molecules behaviour, such as the molecular length. The same molecule can have different lengths in the solutions, leading to slight thickness and SLD changes. Therefore, these experiments did not use constant thickness or SLD for the spacer and tethered molecules. However, the results show the same SLD value for the spacer with slight thickness changes.

4.4.1 DOPC tBLMs with NR

The hydrogenated DOPC membrane shown here had an indicative thickness of 3.92 nm in the buffer, which agrees with the previously reported DOPC bilayer thickness of 4.0 to 3.8 nm [244-246]. Vacklin, H.P. et al. (2015) have studied the phospholipase A_2 effect on DOPC, POPC and DPPC lipid bilayer membranes deposited directly onto a surface using neutron reflectometry [247]. Their study used a *Naja mossambica nossambica* (cobra) PLA_2 0.01 g/mL. The DOPC membrane thickness in the tris buffer was shown to be 3.5 nm, and right after the PLA_2 was added it had reduced to 3.1 nm. After 4 h and 10 mins, their bilayer thickness was 2.6 nm. Their study shows that DOPC membrane thickness changes over time with the PLA_2.

In the current study 1.2 U/mL of PLA_2 sourced from the porcine pancreas was tested on the DOPC tBLMs with electrical impedance spectroscopy, where the results indicated significant hydrolysation occurred (see Chapter 2.3). The NR results suggest that the hydrolysation of the phospholipids was not sufficient for inducing significant changes in the overall membrane structure, unlike the reported bilayer of Vacklin et al, which saw

significant membrane disruption. it could be the tethers provide a more stable framework whereby fatty acids and phospholipase are able to co-exist as the membrane for longer periods. Hydrolysation would still be sufficient for inducing transient pore formation, as is evident from the increased conduction in the EIS data.

In this chapter, each sample has a similar membrane architecture. However, the exact thickness of tethering and spacer layers is different in each sample due to the molecule behaviour in the liquid phase. These molecules might not stretch to their fullest. Therefore, they will form layers of different thicknesses. This being the case, fixed values across different samples cannot be used, as it could present misleading data.

The experimental data for hydrogenated and deuterated triolein membranes could not be fit with bilayer or multilayer structures, whereas the monolayer structure shows the best fitting and reasonable SLD values that are close to the calculated SLD values. This suggests that triolein creates a monolayer membrane with the tethering chemistries employed. C20 phytanyl acts as membrane tethers, which could sit well with the lipid tails of the 18:1 triolein molecules.

The h-triolein membrane at D_2O contrast (SLD profile Figure 4.10B) shows the clear gold substrate and a reservoir (tether) region that is separated from the membrane. This shows the triolein membrane is not formed directly on the gold electrode, rather it is formed between the hydrophilic phytanyl regions of the tethers. However, the d-triolein membrane SLD profile (Figure 4.8B) shows a less separated reservoir region. The lack of a clear reservoir region in the fitting profile of the d-triolein tethered membrane might be due to the low membrane coverage and the high roughness in the membrane. The d-triolein membrane's water volume fraction was 49%, whilst the h-triolein membrane had a 10% water volume fraction. . The water volume fraction is essential in showing how packed the membrane is. A lower water volume fraction indicates a higher membrane packing density.

Hypothetically, these triolein molecules would align themselves between the tethers' hydrophobic C20 phytanyl groups (Figure 4.11). Due to their hydrophobicity, it is more likely that the C18 tails of the triolein molecules would be oriented towards the gold electrode rather than the bulk water, but it is difficult to confirm this experimentally.

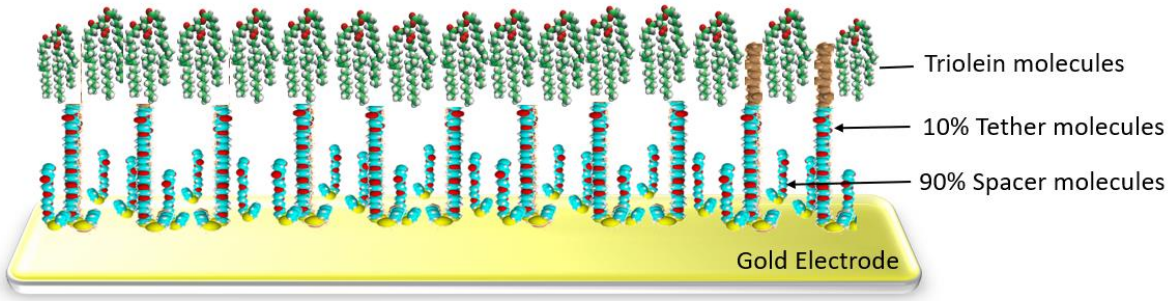

Figure 4.11: Proposed triolein monolayer formation with 10% tethered molecules.

The EIS data showed that the triolein membrane conductance increased with the addition of PPL, and after some time, conductance plateaued. The EIS data with the triolein membranes and industrial lipases showed similar effects. The indicative thickness of the hydrogenous triolein membrane was 1.02 nm before PPL, and after PPL it increased to 3.16 nm. Pancreatic lipase cleaves the sn-1 and 3 positions to form monoglycerides and free fatty acids. Conceivably, these products might rearrange to form micelles on the surface of the tethered membrane, which could be another reason for the membrane thickness increasing. Another possibility could be that the fatty acids and monoglycerides remain in the membrane, and this leads to an altering of the overall critical packing parameter of the monolayer which induces significant membrane curvature. Alternatively, the presence of the enzyme proteins themselves can interact with the membrane substrate leading to a perceived overall membrane thickness change.

The mixture of triolein and DOPC membranes give the best fit with a monolayer rather than bilayer fitting with NR. However, from the contrasts used (H_2O and D_2O), it is unclear where the reservoir region of the tethered membrane starts, and the membrane is. This would suggest that both hydrogenated DOPC and deuterated triolein are present. Interestingly, this mixture with EIS shows the enzymatic reaction only with PPL and not PLA_2 (Chapter 3.3.1). In nature, triglyceride content in cellular membranes is typically between 3 to 5% [248]. Pakkanen, K.I., et al. (2011) have studied the triglyceride-phospholipid membranes' mechanics and dynamics [249]. They used a 1:9 triolein and

POPC mixture ratio to prepare vesicles. They determined that only 5 mol % of triolein could be included in these membranes.

This would suggest that triglycerides are poorly incorporated into phospholipid bilayers. The research presented here suggests the reverse is true as well. This could be due to a combination of factors related to both molecular properties, such as their structure and packing. There are two unsaturated acyl chains in DOPC, which results in a bent structure compared to saturated acyl chains. Triolien has monounsaturated fatty acids with straight acyl chains. Due to their structural differences, DOPC molecules may have trouble fitting comfortably within the triglyceride-lipid bilayer.

Chapter 3 shows the possibility of forming a triolein membrane and then characterisation and enzymatic activity using the EIS. Enzymatic activity on the membrane would not be affected based on a single or double-layer substrate. This would change the membrane's electrical properties, which is why the triolein has different values than well-established bilayers like DOPC.

In this chapter, this new membrane architecture is further characterised by NR. These results suggest that the triolein membrane is a single layer than a bilayer. However, the area effect comparisons in the EIS and NR membrane samples are different. EIS used the SDx-tethered membranes industrial partners sample slide, which gives a small area compared to the NR sample area. The large area might cause the appearance of a single layer of triolein.

As a new membrane architecture, a few further questions can be asked with the triolein membrane, such as does the triolein actually form a homogenous monolayer membrane around the tethers, or are they also capable of forming micelles around the tether groups? The EIS Bode plots discussed in Chapter 3.3.1.1, which are fitted with a simple resistor-capacitor equivalent circuit, along with the NR analysis of hydrogenated triolein, indicate that the triolein forms a cohesive membrane around the tethering molecules, with minimal micelle formation.

4.5 Conclusion

To conclude, neutron reflectometry experiments on d-triolein and h-triolein membranes, compared to the DOPC or phospholipid membranes with and without lipases, strongly support the idea of a *tethered monolayer lipid membrane* (tMLM). The data also indicates that the lipase enzymes do indeed penetrate the membranes during hydrolysis. However, the tMLMs remain intact, even after hydrolysis. This ultimately suggests the possibility of a more robust membrane sensor.

5 Future directions

5.1 Future directions for the PLA_2 activity sensor

Based on the results of Chapter 2, three further blind trials, conducted by others, were done using the phospholipid tBLM array sensor. The results were consistent with the proof-of-concept trial presented here in Chapter 2 in that the PLA_2 sensor is better at sensing PLA_2 activity in the UC than Crohn's samples. The next step in this research will be to create a sensor prototype (Figure 5.1).Mark Cherrill and Simon Doe have developed this prototype at the Australian National Fabrication Facility (ANFF). With this sensor, a longitudinal study could be done on individual patients to determine if their PLA_2 activity increases or reduces with their IBD treatments and to assess if the sensor can assist them in managing their disease. The hope is that patients will be able to use this sensor at home to track their IBD condition. The collector cap (shown in Figure 5.1) contains a spoon that can collect a fixed amount of stool samples into the tube. This tube will contain the appropriate buffers with which the PLA_2 enzymatic reactions can be measured when the tube is plugged into a small electrical impedance spectrometer.

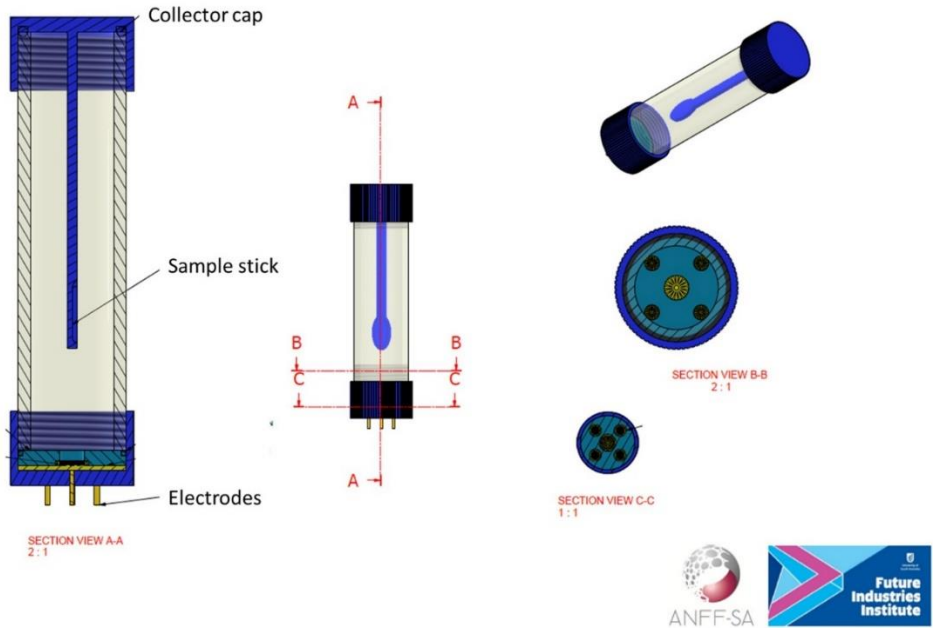

Figure 5.1: The prototype of the PLA_2 sensor created at the South Australian node of the Australian National Fabrication Facility under the National Collaborative Research Infrastructure Strategy.

In the future, experiments with different sn-2 ester PC molecules, other than DOPC, could be conducted to improve the sensitivity of the PLA_2 activity sensor. Other optimisations to be considered could also include:

- Identifying the ideal tether density.
- Identifying the ideal lipid-tether incubation times before solvent exchange.
- Optimizing the delivery buffer solution components.
- Changing the electrode size.

This PLA_2 sensor also has possible applications as a diagnostic for chronic inflammatory diseases and other gastrointestinal diseases like colorectal cancers. For example, colorectal tumour tissues express a high level of PLA_2 group X proteins [250, 251]. Also, synovial fluid from inflamed joints shows the presence of PLA_2 [252]. Not only that, according to recent clinical studies, increased PLA_2 in plasma is a significant independent risk factor for coronary heart disease [253].

5.2 Future directions for the lipase sensor

There is a need for negative control for the triolein sensor; therefore, future studies can perhaps attempt to use ether-linked triglycerides in the creation of triglyceride-tethered membranes. There is not any commercially available ether-linked triglyceride to the best of our knowledge, so these lipids might need to be bespoke produced

Lipase sensors are commonly used in the medical industry as a diagnostic tool to detect lipase levels, triglycerides and cholesterol levels. Therefore, the triolein tMLM sensor could further be developed as a diagnosis point-of-care sensor for these identifications. As some lipases are substrate dependent, there is also the possibility of creating other triglyceride tMLMs besides triolein. To confirm the use of the triolein sensor as a pancreatitis diagnostic sensor, a blind trial with pancreatitis patients' blood samples would need to be done.

Lipases are also currently used in wastewater treatments [254]; therefore, another possible application for the triolein sensor is as a quality test to see if the lipases are functioning properly in the wastewater.

Appendices

Appendix A: Calprotectin protein ELISA protocol

1. For the standard curve, add 100 µL of standards to the appropriate wells (see Dilute standards). For samples, add 100 µL of diluted samples (see Dilute samples) to the wells.

2. Cover wells and incubate for 2.5 hours at room temperature or overnight at 4°C with gentle shaking.

3. Discard the solution and wash it 4 times with 1X Wash Buffer. Wash by filling each well with Wash. Buffer (300 µL) using a multi-channel Pipette or auto washer. Complete removal of the liquid at each step is essential for good performance. After the last wash, remove any remaining Wash Buffer by aspirating or decanting. Invert the plate and blot it against clean paper towels.

4. Add 100 µL of prepared biotin conjugate (see Prepare biotin conjugate) to each well.

5. Incubate for 1 hour at room temperature with gentle shaking.

6. Discard the solution. Repeat the wash as in step 3.

7. Add 100 µL of prepared Streptavidin-HRP solution (see Prepare Streptavidin-HRP solution) to each well.

8. Incubate for 45 minutes at room temperature with gentle shaking.

9. Discard the solution. Repeat the wash as in step 3.

10. Add 100 µL of TMB Substrate to each well. The substrate will begin to turn blue.

11. Incubate for 30 minutes at room temperature in the dark with gentle shaking.

12. Add 50 µL of Stop Solution to each well. Tap the side of the plate gently to mix. The solution in the well changes from blue to yellow.

Appendix B: PLA_2 ELISA protocol

1. For the standard curve, add 100 µL of standards to the appropriate wells (see Dilute standards). For samples, add 100 µL of diluted samples (see Dilute samples) to the wells.

2. Cover wells and incubate for 2.5 hours at room temperature or overnight at 4°C with gentle shaking.

3. Discard the solution and wash it 4 times with 1X Wash Buffer. Wash by filling each well with Wash Buffer (300 µL) using a multi-channel Pipette or auto washer. Complete removal of the liquid at each step is essential for good performance. After the last wash, remove any remaining Wash Buffer by aspirating or decanting. Invert the plate and blot it against clean paper towels.

4. Add biotin conjugate a. Add 100 µL of prepared biotin conjugate (see Prepare biotin conjugate) to each well.

5. Incubate for 1 hour at room temperature with gentle shaking.

6. Discard the solution. Repeat the wash as in step 3.

7. Add Streptavidin-HRP a. Add 100 µL of prepared Streptavidin-HRP solution (see Prepare Streptavidin-HRP solution) to each well.

8. Incubate for 45 minutes at room temperature with gentle shaking.

9. Discard the solution. Repeat the wash as in step 3.

10. Add TMB substrate a. Add 100 µL of TMB Substrate to each well. The substrate will begin to turn blue.

11. Incubate for 30 minutes at room temperature in the dark with gentle shaking.

12. Add stop solution Add 50 µL of Stop Solution to each well. Tap the side of the plate gently to mix. The solution in the well changes from blue to yellow.

Appendix C: PLA_2 ELISA protocol

1. Dilute faeces extract samples 1:100 (e.g. 10 µL sample + 990 µL Sample Dilution Buffer) and mix well by vortexing.

2. Add 100 µL of each standard, control and diluted sample in duplicate wells.

3. Cover the plate with a sealing foil and incubate at room temperature for 40±5 min*) on a horizontal plate shaker (approximately 500 – 700 rpm).

4. At the end of the incubation time, remove the liquid and wash the wells by adding 300 µL. Washing Solution to each well. Remove as much liquid as possible and repeat until a total of three items of washing have been performed. If a plate washer is used, check that all aspirating and filling probes are unblocked to ensure efficient washing of all wells. After the final wash, invert the plate and tap the well openings thoroughly on absorbent tissue to remove any remaining Washing Solution.

5. Mix the content of the Enzyme Conjugate vial gently prior to use (do not shake). Add 100 µL of the conjugate to each well, preferably using a repetitive or multichannel pipette.

6. Cover the plate with sealing foil and incubate at room temperature for 40±5 min*) on a horizontal plate shaker (approximately 500 – 700 rpm).

7. Repeat the washing steps as described above, three times with 300 µL Washing Solution per well.

8. Add 100 µL Enzyme Substrate Solution to each well, preferably using a repetitive or multichannel pipette.

9. Incubate the plate at room temperature (without shaking) for 20 – 30 minutes, protected from light.

10. Optional: Add 100 µL 1M NaOH stop solution to each well if a fixed incubation period is required.

11. Read the optical density (OD) values at 405 nm using an ELISA reader. If the plate reader has this option, shake the plate briefly (2-3 seconds) before reading.

References

1. Green, P.H. and C. Cellier, *Celiac disease.* New england journal of medicine, 2007. **357**(17): p. 1731-1743.

2. Ollis, D.L., et al., *The α/β hydrolase fold.* 1992. **5**(3): p. 197-211.

3. Hermoso, J., et al., *Lipase activation by nonionic detergents: the crystal structure of the porcine lipase-colipase-tetraethylene glycol monooctyl ether complex.* 1996. **271**(30): p. 18007-18016.

4. Villeneuve, P.J.E.J.o.L.S. and Technology, *Plant lipases and their applications in oils and fats modification.* 2003. **105**(6): p. 308-317.

5. Helal, S.E., et al., *Lipase from Rhizopus oryzae R1: in-depth characterization, immobilization, and evaluation in biodiesel production.* 2021. **19**(1): p. 1-13.

6. Yao, W., et al., *A valuable product of microbial cell factories: Microbial lipase.* Frontiers in Microbiology, 2021. **12**: p. 743377.

7. Kapoor, M. and M.N. Gupta, *Lipase promiscuity and its biochemical applications.* Process Biochemistry, 2012. **47**(4): p. 555-569.

8. Rajendran, A., et al., *Lipase catalyzed ester synthesis for food processing industries.* 2009. **52**: p. 207-219.

9. Cipolatti, E.P., et al., *Production of new nanobiocatalysts via immobilization of lipase B from C. antarctica on polyurethane nanosupports for application on food and pharmaceutical industries.* 2020. **165**: p. 2957-2963.

10. Hasan, F., et al., *Industrial applications of microbial lipases.* 2006. **39**(2): p. 235-251.

11. Hwang, H.T., et al., *Lipase-catalyzed process for biodiesel production: Protein engineering and lipase production.* Biotechnology and bioengineering, 2014. **111**(4): p. 639-653.

12. Bora, L., D. Gohain, and R. Das, *Recent advances in production and biotechnological applications of thermostable and alkaline bacterial lipases.* Journal of Chemical Technology & Biotechnology, 2013. **88**(11): p. 1959-1970.

13. Treichel, H., et al., *A review on microbial lipases production.* Food and bioprocess technology, 2010. **3**(2): p. 182-196.

14. Kumar, A. and S.S. Kanwar, *Lipase production in solid-state fermentation (SSF): recent developments and biotechnological applications.* Dynamic Biochemistry, Process Biotechnology and Molecular Biology, 2012. **6**(1): p. 13-27.

15. Facin, B.R., et al., *Driving immobilized lipases as biocatalysts: 10 years state of the art and future prospects.* Industrial & Engineering Chemistry Research, 2019. **58**(14): p. 5358-5378.

16. Chandra, P., R. Singh, and P.K. Arora, *Microbial lipases and their industrial applications: a comprehensive review.* Microbial Cell Factories, 2020. **19**(1): p. 1-42.

17. Chapus, C., et al., *Minireview on pancreatic lipase and colipase.* Biochimie, 1988. **70**(9): p. 1223-1233.

18. Giller, T., et al., *Two novel human pancreatic lipase related proteins, hPLRP1 and hPLRP2. Differences in colipase dependence and in lipase activity.* Journal of Biological Chemistry, 1992. **267**(23): p. 16509-16516.

19. Thirstrup, K., R. Verger, and F. Carriere, *Evidence for a pancreatic lipase subfamily with new kinetic properties.* Biochemistry, 1994. **33**(10): p. 2748-2756.

20. Winkler, F., A. d'Arcy, and W.J.N. Hunziker, *Structure of human pancreatic lipase.* 1990. **343**(6260): p. 771.

21. Lowe, M.E., *Structure and function of pancreatic lipase and colipase.* Annual review of nutrition, 1997. **17**: p. 141.

22. Van Tilbeurgh, H., et al., *Colipase: structure and interaction with pancreatic lipase.* Biochimica et Biophysica Acta (Bba)-Molecular and Cell Biology of Lipids, 1999. **1441**(2-3): p. 173-184.

23. Crockett, S.D., et al., *American Gastroenterological Association Institute guideline on initial management of acute pancreatitis.* Gastroenterology, 2018. **154**(4): p. 1096-1101.

24. McPherson, R.A. and M.R. Pincus, *Henry's clinical diagnosis and management by laboratory methods E-book*. 2021: Elsevier Health Sciences.

25. Godfrey, T. and S. West, *Introduction to industrial enzymology. Industrial enzymology, Mac*. 1996, Millan Press, London.

26. Costa, T.M., et al., *Lipase production by Aspergillus niger grown in different agro-industrial wastes by solid-state fermentation.* Brazilian Journal of Chemical Engineering, 2017. **34**: p. 419-427.

27. Timberlake, W.E. and M.A.J.S. Marshall, *Genetic engineering of filamentous fungi.* 1989. **244**(4910): p. 1313-1317.

28. Mushtaq, S., et al., *Natural products as reservoirs of novel therapeutic agents.* EXCLI journal, 2018. **17**: p. 420.

29. Sugihara, A., et al., *Purification and characterization of Aspergillus niger lipase.* 1988. **52**(6): p. 1591-1592.

30. Utami, T.S., et al., *Production of dry extract extracellular lipase from Aspergillus niger by solid state fermentation method to catalyze biodiesel synthesis.* 2017. **136**: p. 41-46.

31. Adham, N.Z. and E. Ahmed, *Extracellular lipase of Aspergillus niger NRRL3; production, partial purification and properties.* Indian Journal of Microbiology, 2009. **49**(1): p. 77-83.

32. Nema, A., et al., *Production and optimization of lipase using Aspergillus niger MTCC 872 by solid-state fermentation.* Bulletin of the National Research Centre, 2019. **43**(1): p. 1-8.

33. Xing, S., et al., *Gene cloning, expression, purification and characterization of a sn-1, 3 extracellular lipase from Aspergillus niger GZUF36.* Journal of Food Science and Technology, 2020. **57**(7): p. 2669-2680.

34. Zheng-Yu, S., Y. Jiang-Ke, and Y. Yun-Jun, *Purification and characterization of a lipase from Aspergillus niger F044.* Chinese Journal of Biotechnology, 2007. **23**(1): p. 96-101.

35. Qiao, H., et al., *Optimisation of combi-lipases from Aspergillus niger for the synergistic and efficient hydrolysis of soybean oil.* Animal science journal, 2017. **88**(5): p. 772-780.

36. Mhetras, N., K. Bastawde, and D. Gokhale, *Purification and characterization of acidic lipase from Aspergillus niger NCIM 1207.* Bioresource technology, 2009. **100**(3): p. 1486-1490.

37. Contesini, F.J., et al., *Aspergillus sp. lipase: potential biocatalyst for industrial use.* 2010. **67**(3-4): p. 163-171.

38. Yang, J., J. Sun, and Y. Yan, *lip2, a novel lipase gene cloned from Aspergillus niger exhibits enzymatic characteristics distinct from its previously identified family member.* Biotechnology letters, 2010. **32**(7): p. 951-956.

39. Pfaller, M.A., et al., *Candida rugosa, an emerging fungal pathogen with resistance to azoles: geographic and temporal trends from the ARTEMIS DISK antifungal surveillance program.* Journal of clinical microbiology, 2006. **44**(10): p. 3578-3582.

40. De Maria, P.D., et al., *Understanding Candida rugosa lipases: an overview.* Biotechnology advances, 2006. **24**(2): p. 180-196.

41. Menden, A., et al., *Candida rugosa lipase alters the gastrointestinal environment in wild-type mice.* Biomedicine & Pharmacotherapy, 2020. **130**: p. 110579.

42. Benjamin, S. and A.J.Y. Pandey, *Candida rugosa lipases: molecular biology and versatility in biotechnology.* 1998. **14**(12): p. 1069-1087.

43. Sri Kaja, B., et al., *Investigating enzyme activity of immobilized Candida rugosa lipase.* 2018. **2018**.

44. Öztürk, B., *Immobilization of lipase from Candida rugosa on hydrophobic and hydrophilic supports*. 2001: Izmir Institute of Technology (Turkey).

45. Rúa, M.L. and A. Ballesteros, *Rapid purification of two lipase isoenzymes from Candida rugosa.* Biotechnology Techniques, 1994. **8**(1): p. 21-26.

46. Lee, G.-C., et al., *Analysis of the gene family encoding lipases in Candida rugosa by competitive reverse transcription-PCR.* Applied and environmental microbiology, 1999. **65**(9): p. 3888-3895.

47. Barriuso, J., et al., *Structural traits and catalytic versatility of the lipases from the Candida rugosa-like family: A review.* Biotechnology Advances, 2016. **34**(5): p. 874-885.

48. Mancheño, J.M., et al., *Structural insights into the lipase/esterase behavior in the Candida rugosa lipases family: crystal structure of the lipase 2 isoenzyme at 1.97 Å resolution.* Journal of Molecular Biology, 2003. **332**(5): p. 1059-1069.

49. A Jarjes, Z., M. Razip Samian, and S. Ab Ghani, *Bio-electrode in mechanistic study of lipoxygenase with fatty acids from cooking palm oil.* The Open Electrochemistry Journal, 2012. **4**(1).

50. Sri Kaja, B., et al., *Investigating enzyme activity of immobilized Candida rugosa lipase.* Journal of Food Quality, 2018. **2018**.

51. Katiyar, M. and A. Ali, *Effect of metal ions on the hydrolytic and transesterification activities of Candida rugosa lipase.* Journal of Oleo Science, 2013. **62**(11): p. 919-924.

52. Carrière, F., S. Bezzine, and R.J.J.o.M.C.B.E. Verger, *Molecular evolution of the pancreatic lipase and two related enzymes towards different substrate selectivities.* 1997. **3**(1-4): p. 55-64.

53. Andualema, B. and A. Gessesse, *Microbial lipases and their industrial applications.* Biotechnology, 2012. **11**(3): p. 100.

54. Hiol, A., et al., *Purification and characterization of an extracellular lipase from a thermophilic Rhizopus oryzae strain isolated from palm fruit.* 2000. **26**(5-6): p. 421-430.

55. Sayari, A., et al., *N-terminal peptide of Rhizopus oryzae lipase is important for its catalytic properties.* 2005. **579**(5): p. 976-982.

56. Li, C., et al., *Preparation and properties of Rhizopus oryzae lipase immobilized using an adsorption-crosslinking method.* 2016. **19**(8): p. 1776-1785.

57. Chiou, S.-H. and W.-T.J.B. Wu, *Immobilization of Candida rugosa lipase on chitosan with activation of the hydroxyl groups.* 2004. **25**(2): p. 197-204.

58. Singer, T.P. and B. Hofstee, *Studies on wheat germ lipase; methods of estimation, purification, and general properties of the enzyme.* Archives of biochemistry, 1948. **18**(2): p. 229-243.

59. Kublicki, M., et al., *Wheat germ lipase: Isolation, purification and applications.* Critical Reviews in Biotechnology, 2022. **42**(2): p. 184-200.

60. Jing, F., X. An, and W. Shen, *The characteristics of hydrolysis of triolein catalyzed by wheat germ lipase in water-in-oil microemulsions.* Journal of Molecular Catalysis B: Enzymatic, 2003. **24**: p. 53-60.

61. Barros, M., L. Fleuri, and G. Macedo, *Seed lipases: sources, applications and properties-a review.* Brazilian Journal of Chemical Engineering, 2010. **27**: p. 15-29.

62. Xia, X., et al., *Wheat germ lipase catalyzed kinetic resolution of secondary alcohols in non-aqueous media.* Biotechnology letters, 2009. **31**(1): p. 83-87.

63. Stauffer, C. and R. Glass, *The glycerol ester hydrolases of wheat germ.* Cereal Chem, 1966. **43**: p. 644-657.

64. Rose, D.J. and O.A. Pike, *A simple method to measure lipase activity in wheat and wheat bran as an estimation of storage quality.* Journal of the American Oil Chemists' Society, 2006. **83**(5): p. 415-419.

65. Yang, F. and A.J. Russell, *A comparison of lipase-catalyzed ester hydrolysis in reverse micelles, organic solvents, and biphasic systems.* Biotechnology and bioengineering, 1995. **47**(1): p. 60-70.

66. Aloulou, A., et al., *Phospholipases: an overview*, in *Lipases and phospholipases*. 2012, Springer. p. 63-85.

67. Richmond, G.S. and T.K.J.I.j.o.m.s. Smith, *Phospholipases A1.* 2011. **12**(1): p. 588-612.

68. Sun, G.Y., et al., *Dynamic Role of Phospholipases A2 in Health and Diseases in the Central Nervous System.* Cells, 2021. **10**(11): p. 2963.

69. Stephens, J.W.W., W.J.T.J.o.P. Myers, and Bacteriology, *The action of cobra poison on the blood: a contribution to the study of passive immunity.* 1898. **5**(3): p. 279-301.

70. Nevalainen, T.J., et al., *Conservation of group XII phospholipase A2 from bacteria to human.* 2012. **7**(4): p. 340-350.

71. Karray, A., et al., *Antibacterial properties of chicken intestinal phospholipase A2.* 2011. **10**(1): p. 4.

72. Burke, J.E. and E.A.J.J.o.l.r. Dennis, *Phospholipase A2 structure/function, mechanism, and signaling.* 2009. **50**(Supplement): p. S237-S242.

73. Dennis, E.A., et al., *Phospholipase A2 enzymes: physical structure, biological function, disease implication, chemical inhibition, and therapeutic intervention.* 2011. **111**(10): p. 6130-6185.

74. Pan, Y.H., B.J.J.B.e.B.A.-P. Bahnson, and Proteomics, *Structure of a premicellar complex of alkyl sulfates with the interfacial binding surfaces of four subunits of phospholipase A2.* 2010. **1804**(7): p. 1443-1448.

75. Ishizaki, J., et al., *cDNA cloning and sequence determination of rat membrane-associated phospholipase A2.* Biochemical and biophysical research communications, 1989. **162**(3): p. 1030-1036.

76. Dong, L., et al., *Group II phospholipase A2 gene expression is transcriptionally regulated in rat liver during sepsis.* American Journal of Physiology-Gastrointestinal and Liver Physiology, 1997. **273**(3): p. G706-G712.

77. Hara, S., et al., *Detection and purification of two 14 kDa phospholipase A2 isoforms in rat kidney: their role in eicosanoid synthesis.* Biochimica et Biophysica Acta (BBA)-Lipids and Lipid Metabolism, 1995. **1257**(1): p. 11-17.

78. Rozenfeld, R.A., et al., *Role of gut flora on intestinal group II phospholipase A2 activity and intestinal injury in shock.* 2001. **281**(4): p. G957-G963.

79. Murakami, M., et al., *The functions of five distinct mammalian phospholipase A2s in regulating arachidonic acid release: type IIA and type V secretory phospholipase A2s*

are functionally redundant and act in concert with cytosolic phospholipase A2. Journal of Biological Chemistry, 1998. **273**(23): p. 14411-14423.

80. Koduri, R.S., et al., *Bactericidal properties of human and murine groups I, II, V, X, and XII secreted phospholipases A2.* 2002. **277**(8): p. 5849-5857.

81. van Hensbergen, V.P., et al., *Type IIA Secreted Phospholipase A2 in Host Defense against Bacterial Infections.* 2020.

82. Six, D.A., E.A.J.B.e.B.A.-M. Dennis, and C.B.o. Lipids, *The expanding superfamily of phospholipase A2 enzymes: classification and characterization.* 2000. **1488**(1-2): p. 1-19.

83. Schaloske, R.H., E.A.J.B.e.B.A.-M. Dennis, and C.B.o. Lipids, *The phospholipase A2 superfamily and its group numbering system.* 2006. **1761**(11): p. 1246-1259.

84. Herrera-López, E.J., *Lipase and phospholipase biosensors: a review.* Methods in molecular biology (Clifton, N.J.), 2012. **861**: p. 525-543.

85. Sandoval, G. and E.J. Herrera-López, *Lipase, phospholipase, and esterase biosensors.* Lipases and Phospholipases, 2018: p. 391-425.

86. Nguyen, H.H., et al., *Immobilized enzymes in biosensor applications.* Materials, 2019. **12**(1): p. 121.

87. Needham, D., et al., *A new temperature-sensitive liposome for use with mild hyperthermia: characterization and testing in a human tumor xenograft model.* Cancer research, 2000. **60**(5): p. 1197-1201.

88. Yatvin, M.B., T.C. Cree, and J.J. Gipp, *Hyperthermia-Mediated Targeting of Liposome-Associated Anti-Neoplastic Drugs*, in *Targeting of Drugs*. 1982, Springer. p. 223-234.

89. Adlakha-Hutcheon, G., et al., *Controlled destabilization of a liposomal drug delivery system enhances mitoxantrone antitumor activity.* Nature biotechnology, 1999. **17**(8): p. 775-779.

90. Connor, J., M.B. Yatvin, and L. Huang, *pH-sensitive liposomes: acid-induced liposome fusion.* Proceedings of the National Academy of Sciences, 1984. **81**(6): p. 1715-1718.

91. Hong, M.S., et al., *pH-sensitive, serum-stable and long-circulating liposomes as a new drug delivery system.* Journal of pharmacy and pharmacology, 2002. **54**(1): p. 51-58.

92. Zhang, W., et al., *Colorimetric assay for heterogeneous-catalyzed lipase activity: enzyme-regulated gold nanoparticle aggregation.* Journal of agricultural and food chemistry, 2015. **63**(1): p. 39-42.

93. Chakraborty, D., et al., *Lipase sensing by naphthalene diimide based fluorescent organic nanoparticles: a solvent induced manifestation of self-assembly.* Soft Matter, 2021. **17**(8): p. 2170-2180.

94. Pijanowska, D., et al., *The pH-detection of triglycerides.* Sensors and Actuators B: Chemical, 2001. **78**(1-3): p. 263-266.

95. Bi, X., D. Hartono, and K.L. Yang, *Real-time liquid crystal pH sensor for monitoring enzymatic activities of penicillinase.* Advanced Functional Materials, 2009. **19**(23): p. 3760-3765.

96. Choudhury, P. and B. Bhunia, *Industrial application of lipase: a review.* Biopharm J, 2015. **1**(2): p. 41-47.

97. Pijanowska, D., et al., *The pH-detection of triglycerides.* 2001. **78**(1-3): p. 263-266.

98. Alkanhal, H., J. Frank, and G. Christen, *Microbial protease and phospholipase C stimulate lipolysis of washed cream.* Journal of dairy science, 1985. **68**(12): p. 3162-3170.

99. Shi, J., et al., *Fluorometric probing of the lipase level as acute pancreatitis biomarkers based on interfacially controlled aggregation-induced emission (AIE).* Chemical science, 2017. **8**(9): p. 6188-6195.

100. Whitcomb, D.C., *Clinical practice. Acute pancreatitis.* N Engl J Med, 2006. **354**: p. 2142-2150.

101. Aili, D., et al., *Hybrid nanoparticle− liposome detection of phospholipase activity.* Nano letters, 2011. **11**(4): p. 1401-1405.

102. Mirsky, V.M., et al., *Capacitive approach to determine phospholipase A2 activity toward artificial and natural substrates.* Analytical chemistry, 1998. **70**(17): p. 3674-3678.

103. Zehani, N., et al., *Impedimetric biosensor for the determination of phospholipase A2 activity in snake venom.* Analytical Letters, 2018. **51**(3): p. 401-410.

104. Lisdat, F. and D. Schäfer, *The use of electrochemical impedance spectroscopy for biosensing.* Analytical and bioanalytical chemistry, 2008. **391**(5): p. 1555-1567.

105. Zlatev, R., et al., *Rapid disposable lipase activity sensor for automatic industrial application.* Biotechnology & Biotechnological Equipment, 2021. **35**(1): p. 323-332.

106. Guda, N.M. and C.J.P.T.E.P.K.B. Nøjgaard, *Recurrent acute pancreatitis and progression to chronic pancreatitis.* 2015.

107. Herreros-Villanueva, M., et al., *Alcohol consumption on pancreatic diseases.* 2013. **19**(5): p. 638.

108. Melamed, P. and F.J.J.J.o.t.P. Melamed, *Chronic metabolic acidosis destroys pancreas.* 2014. **15**(6): p. 552-560.

109. Braganza, J.M., et al., *Chronic pancreatitis.* The Lancet, 2011. **377**(9772): p. 1184-1197.

110. DiMagno, E.P. and G.J.C.O.i.G. Holtmann, *Chronic pancreatitis.* 1991. **7**(5): p. 720-725.

111. Lucas, F.R.C.J.E.G. and D. System, *Critical Shock-Related Acute Pancreatitis.* 2019. **6**: p. 19-22.

112. Beger, H.G., S. Matsuno, and J.L. Cameron, *Diseases of the pancreas: current surgical therapy*. 2008: Springer Science & Business Media.

113. Szabo, G. and B.J.A.r.c.r. Saha, *Alcohol's effect on host defense.* 2015. **37**(2): p. 159.

114. Apte, M.V., et al., *Alcohol-related pancreatic damage.* 1997. **21**(1): p. 13-20.

115. Leppäniemi, A., et al., *2019 WSES guidelines for the management of severe acute pancreatitis.* 2019. **14**(1): p. 27.

116. Zhu, A.-J., J.-S. Shi, and X.-J.J.W.j.o.g. Sun, *Organ failure associated with severe acute pancreatitis.* 2003. **9**(11): p. 2570.

117. Ah-Tye, P.J.J.A.J.o.R.H., *Pancreatitis in remote Australia: an indigenous perspective.* 2001. **9**(3): p. 134-137.

118. Turner, R.C. and R. McDermott, *Clinical predictors of severe acute pancreatitis: value-adding the view from the end of the bed.* ANZ journal of surgery, 2014. **84**(9): p. 672-676.

119. Carroll, J.K., et al., *Acute pancreatitis: diagnosis, prognosis, and treatment.* 2007. **75**(10).

120. Nesvaderani, M., G.D. Eslick, and M.R.J.T.M.J.o.A. Cox, *Acute pancreatitis: update on management.* 2015. **202**(8): p. 420-423.

121. Yadav, D., N. Agarwal, and C.J.T.A.j.o.g. Pitchumoni, *A critical evaluation of laboratory tests in acute pancreatitis.* 2002. **97**(6): p. 1309.

122. Shah, A.P., M.M. Mourad, and S.R.J.J.o.i.r. Bramhall, *Acute pancreatitis: current perspectives on diagnosis and management.* 2018. **11**: p. 77.

123. Rompianesi, G., et al., *Serum amylase and lipase and urinary trypsinogen and amylase for diagnosis of acute pancreatitis.* Cochrane Database of Systematic Reviews, 2017(4).

124. Batra, H., et al., *Comparative study of serum amylase and lipase in acute pancreatitis patients.* 2015. **30**(2): p. 230-233.

125. Posthuma-Trumpie, G.A., J. Korf, and A. van Amerongen, *Lateral flow (immuno) assay: its strengths, weaknesses, opportunities and threats. A literature survey.* Analytical and bioanalytical chemistry, 2009. **393**(2): p. 569-582.

126. Gudgeon, A., et al., *Trypsinogen activation peptides assay in the early prediction of severity of acute pancreatitis.* The Lancet, 1990. **335**(8680): p. 4-8.

127. Basnayake, C. and D.J.A.p. Ratnam, *Abnormal laboratory results: blood tests for acute pancreatitis.* 2015. **38**(4): p. 128.

128. Asvesta, S., K. Pantopoulos, and P.J.A.B.C. Arzoglou, *Lipase activity and properties in serum of chronic alcoholics.* 1988. **46**: p. 435-438.

129. Li, X., et al., *Serum trypsinogen levels in type 1 diabetes.* 2017. **40**(4): p. 577-582.

130. Dalal, S.R. and E.B.J.T.J.o.c.i. Chang, *The microbial basis of inflammatory bowel diseases.* 2014. **124**(10): p. 4190-4196.

131. Baumgart, D.C. and W.J.J.T.L. Sandborn, *Crohn's disease.* 2012. **380**(9853): p. 1590-1605.

132. Barton, J. and A.J.Q.A.I.J.o.M. FERGUSON, *Clinical features, morbidity and mortality of Scottish children with inflammatory bowel disease.* 1990. **75**(2): p. 423-439.

133. Hendrickson, B.A., R. Gokhale, and J.H.J.C.m.r. Cho, *Clinical aspects and pathophysiology of inflammatory bowel disease.* 2002. **15**(1): p. 79-94.

134. Okazaki, K., et al., *Autoimmune-related pancreatitis is associated with autoantibodies and a Th1/Th2-type cellular immune response.* 2000. **118**(3): p. 573-581.

135. Stöcker, W., et al., *Autoimmunity to Pancreatic Juice in Crohn's Disease Results of an Autoantibody Screening in Patients with Chronic Inflammatory Bowel Disease.* 1987. **22**(sup139): p. 41-52.

136. Apple, F., et al., *Lipase and pancreatic amylase activities in tissues and in patients with hyperamylasemia.* 1991. **96**(5): p. 610-614.

137. ZhM, I., V. Rogozina, and O.J.K.m. Zinov'ev, *Amylolytic and lipolytic activities of the large intestine mucosa in various intestinal diseases.* 1984. **62**(1): p. 121-126.

138. Cho, J.H.J.N.R.I., *The genetics and immunopathogenesis of inflammatory bowel disease.* 2008. **8**(6): p. 458-466.

139. Morgan, X.C., et al., *Dysfunction of the intestinal microbiome in inflammatory bowel disease and treatment.* 2012. **13**(9): p. R79.

140. Carter, M.J., A.J. Lobo, and S.P.J.G. Travis, *Guidelines for the management of inflammatory bowel disease in adults.* 2004. **53**(suppl 5): p. v1-v16.

141. Yang, Z., et al., *Effectiveness and cost-effectiveness of measuring fecal calprotectin in diagnosis of inflammatory bowel disease in adults and children.* 2014. **12**(2): p. 253-262. e2.

142. Peterson, J., et al., *Phospholipase A2 activating protein and idiopathic inflammatory bowel disease.* 1996. **39**(5): p. 698-704.

143. Stremmel, W., et al., *Phospholipase A2 of microbiota as pathogenetic determinant to induce inflammatory states in ulcerative colitis: therapeutic implications of phospholipase A2 inhibitors.* 2017. **2**(3): p. 180-187.

144. Minami, T., et al., *Increased group II phospholipase A2 in colonic mucosa of patients with Crohn's disease and ulcerative colitis.* 1994. **35**(11): p. 1593-1598.

145. Stange, E.F., B.O.J.E.r.o.g. Schroeder, and hepatology, *Microbiota and mucosal defense in IBD: an update.* 2019. **13**(10): p. 963-976.

146. Adeagbo, A.S. and M.K.J.J.o.v.r. Henzel, *Calcium-dependent phospholipase A2 mediates the production of endothelium-derived hyperpolarizing factor in perfused rat mesenteric prearteriolar bed.* 1998. **35**(1): p. 27-35.

147. Buhmeida, A., et al., *PLA2 (group IIA phospholipase A2) as a prognostic determinant in stage II colorectal carcinoma.* 2009. **20**(7): p. 1230-1235.

148. Paganelli, F.L., et al., *Group IIA-secreted phospholipase A2 in human serum kills commensal but not clinical Enterococcus faecium isolates.* 2018. **86**(8).

149. Harwig, S., et al., *Bactericidal properties of murine intestinal phospholipase A2.* 1995. **95**(2): p. 603-610.

150. Sitkiewicz, I., K.E. Stockbauer, and J.M.J.T.i.m. Musser, *Secreted bacterial phospholipase A2 enzymes: better living through phospholipolysis.* 2007. **15**(2): p. 63-69.

151. Tibble, J., et al., *A simple method for assessing intestinal inflammation in Crohn's disease.* Gut, 2000. **47**(4): p. 506-513.

152. Tillett, W.S. and T. Francis Jr, *Serological reactions in pneumonia with a non-protein somatic fraction of pneumococcus.* The Journal of experimental medicine, 1930. **52**(4): p. 561.

153. Sugi, K., et al., *Fecal lactoferrin as a marker for disease activity in inflammatory bowel disease: comparison with other neutrophil-derived proteins.* American Journal of Gastroenterology (Springer Nature), 1996. **91**(5).

154. Bjerrum, O., M. Nissen, and N. Borregaard, *Neutrophil beta-2 microglobulin: an inflammatory mediator.* Scandinavian journal of immunology, 1990. **32**(3): p. 233-242.

155. Simard, J.C., D. Girard, and P.A. Tessier, *Induction of neutrophil degranulation by S100A9 via a MAPK-dependent mechanism.* Journal of leukocyte biology, 2010. **87**(5): p. 905-914.

156. Pathirana, W.G.W., et al., *Faecal calprotectin.* The Clinical Biochemist Reviews, 2018. **39**(3): p. 77.

157. Pintre, I.C. and S.J. Webb, *Binding and reactivity at bilayer membranes*, in *Advances in Physical Organic Chemistry*. 2013, Elsevier. p. 129-183.

158. Tien, H.T. and A. Ottova-Leitmannova, *Membrane biophysics: as viewed from experimental bilayer lipid membranes*. 2000: Elsevier.

159. Andersson, J. and I. Köper, *Biomimetic membranes*, in *Comprehensive Nanoscience and Nanotechnology*. 2019, Elsevier. p. 49-64.

160. Kurniawan, J., et al., *Preparation and characterization of solid-supported lipid bilayers formed by Langmuir–Blodgett deposition: a tutorial.* Langmuir, 2018. **34**(51): p. 15622-15639.

161. Villar, A.V., F.M. Goñi, and A. Alonso, *Diacylglycerol effects on phosphatidylinositol-specific phospholipase C activity and vesicle fusion.* FEBS letters, 2001. **494**(1-2): p. 117-120.

162. Andersson, J. and I. Köper, *Tethered and polymer supported bilayer lipid membranes: Structure and function.* Membranes, 2016. **6**(2): p. 30.

163. Naumann, R., et al., *Incorporation of membrane proteins in solid-supported lipid layers.* Angewandte Chemie International Edition in English, 1995. **34**(18): p. 2056-2058.

164. Lang, H., C. Duschl, and H.J.L. Vogel, *A new class of thiolipids for the attachment of lipid bilayers on gold surfaces.* 1994. **10**(1): p. 197-210.

165. Andersson, J., I. Köper, and W. Knoll, *Tethered membrane architectures—design and applications.* Frontiers in Materials, 2018. **5**: p. 55.

166. Alberts, B., et al., *The lipid bilayer*, in *Molecular Biology of the Cell. 4th edition*. 2002, Garland Science.

167. Israelachvili, J.N., D.J. Mitchell, and B.W. Ninham, *Theory of self-assembly of hydrocarbon amphiphiles into micelles and bilayers.* Journal of the Chemical Society, Faraday Transactions 2: Molecular and Chemical Physics, 1976. **72**: p. 1525-1568.

168. Israelachvili, J., S. Marčelja, and R.G. Horn, *Physical principles of membrane organization.* Quarterly reviews of biophysics, 1980. **13**(2): p. 121-200.

169. Dopazo, G.A., et al., *Modeling the Behavior of Amphiphilic Aqueous Solutions*, in *Deep Learning Applications*. 2021, IntechOpen.

170. Salim, M., et al., *Amphiphilic designer nano-carriers for controlled release: from drug delivery to diagnostics.* MedChemComm, 2014. **5**(11): p. 1602-1618.

171. Cranfield, C.G., et al., *Evidence of the key role of H3O+ in phospholipid membrane morphology.* Langmuir, 2016. **32**(41): p. 10725-10734.

172. Cranfield, C.G., et al., *Kalata b1 and kalata b2 have a surfactant-like activity in phosphatidylethanolomine-containing lipid membranes.* Langmuir, 2017. **33**(26): p. 6630-6637.

173. Yu, T.T., et al., *Design, Synthesis and Biological Evaluation of N-Sulfonylphenyl glyoxamide-Based Antimicrobial Peptide Mimics as Novel Antimicrobial Agents.* ChemistrySelect, 2017. **2**(12): p. 3452-3461.

174. Li, S., Q. Zhou, and H. Cong, *Electrochemical techniques, impedance, and spectroscopy.* Handbook of Advanced Non-Destructive Evaluation, 2018: p. 1-27.

175. Luan, Y., et al., *A hierarchical porous carbon material from a loofah sponge network for high performance supercapacitors.* Rsc Advances, 2015. **5**(53): p. 42430-42437.

176. Mathis, T.S., et al., *Energy storage data reporting in perspective—guidelines for interpreting the performance of electrochemical energy storage systems.* Advanced Energy Materials, 2019. **9**(39): p. 1902007.

177. Montemor, M. and M. Ferreira, *Cerium salt activated nanoparticles as fillers for silane films: Evaluation of the corrosion inhibition performance on galvanised steel substrates.* Electrochimica Acta, 2007. **52**(24): p. 6976-6987.

178. Montemor, M. and M. Ferreira, *Electrochemical study of modified bis-[triethoxysilylpropyl] tetrasulfide silane films applied on the AZ31 Mg alloy.* Electrochimica Acta, 2007. **52**(27): p. 7486-7495.

179. Cornell, B.A., et al., *A biosensor that uses ion-channel switches.* Nature, 1997. **387**(6633): p. 580-583.

180. Raguse, B., et al., *Tethered lipid bilayer membranes: formation and ionic reservoir characterization.* Langmuir, 1998. **14**(3): p. 648-659.

181. Garcia, A., et al., *Label-Free, Real-Time Phospholipase-A Isoform Assay.* ACS Biomaterials Science & Engineering, 2020. **6**(8): p. 4714-4721.

182. Fagerhol, M., *Calprotectin (the L1 leukocyte protein).* Stimulus response coupling: the role of intracellular calcium-binding proteins, 1990: p. 187-210.

183. Røseth, A., et al., *Assessment of the neutrophil dominating protein calprotectin in feces: a methodologic study.* Scandinavian journal of gastroenterology, 1992. **27**(9): p. 793-798.

184. Fagerhol, M., I. Dale, and T. Andersson, *A RADIOIMMUNOASSAY FOR A GRANULOCYTE PROTEIN AS A MARKER IN STUDIES ON THE TURNOVER OF SUCH CELLS: DOSAGE RADIO-IMMUNOLOGIQUE D'UNE PROTÉINE GRANULOCYTAIRE, UTILISÉE COMME MARQUEUR DANS LES ÉTUDES DU TAUX DE RENOUVELLEMENT LEUCOCYTAIRE*, in *Biochemistry, Pathology and Genetics of Pulmonary Emphysema*. 1981, Elsevier. p. 273-282.

185. DALE, I., M.K. FAGERHOL, and I. NAESGAARD, *Purification and partial characterization of a highly immunogenic human leukocyte protein, the L1 antigen.* European Journal of Biochemistry, 1983. **134**(1): p. 1-6.

186. Fagerhol, M., *Nomenclature for proteins: is calprotectin a proper name for the elusive myelomonocytic protein?* Clinical molecular pathology, 1996. **49**(2): p. M74.

187. Mumolo, M.G., et al., *From bench to bedside: Fecal calprotectin in inflammatory bowel diseases clinical setting.* World journal of gastroenterology, 2018. **24**(33): p. 3681.

188. Gaya, D., et al., *Faecal calprotectin in the assessment of Crohn's disease activity.* Qjm, 2005. **98**(6): p. 435-441.

189. Chahwan, B., et al., *Gut feelings: a randomised, triple-blind, placebo-controlled trial of probiotics for depressive symptoms.* 2019. **253**: p. 317-326.

190. Tamm, L.K. and H.M.J.B.j. McConnell, *Supported phospholipid bilayers.* 1985. **47**(1): p. 105-113.

191. Alghalayini, A., et al., *The use of tethered bilayer lipid membranes to identify the mechanisms of antimicrobial peptide interactions with lipid bilayers.* 2019. **8**(1): p. 12.

192. Krishna, G., et al., *Tethered bilayer membranes containing ionic reservoirs: selectivity and conductance.* Langmuir, 2003. **19**(6): p. 2294-2305.

193. Krishna, G., et al., *Tethered bilayer membranes containing ionic reservoirs: the interfacial capacitance.* Langmuir, 2001. **17**(16): p. 4858-4866.

194. Cornell, B.A., et al., *Tethered-bilayer lipid membranes as a support for membrane-active peptides.* Biochemical Society Transactions, 2001. **29**(3): p. 56-56.

195. de Buhr, M.F., et al., *Cd14, Gbp1, and Pla2g2a: three major candidate genes for experimental IBD identified by combining QTL and microarray analyses.* Physiological genomics, 2006. **25**(3): p. 426-434.

196. Swets, J.A., *Signal detection theory and ROC analysis in psychology and diagnostics: Collected papers*. 2014: Psychology Press.

197. Fogarty, J., R.S. Baker, and S.E. Hudson. *Case studies in the use of ROC curve analysis for sensor-based estimates in human computer interaction*. in *Proceedings of Graphics Interface 2005*. 2005. Citeseer.

198. Berrar, D. and P. Flach, *Caveats and pitfalls of ROC analysis in clinical microarray research (and how to avoid them).* Briefings in bioinformatics, 2012. **13**(1): p. 83-97.

199. Brown, C.D., H.T.J.C. Davis, and I.L. Systems, *Receiver operating characteristics curves and related decision measures: A tutorial.* 2006. **80**(1): p. 24-38.

200. Mandrekar, J.N.J.J.o.T.O., *Receiver operating characteristic curve in diagnostic test assessment.* 2010. **5**(9): p. 1315-1316.

201. Siqueira, F.F., et al., *Characterization of polymorphisms and isoforms of the Clostridium perfringens phospholipase C gene (plc) reveals high genetic diversity.* Veterinary microbiology, 2012. **159**(3-4): p. 397-405.

202. Fach, P. and J. Guillou, *Detection by in vitro amplification of the alpha-toxin (phospholipase C) gene from Clostridium perfringens.* Journal of applied bacteriology, 1993. **74**(1): p. 61-66.

203. Wolf, M.J. and R.W. Gross, *The calcium-dependent association and functional coupling of calmodulin with myocardial phospholipase A2: implications for cardiac cycle-dependent alterations in phospholipolysis.* Journal of Biological Chemistry, 1996. **271**(35): p. 20989-20992.

204. Sharma, S., *Melittin-induced hyperactivation of phospholipase A2 activity and calcium influx in ras-transformed cells.* Oncogene, 1993. **8**(4): p. 939-947.

205. Yoshihara, Y. and Y. Watanabe, *Translocation of phospholipase A2 from cytosol to membranes in rat brain induced by calcium ions.* Biochemical and biophysical research communications, 1990. **170**(2): p. 484-490.

206. Burack, W.R. and R.L. Biltonen, *Lipid bilayer heterogeneities and modulation of phospholipase A2 activity.* Chemistry and physics of lipids, 1994. **73**(1-2): p. 209-222.

207. Hutchison, J.S., et al., *Hypothermia therapy after traumatic brain injury in children.* New England Journal of Medicine, 2008. **358**(23): p. 2447-2456.

208. Santosh, L., *The effects of temperature on enzyme activity and biology*. 2018, Sciencing.

209. Donohoe, P.H., T.G. West, and R.G. Boutilier, *Factors affecting membrane permeability and ionic homeostasis in the cold-submerged frog.* Journal of Experimental Biology, 2000. **203**(2): p. 405-414.

210. Tanca, A., et al., *A human gut metaproteomic dataset from stool samples pretreated or not by differential centrifugation.* Data in Brief, 2015. **4**: p. 559-562.

211. Verberkmoes, N.C., et al., *Shotgun metaproteomics of the human distal gut microbiota.* The ISME journal, 2009. **3**(2): p. 179-189.

212. Cranfield, C., et al., *The impact of pH on packing in tethered lipid bilayers.* 2016.

213. Holt, S., C. Cranfield, and I. Koeper, *Probing the structure and function of tethered bilayer membranes by neutron reflection.* 2018.

214. Akita, C., T. Kawaguchi, and F. Kaneko, *Structural study on polymorphism of cis-unsaturated triacylglycerol: triolein.* The Journal of Physical Chemistry B, 2006. **110**(9): p. 4346-4353.

215. Deplazes, E., et al., *Calcium ion binding at the lipid–water interface alters the ion permeability of phospholipid bilayers.* Langmuir, 2021. **37**(48): p. 14026-14033.

216. Krokan, H.E., K.S. Bjerve, and E. Mørk, *The enteral bioavailability of eicosapentaenoic acid and docosahexaenoic acid is as good from ethyl esters as from glyceryl esters in spite of lower hydrolytic rates by pancreatic lipase in vitro.* Biochimica et Biophysica Acta (BBA)-Lipids and Lipid Metabolism, 1993. **1168**(1): p. 59-67.

217. Dumonde, D. and L. Glynn, *The production of arthritis in rabbits by an immunological reaction to fibrin.* British journal of experimental pathology, 1962. **43**(4): p. 373.

218. Andersson, R., M. Nyström, and K. Holmqvist, *Sampling frequency and eye-tracking measures: how speed affects durations, latencies, and more.* Journal of Eye Movement Research, 2010. **3**(3).

219. Cranfield, C.G., T. Bettler, and B. Cornell, *Nanoscale ion sequestration to determine the polarity selectivity of ion conductance in carriers and channels.* Langmuir, 2015. **31**(1): p. 292-298.

220. Xin, R., et al., *A comparative study on kinetics and substrate specificities of Phospholipase A1 with Thermomyces lanuginosus lipase.* Journal of Colloid and Interface Science, 2017. **488**: p. 149-154.

221. Fauvel, J., et al., *Substrate specificity of two cationic lipases with high phospholipase A1 activity purified from guinea pig pancreas I. Studies on neutral glycerides.* Biochimica et Biophysica Acta (BBA)-Lipids and Lipid Metabolism, 1984. **792**(1): p. 65-71.

222. Bagi, K., L. Simon, and B. Szajáni, *Immobilization and characterization of porcine pancreas lipase.* Enzyme and Microbial Technology, 1997. **20**(7): p. 531-535.

223. Lowe, L.A., et al., *Subtle changes in pH affect the packing and robustness of fatty acid bilayers.* Soft Matter, 2022. **18**(18): p. 3498-3504.

224. Zambrzycka, A., R.P. Strosznajder, and J.B. Strosznajder, *Aggregated beta amyloid peptide 1–40 decreases Ca2+-and cholinergic receptor-mediated phosphoinositide degradation by alteration of membrane and cytosolic phospholipase C in brain cortex.* Neurochemical research, 2000. **25**(2): p. 189-196.

225. Wang, G., S. Ryu, and X. Wang, *Plant phospholipases: an overview.* Lipases and phospholipases, 2012: p. 123-137.

226. Kimura, H., et al., *Activation of human pancreatic lipase activity by calcium and bile salts.* The Journal of Biochemistry, 1982. **92**(1): p. 243-251.

227. Borgström, B., et al., *Studies of intestinal digestion and absorption in the human.* The Journal of clinical investigation, 1957. **36**(10): p. 1521-1536.

228. Engel, K.M., et al., *Phospholipases and Reactive Oxygen Species Derived Lipid Biomarkers in Healthy and Diseased Humans and Animals–A Focus on Lysophosphatidylcholine.* Frontiers in Physiology, 2021: p. 2019.

229. Ditz, T., et al., *Phospholipase A2 products predict the hematopoietic support capacity of horse serum.* Differentiation, 2019. **105**: p. 27-32.

230. Vines, C.M., *Phospholipase C.* Calcium Signaling, 2012: p. 235-254.

231. Kadamur, G. and E.M. Ross, *Mammalian phospholipase C.* Annu Rev Physiol, 2013. **75**(1): p. 127-154.

232. Terra, W.R. and C. Ferreira, *Biochemistry and molecular biology of digestion*, in *Insect molecular biology and biochemistry*. 2012, Elsevier. p. 365-418.

233. Van Der Kolk, J., et al., *Heparinised blood ionised calcium concentrations in horses with colic or diarrhoea compared to normal subjects.* Equine veterinary journal, 2002. **34**(5): p. 528-531.

234. White, R., et al., *New sample environment projects and developments at the Australian Centre for Neutron Scattering.* 2019.

235. Cubitt, R. and G. Fragneto, *Neutron reflection:: Principles and examples of applications*, in *Scattering*. 2002, Elsevier. p. 1198-1208.

236. Sears, V.F., *Fundamental aspects of neutron optics.* Physics Reports, 1982. **82**(1): p. 1-29.

237. Utsuro, M. and V.K. Ignatovich, *Handbook of neutron optics*. 2010: John Wiley & Sons.

238. Jackson, A.J., *Introduction to small-angle neutron scattering and neutron reflectometry.* NIST Center for Neutron Research, 2008: p. 1-24.

239. Cousin, F. and G. Fadda. *An introduction to neutron reflectometry*. in *EPJ Web of Conferences*. 2020. EDP Sciences.

240. Efimova, Y., et al., *On the neutron scattering length density of proteins in H2O/D2O.* Physica B: Condensed Matter, 2004. **350**(1-3): p. E877-E880.

241. James, M., et al., *The multipurpose time-of-flight neutron reflectometer "Platypus" at Australia's OPAL reactor.* Nuclear Instruments and Methods in Physics Research Section A: Accelerators, Spectrometers, Detectors and Associated Equipment, 2011. **632**(1): p. 112-123.

242. Pirali, T., et al., *Applications of deuterium in medicinal chemistry.* Journal of medicinal chemistry, 2019. **62**(11): p. 5276-5297.

243. King, G.I. and S.H. White, *Determining bilayer hydrocarbon thickness from neutron diffraction measurements using strip-function models.* Biophysical journal, 1986. **49**(5): p. 1047-1054.

244. Motlaq, V.F., et al., *Dissolution mechanism of supported phospholipid bilayer in the presence of amphiphilic drug investigated by neutron reflectometry and quartz crystal microbalance with dissipation monitoring.* Biochimica et Biophysica Acta (BBA)-Biomembranes, 2022: p. 183976.

245. Nagle, J.F. and S. Tristram-Nagle, *Structure of lipid bilayers.* Biochimica et Biophysica Acta (BBA)-Reviews on Biomembranes, 2000. **1469**(3): p. 159-195.

246. Tristram-Nagle, S., H.I. Petrache, and J.F. Nagle, *Structure and interactions of fully hydrated dioleoylphosphatidylcholine bilayers.* Biophysical journal, 1998. **75**(2): p. 917-925.

247. Vacklin, H.P., et al., *Phospholipase A2 hydrolysis of supported phospholipid bilayers: a neutron reflectivity and ellipsometry study.* Biochemistry, 2005. **44**(8): p. 2811-2821.

248. Hamilton, J.A., *Interactions of triglycerides with phospholipids: incorporation into the bilayer structure and formation of emulsions.* Biochemistry, 1989. **28**(6): p. 2514-2520.

249. Pakkanen, K.I., et al., *Mechanics and dynamics of triglyceride-phospholipid model membranes: Implications for cellular properties and function.* Biochimica et Biophysica Acta (BBA)-Biomembranes, 2011. **1808**(8): p. 1947-1956.

250. Hiyoshi, M., et al., *The expression of phospholipase A2 group X is inversely associated with metastasis in colorectal cancer.* Oncology letters, 2013. **5**(2): p. 533-538.

251. Gonzalez-Buritica, H., M. Khamashita, and G. Hughes, *Synovial fluid phospholipase A2s and inflammation.* Annals of the rheumatic diseases, 1989. **48**(4): p. 267-269.

252. Duchez, A.-C., et al., *Respective contribution of cytosolic phospholipase A2α and secreted phospholipase A2 IIA to inflammation and eicosanoid production in arthritis.* Prostaglandins & Other Lipid Mediators, 2019. **143**: p. 106340.

253. Hurt-Camejo, E., et al., *Phospholipase A2 in vascular disease.* Circulation research, 2001. **89**(4): p. 298-304.

254. Nimkande, V.D. and A. Bafana, *A review on the utility of microbial lipases in wastewater treatment.* Journal of Water Process Engineering, 2022. **46**: p. 102591.